People's Democratic Republic of Algeria
Ministry of Higher Education and Scientific Research
Larbi Ben M'hidi, University-Oum El Bouaghi
Faculty of Sciences and Applied Sciences
Department of Electrical Engineering
LGEA Laboratory

A Dissertation

Submitted in partial fulfillment of the requirements for the degree of

LMD Doctorate

Option: Electrical Engineering and Automation

Title :

"Réalisation d'une plate-forme expérimentale pour la commande prédictive d'une chaine de conversion d'énergie photovoltaïque raccordée au réseau basse tension"

Implementation of an experimental bench of the predictive control applied on photovoltaic low voltage grid connected system

By

REMACHE Seif El Islam

Submitted on 11/07/2021

Board of Examiners

Mr. Noureddine Goléa	Professor	Chairman	OEB University
Mr. Kamel Barra	Professor	Supervisor	OEB University
Mr. Abdellatif Reama	Professor	Co-Supervisor	Gustave Eiffel University-France
Mr. Achour Betka	Professor	Examiner	Biskra University
Mr. Youcef Soufi	Professor	Examiner	Tebessa University
Mr. Said Drid	Professor	Examiner	Batna University

Dedication

My aim dedication goes to my father Laid, Mom Saida, My lovely sister Soundous, and my only brother Ayoub

To my wife Nour.

Acknowledgements

First, I 'am grateful to **the Almighty GOD** for establishing me to complete this work.

In the beginning, I would like to express my special appreciation and thanks to my academic advisor Professor Barra Kamel, head of the LGEA laboratory. During my thesis work, you contribute to a rewarding my graduate school experience by giving me intellectual freedom, supporting my attendance at various conferences, engaging me in new ideas and demanding a high quality of work in all my endeavors. Your advice on both research as well as on my career have been invaluable.

In addition, I want to thank my co-advisor in France Professor Reama Abdellatif for accepting me into his group in ESIEE-Paris-France. By this word, I would like to thank you for encouraging my research and for allowing me to grow as a research scientist.

I am deeply grateful to my committee members: Pr. Noureddine Goléa, Pr. Youcef Soufi, Pr. Achour Betka, and Pr. Drid Said, for their interest in my work.

I would like to say thank you so much to my sister, you were the reason that led me to my PhD, thank you for supporting me, helping me, and giving me the energy to complete what I did before, so thank you again Soundous. In addition, every result described in this thesis was accomplished with the help and support of my lab-mate and collaborator Yahia Cherif Ali, a special thanks to you my friend, I greatly benefited from your keen scientific insight.

I am also indebted to all the staff of the LGEA laboratory; I had the opportunity to work with you. I would be remiss if I did not thank, Algerian Ministry of Higher Education and Scientific Research, I am grateful for the funding sources that allowed me to pursue my graduate researches.

Finally, I would like to acknowledge friends and family members who supported me during my PhD timework.

Table of contents

Chapter III: Optimal cascaded predictive control for photovoltaic systems: application based on predictive emulator

Chapter IV: Cascaded predictive direct power control for photovoltaic systems: stand-alone system with integrated energy storage and grid-connected system

List of figures

Chapter I: State of the art - photovoltaic power sharing with interface converters in stand-alone and grid connected systems

Chapter II: Finite set model predictive control applied to photovoltaic systems

Chapter III: Optimal cascaded predictive control for photovoltaic systems: application based on predictive emulator

Chapter IV: Cascaded predictive direct power control for photovoltaic systems: stand-alone system with integrated energy storage and grid-connected system

List of Tables

Chapter I: State of the art - photovoltaic power sharing with interface converters in stand-alone and grid connected systems

Chapter II: Finite set model predictive control applied to photovoltaic systems

Chapter III: Optimal cascaded predictive control for photovoltaic systems: application based on predictive emulator

Chapter IV: Cascaded predictive direct power control for photovoltaic systems: stand-alone system with integrated energy storage and grid-connected system

GENERAL INTRODUCTION

General introduction

The world is running out of conventional energies and makes more importance on renewables. Furthermore, and in contrast to all other fossil fuels used in energy production, renewables in 2020 proved that were resilient to the crisis of Covid-19 by generating clean electricity that grow by almost 7%. In fact, the International Energy Agency (IEA) forecasts declare that global energy demand on fossil one will be decreased by 5%, whereas in long term, the green energy plants continue to grow strongly, and green projects are in progress to be realized [1]. The growing demand for renewable energies can help our planet to overcome the global warming by allowing the atmospheric gases to cover the Ozone hole.

In the last decades, the global energy demands are switched to Micro-grids that uses renewable energy sources such as: biomass, wind and solar energies. However, the global electricity production is now connected to several hybrid electrical distribution systems and controllable loads that constitute an active electrical network or as it called Distributed Energy Resources (DERs). The rapid expansion of DERs has made important changes in the electricity systems around the world, in terms of availability, reliability and high efficiency. Fast penetration of renewables in DERs makes the system more complex and in need of new architectures. Community Micro-grids (MGs) integrate several renewable sources (such as wind and solar), loads and central battery bank. These parts are connected between them by a DC bus through many power electronic interfaces. In contrast, these MGs operate in parallel with the AC existing distributed system to provide high power quality and low electricity cost for customers.

Solar energy is the most preferred kind of energy source for Algeria economy since our country is the largest one in Africa where the desert occupies more than 80% of its total area. In the Algerian south area, the irradiance level is always greater than 1000 W/m², which gives the opportunity to generate more KWs/day of green PV energy.

According to the IEA statistics, solar PV installations is growing by over 22% and reached 720 TWh in 2019, these results lead to say that the PV generated electricity represents the second vast growth in all renewables behind wind energy. Moreover, the cumulative PV panels installation in the world increases rapidly and will attain the Sustainable Development Scenario (SDS) level by the end of 2029, which requires a rate of 15% of PV solar electricity generated annually, by means it can rise up to 3300 TWh in 2030. These statistics must be accomplished

by integrating PV systems in several area like commercial buildings, homes, industry and transport vehicles…etc. For example, new industrial and commercial PV applications and residential systems are installed in China where 30.1 GW is achieved in 2019 despite the sever policy uncertainties, and now there are many subsides-green projects in development. In addition, the United-States continue to adopt PV solar projects with a growth of 13.2 GW in 2019, and in the European Union have had the fastest PV solar additions in 2019 with a rate of 98% in Germany, the Netherlands, and Spain. The proliferation of PV solar systems and the integration into the grid have open the door for advanced studies of power electronic interfaces.

Power electronic converters are the interface blocks used in DERs linking renewable systems, electrical grid, and customers. Due to its important role in power quality, many advanced researches and investigations were carried out in order to develop new power converter topologies with high efficacy and reduced components such as K-Type Multilevel inverter [2]. Moreover, the control strategy has a key role on the system stability and controllability. From the advanced controls used for power electronic converters, Finite-Set Model Predictive Control FS-MPC is the most advanced used one, where it proved high performance and robustness with a simple design based on converter switches states.

The main objective of this dissertation is the design and implementation by experimental validation of PV grid connected systems using FS-MPC as an advanced control method of power converters. This dissertation has many contributions:

- Analysis, simulations and comparison of different PV systems using FS-MPC.
- Design of a new predictive PV emulator (P-PVE) used to test PV systems under real climatic conditions.
- Proposing of an efficient cascaded predictive control method (CPC) for PV stand-alone and grid connected systems.
- Integrating of an energy storage system with the studied system.

This dissertation consists of four chapters that are presented as follows:

In chapter 1, we investigate the state of the art of PV solar conversion systems, their connection architectures and the different power electronic converters used to ensure interfaces functioning between PV panels, grid, batteries and loads. In addition, we discuss the advanced control methods and their benefits proposed in the literature.

In chapter 2, we present the FS-MPC basic principle applied to a photovoltaic system. The research in this chapter deals with the modeling and simulation of a PV stand-alone and grid-connected systems using two different topologies of DC/DC converters and their comparison in terms of DC-link voltage oscillations, reference tracking, switching's number and efficiency.

In chapter 3, the research aims to develop an experimental bench for the previously studied systems and to develop efficient control methods based on the FS-MPC. Therefore, a Predictive PV Emulator P-PVE is proposed and realized; also, a Cascaded Predictive Control CPC for a single-phase grid-tied system is developed and tested experimentally under several tests using the P-PVE. A set of simulation and experiment results are carried out to prove the robustness and correctness of the proposed method for such systems.

In chapter 4, the contribution aims to two goals, the fist is to propose a Cascaded Predictive Power Control (CPPC) that uses the decoupled active and reactive power control strategy. This control method provides flexibility and simple controllability to the system, by means that the PV grid system has had a robust control on reactive power and MPPT at the same time without any perturbation on the system. The second goal is to integrate an energy storage system into a stand-alone PV system using the proposed CPPC and a power management algorithm. The two studied systems were tested experimentally and they proved high performances.

This dissertation ends with a general conclusion that collects the benefits of the contributions and presents the future work that will be developed later.

Chapter I

State Of The Art - Photovoltaic Power Sharing With Interface Converters in Stand-alone and Grid Connected Systems

I. State of the art-photovoltaic power sharing with interface converters in stand-alone and grid connected systems

I.1. Introduction

Photovoltaic solar power is one of the reliable future green energy source that provides available electricity due to its inexhaustible natural renewable. Today's high PV penetration in Distributed Energy Resources (DERs) can make PV energy to be the first source for humanity before the end of this decade. Moreover, according to the International Energy Agency (IEA) report, the decrease in PV solar panels manufacturing costs of 70% allows for more future-scale PV plant installations, and of course, it creates new obstacles and challenges. From these, we can find the requirements of a large area, good irradiance concentration, advanced and efficient control systems with new architectures of power converter interfaces.

The power converter interfaces used in DERs make the system able to connect more energy resources such as PVs, wind and hydrogen energy regardless of the electricity nature DC or AC. They create a power balancing between the connected resources, batteries and the loads. Moreover, these interfaces make the generating system bi-directional with customers and give more flexibility in providing the demanded power or receiving the excess power before injecting it into the grid side. In recent years, there are many advanced interface architectures that connect systems with reduced components and high efficacy. For example, in PV grid-tied systems we can find double and single stage systems such as the quasi Z-source inverter that offers a grid current injection with DC voltage booster and inversion stage at the same time. The multilevel converters are also used to give their benefits of high-gain output voltage or low current and voltage oscillations with low THDs such as in [2]. Each interface topology has advantages and drawbacks related to component losses or the control complexity.

To ensure the system reliability, efficacy, and flexibility of the connected energies, the DER needs a wide range of advanced control methods. Finite set Model Predictive control (FS-MPC) is the recent control method applied to power converter interfaces such as single-phase inverters [4-5], multi-level voltage source inverters [6], DC/DC converters [7], and quasi Z-source inverters [8]. In addition, it can be applied as an energy management algorithm in fuel-cell vehicles [9], or as an optimizer for battery-supercapacitors energy in electric vehicles [10].

Furthermore, and regardless to its application in other domains, FS-MPC gains popularity in advanced researches and in industrial electronic applications thanks to the rapid development of new and fast microprocessors and microcontrollers. For that reason, it is chosen to be the primary objective of this dissertation.

I.2. Power converters in stand-alone and grid connected PV systems

In PV systems, the power electronic converters are the adaptation stages between PV panels and loads or the electrical grid, where they ensure the power boosting, inversion and transmission to the customers with the demanded characteristics. These interfaces are based on advanced and developed switches such as MOSFETs, IGBTs, IGCTs, IEGTs, and MCTs…etc, used to compensate for courant and voltage harmonics, to enhance power quality and to ensure voltage stability. We investigate in this chapter the different architectures of stand-alone and grid connected PV systems and the topologies of the power electronic converters with their control systems.

I.2.1. Stand-alone PV systems

Stand-alone PV systems, also called islanded PV systems, are sized and designed to supply DC loads, batteries or AC loads without the need of the utility grid. These systems will continue to deliver the demanded power during the day until the irradiance level becomes insufficient, then, the system switches to extract the stored energy from batteries in order to feed the loads during the night or on the cloudy days. Power electronic converters play the crucial role in PV systems functioning where DC/DC converters ensure the MPPT PV power extraction feeding the loads and batteries whatever the climatic conditions. In stand-alone PV systems, DC/AC converters ensure the inversion stages for supplying AC loads, the utility grid can be dispensed [11]. Fig.I.1 depicts a PV system scheme with integrated energy storage and feeding AC loads.

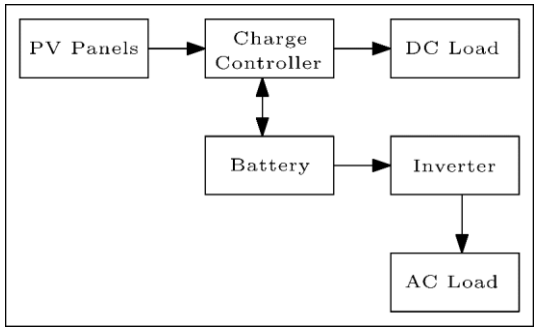

Figure I.1: Stand-alone PV system with integrated energy storage and feeding AC loads [11].

Another kind of PV stand-alone systems called hybrid PV systems include batteries that can balance the energy with utility grid when the panels stop giving energy. Fig.I.2 presents the hybrid PV system.

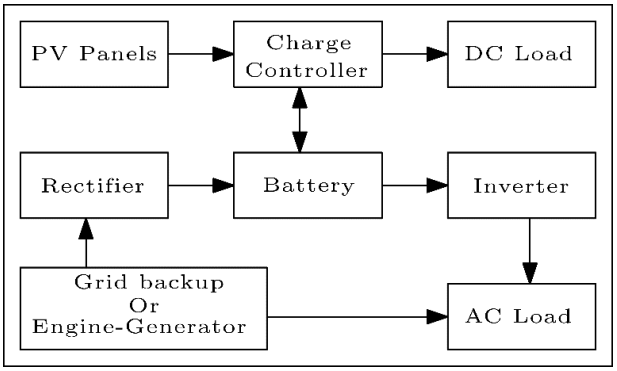

Figure I.2: Hybrid PV system [11].

I.2.1.1. DC/DC converters in stand-alone PV systems

The DC/DC converters in PV systems are often used to enhance the system efficacy. For example, the Boost converter is controlled by an MPPT algorithm to extract the maximum PV power and to boost the PV voltage to an appropriate value. We will investigate the most used topologies in PV systems with their benefits and drawbacks.

- **Boost converter topology**

The conventional boost converter is shown in Fig.I.3. It is the most used topology in PV systems having the role to step up the input DC voltage to a desired value for supplying a load or charging a battery. This converter operates in Continuous Current Mode (CCM) or in Discontinued Current Mode (DCM). This topology has a simple design and concept but needs an exact sizing to eliminate output current and voltage ripples with reduced voltage stress [12].

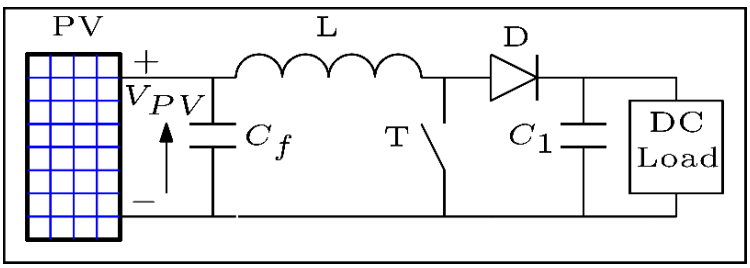

Figure I.3: Conventional boost converter.

▪ Interleaved boost converter

The interleaved boost converter topology is shown in Fig.I.4. It is used in the PV system to improve the efficiency by decreasing the current and voltage ripples against increasing the switching frequency. Its basic principle lays on two parallel conventional boosts with the same input and the same output, where the switches' triggers are controlled in a complimentary way (180-degree out-of-phase from each other). This topology allows sizing the converter with low values of the inductors and capacitors, but these double components can increase the cost of the converter for practical application [12].

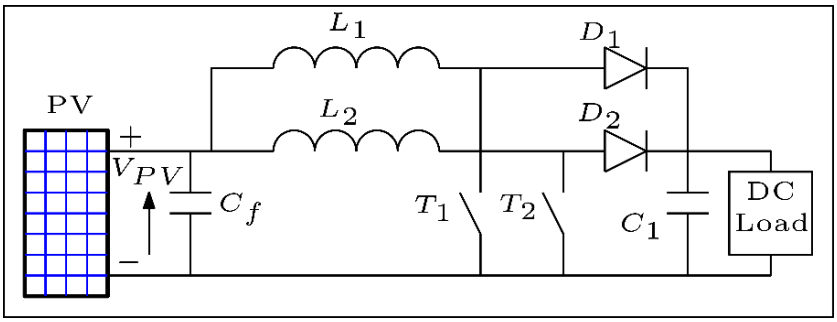

Figure I.4: Interleaved boost converter.

▪ Quadratic boost/buck converter

The circuit design of the quadratic boost converter is shown in Fig.I.5. It is based on two series boost converters with the elimination of the second controllable switch, where it can operate as a boost or buck converter according to the application need. The output gain is the same as two cascaded boost converters but its efficiency is lower than the conventional boost or buck converter in such low voltage PV application. This deficiency can classify the converter for specified power range in PV system applications [13].

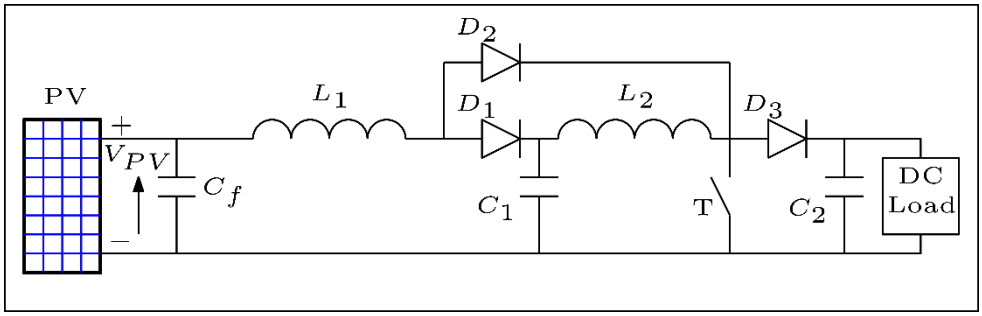

Figure I.5: Quadratic boost converter.

▪ Multilevel boost converter:

The multilevel boost converter is shown in Fig.I.6. It operates as a multiplier of the output voltage that is proportional to the number of the converter levels. It can increase the output voltage by adding two diodes and two capacitors. Therefore, since it has one controllable switch, its principle stays simple. The efficiency is also proportional to the added components and the internal series resistances of the capacitors, inductors and the turn on switch. The sizing procedure is the same for a conventional boost converter. This topology is applicable for a wide range of high gain voltage application and especially for PV systems [14].

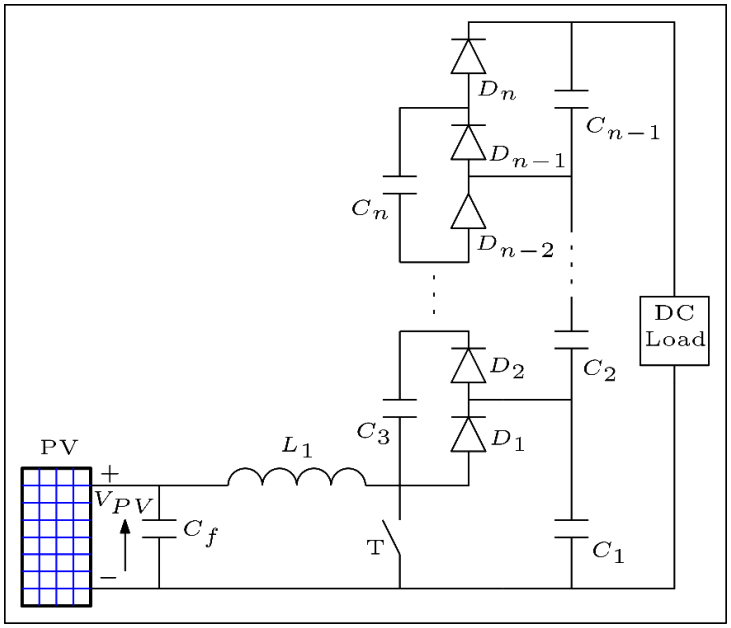

Figure I.6: Multilevel boost converter.

▪ Fly-back boost/buck converter

The fly-back converter illustrated in Fig.I.7 is based on an isolated AC/DC or DC/DC conversion. It can step up or step down the input voltage according to the application need. Based on a coupled inductor or high-frequency transformer, it provides many output voltages to drive multiple loads with the same input voltage. It gives many benefits such as isolated circuit between high voltage side and low voltage one, multiple voltages in the output and simple implementation. It is widely used in industries and household appliances and also recommended for PV system application such as in [15]. Moreover, it became a very interesting research focus, where many papers investigate new fly-back circuits with enhanced power efficiency by adding extra-circuits such as in [16].

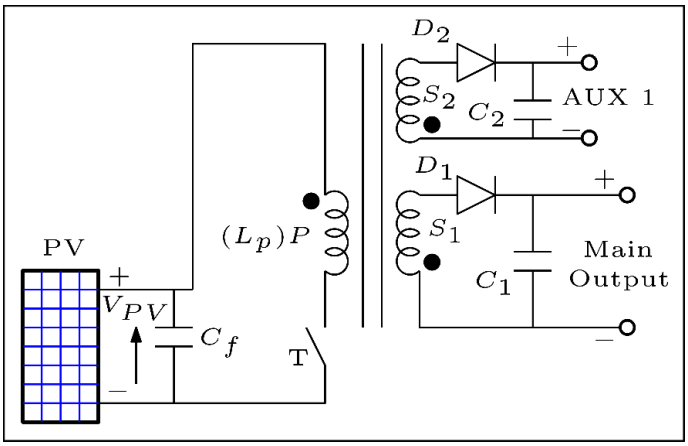

Figure I.7: Fly-back converter.

- **Quasi Z-source converter**

The quasi Z-source converter is shown in Fig.I.8. It is the recent topology version of the Z-source one. This topology uses the switched-capacitor/switched-inductor method in order to provide high voltage in the output. It avoids many drawbacks of the other DC/DC converters like the low voltage stress applied on capacitors and the continuous input current. The converter is used for supplying DC loads or it is cascaded by a Voltage Source Inverter (VSI) to fed AC loads. In recent researches, the quasi Z-source is investigated and developed by adding extra blocks to eliminate the leak of the limited output ratio without any supplementary voltage stress that will be applied on capacitors such as in [17]. Furthermore, this converter is widely used on PV systems and especially for grid-tied PV systems under the name of Quasi Z-source Inverter such as in [18].

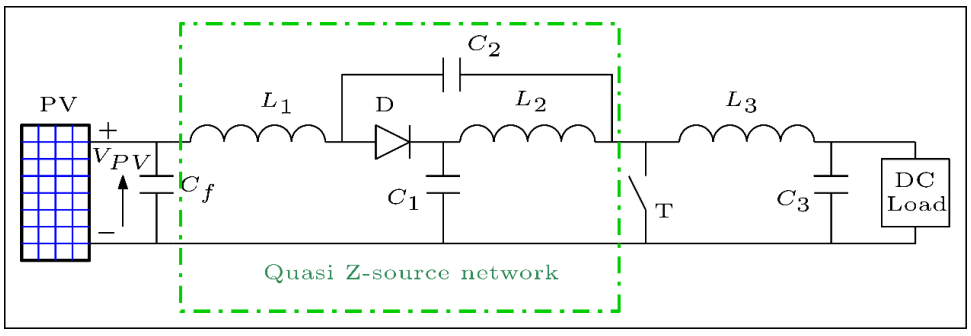

Figure I.8: The Quasi Z-source Converter.

A comparative abstract of the presented converters is summarized in Table I.1.

Table I.1: Characteristics comparison of the presented converters [12-17].

	Conventional Boost Converter	**Interleaved Boost Converter**	**Quadratic Boost Converter**	**Multilevel Boost Converter (N = 2)**	**Fly-back Boost Converter**	**Quasi Z-source Boost Converter**
Required Components Number	5	8	8	8	5	9
Expected implementation Cost	Very low	Moderate	Low	Moderate	High	Moderate
Voltage Conversion ratio V_O	$\frac{1}{1-D}V_{in}$	$\frac{1}{1-D}V_{in}$	$\frac{1}{(1-D)^2}V_{in}$	$n\frac{1+D}{1-D}V_{in}$	$\frac{N_S}{N_P}.\frac{D}{1-D}V_{in}$	$\frac{1}{1-2D}V_{in}$ With $D_{max} \leq 0.5$

I.2.1.2. DC/AC converters in stand-alone PV systems

To supply AC loads in Stand-alone PV systems, second adaptation stages are used, which are DC/AC converters. These inversion stages are used to convert the DC voltage and current into AC voltage and current with the desired values and frequency. From these converters, we will investigate the single-phase and the three-phase two-level inverters.

- **H-bridge two levels inverter**

The single-phase inverter is depicted by Fig.I.9. It is used in Stand-alone PV systems to ensure the inversion of the produced PV power in order to supply AC loads. The waveforms of the inverter output can be in the forms of semi-square or square-wave types. These voltage types are adequate for low or medium power applications, but for high power applications, the sine-wave form is highly requested [19].

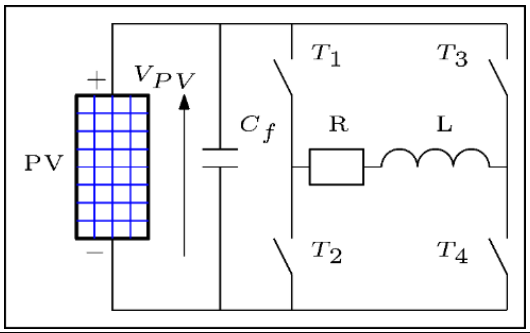

Figure I.9: Single-phase H-bridge inverter.

- **Three-phase voltage source inverter**

The three-phase VSI is illustrated by Fig.I.10. It is able to provide AC voltage with different magnitudes and frequencies according to the load need. It consists of six power switches that can be IGBTs or MOSFETs used for high-power and low frequency or medium-power and high frequency respectively and respect to the application specifications.

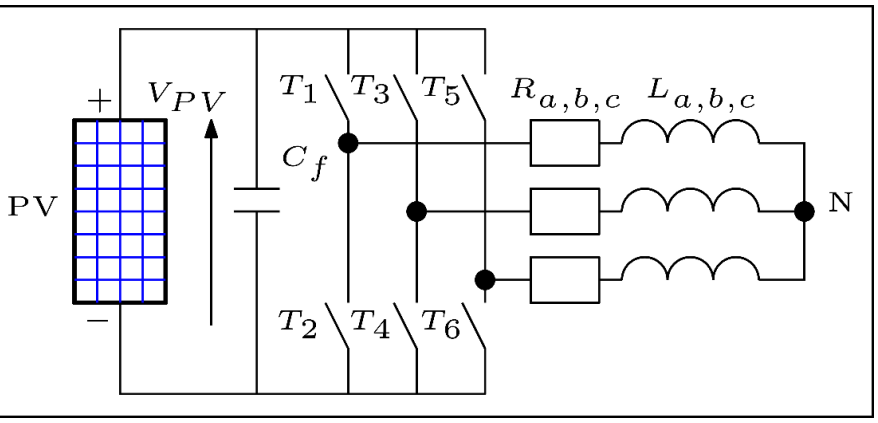

Figure I.10: Three-phase voltage source inverter.

I.2.2. Grid connected PV systems

Grid-connected PV systems are designed to ensure energy sharing between customers and the utility grid, as well as to operate in parallel with other kinds of energies in DERs. These grid-tied PV systems gain popularity in industries and academia as of means they able to generate green and available energy with the desired specifications as long as they based on advanced power electronic interfaces. For Grid PV system configurations, four kinds can be defined as (a) string inverter architecture, (b) module inverter architecture, (c) central inverter architecture, (d) multi-string inverter architecture, where Fig.I.11-(a, b, c, d) represents these configurations.

Fig.I.11.a presents the string inverter architecture for single-phase grid injection, which is developed for a low range PV power (less than 5 KW) [20]. This structure proved that its efficiency is better when compared to the other structures of single-phase injection because it uses an MPPT algorithm for each PV string inverter in an individual way that allows the extraction of the maximum of power from each side in the PV system [20]. Fig.I.11.b presents the module inverter architecture for single-phase grid injection; this structure uses the PV panel and the inverter as a single module, which leads to a simple MPPT control. The high cost of

this structure in using many power converters allows to medium efficiency with some drawbacks [21]. In addition, approximately there are ten years of difference between the lifetimes of the module components that making the system inefficient and very expensive [22-23].

Fig.I.11.c presents the central inverter architecture, which is used for high PV power plants for three-phase grid connection. This structure uses a central inverter for a high number of panels connected in series and parallel. The cost of this architecture is low because it uses fewer power converters and a software MPPT integrated into the control of the central inverter. The efficiency of this structure is moderated due to the panel losses, which makes it an unreliable one [20].

Fig.I.11.d depicts the multi-string inverter architecture, which is the preferred one for high PV power systems in three-phase grid connection. This structure combines the module inverter and the string inverter architectures; it uses a DC/DC converter for each quantity of panels connected in series [24]. It uses an MPPT control for each DC/DC converter making the system more efficient and more reliable. The structure connects each DC side of the system in a centralized DC bus then cascaded to a three-phase grid inverter. This connection is known as the double stage system, where each stage is controlled separately, and thus limiting the efficiency of the global system. For that, recent focus searches are based on the optimization of the control system by controlling the whole system at the same time in a simultaneous way.

These inverter topologies provide AC power with acceptable quality, moderated efficiency, and they work with medium/high switching frequencies. To overcome some practical drawbacks, researchers have suggested two solutions, advanced inverter control methods such as in [25], or efficient topologies of multi-level converters (MLIs) [26]. The proposed solutions take part of enhancing the quality of the output power, decreasing the stress applied on system components and increasing the efficacy of the system.

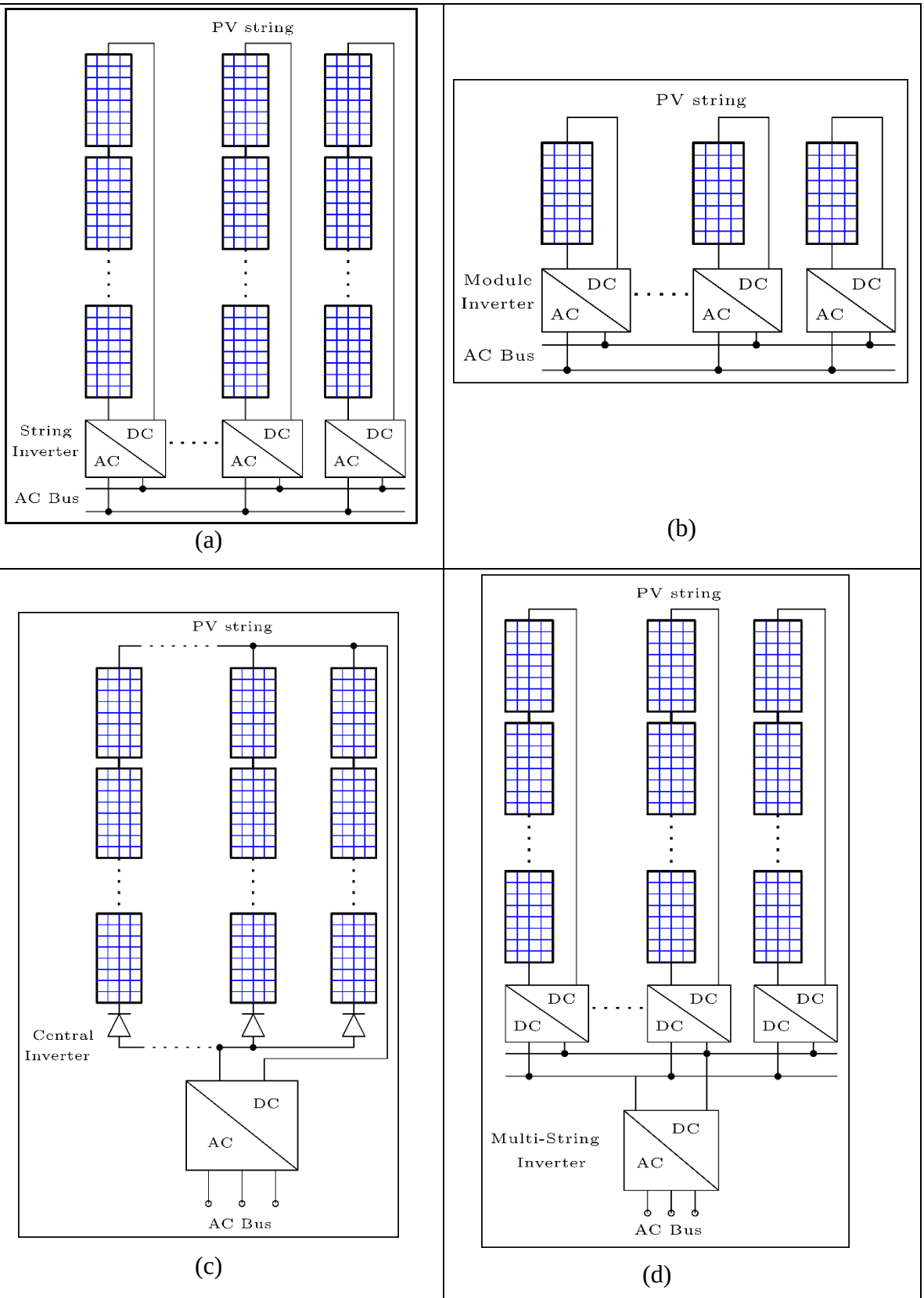

Figure I.11: (a) The string inverter architecture, (b) The module inverter architecture, (c) The central inverter architecture, (d) The multi-string inverter architecture.

I.2.2.1. Multilevel inverter topologies for grid-tied PV systems

The Multilevel inverter (MLI) topology uses several connected converters instead of one power converter, and it has a series of semiconductor power devices that can generate AC power for high-power applications. The topology gains more attention than the conventional two-level one due to the high-voltage operation capability providing high power quality with low switching frequency. It minimizes switching losses and increases the efficacy of the system [26]. We can cite below the attractive features of MLIs:

- They provide output voltage with low distortion and fewer oscillations.
- They generate a negligible value of Common Mode Voltage (CMV).
- They operate with low switching frequency and power losses.
- They improve the electromagnetic interference (EMI).

In the previous decades, the conventional MLIs given in Fig.I.12 are highly merged in PV systems, and they become a part of solutions in improving the PV system's functioning and efficacy.

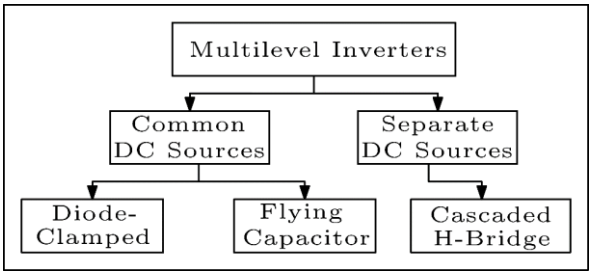

Figure I.12: Classification of the classical MLIs [26-27].

- **Cascaded H-bridge MLI**

This topology is a connection of several single-phase H-bridge inverters shown by Fig.I.9 with separate DC sources as mentioned in [27], each connected H-bridge called a ‘’cell’’. The separate DC sources can be a PV panels cascaded to DC/DC converters to ensure the MPPT functioning and high output efficiency such as in [28-29]. The Cascaded H-Bridge CHB-MLI requires less components compared to the other classical MLIs because it does not use the clamping diodes or flying capacitors [27].

▪ Flying capacitor MLI

The Flying Capacitor FC-MLI is a topology that uses flying capacitors, by means the capacitors are not directly related to the positive or negative DC sides, they are floating. The magnitude of the output voltage is subject to the variation of the voltage in the adjacent capacitors [27]. Fig.I.13 shows a leg of three-level FC-MLI. This structure suffers the drawbacks of unbalanced capacitors voltages as well as the clamping diode MLI.

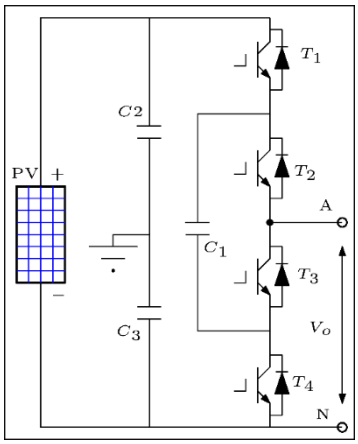

Figure I.13: A leg of three-level FC-MLI.

▪ Clamping diode MLI

The Clamping Diodes CD-MLI is a topology that does not use any flying capacitors. Instead, it uses clamping diodes, where diodes are connected in series in order to share the blocking voltage. This structure is also known as Neutral Point Clamped Inverter (NPC). A leg of three-level NPC inverter is shown by Fig.I.14.

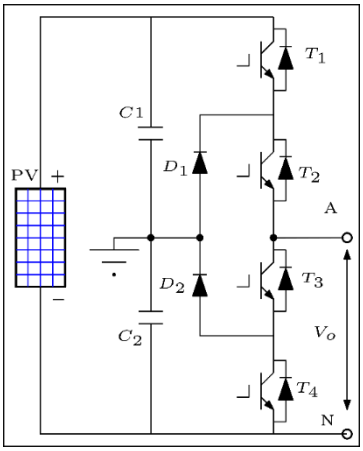

Figure I.14: A leg of three-level NPC inverter.

I.2.2.2. Advanced multilevel inverters for grid-tied PV systems

Over the past decades, MLIs were solutions of many hindrances of power quality. The classical MLIs mentioned above are gaining more and more attention from industry and academia especially in the field of grid-tied PV systems. Each topology presents some benefits and drawbacks where a given one can be suitable in some cases and totally not adapted in others. For that, researchers continue to develop new structures with the application-oriented approach.

In [30], a modified single-phase voltage source MLI is presented for photovoltaic application. The structure uses a combination of both unidirectional and bidirectional switches and separate sources required for PV solar panels. In [31], a modified FC-MLI is presented which uses a specific modulation to maintain the capacitor's voltage balance. In addition, a topology that combines the benefits of the FC and NPC MLIs to generate multilevel output voltage is presented in [32], it is called the active neutral point clamped (ANPC).

There are an uncounted published research papers in the context of developing new topologies and increasing the output voltage levels. For PV application, we can present an interesting structure that is the T-Type inverter.

- **Three-level T-type NPC**

The T-type NPC is a recent topology that is gaining attention in PV system application [33]; it is widely commercialized because of its interesting structure. The SEMIKRON Company developed this type of inverters, which is compared to the classical one [34]. Fig.I.15 shows a leg of three-level T-type inverter, this structure gives benefits over the NPC one in terms of output voltage waveforms while there are no restrictions to the switching schemes as in three-level NPC and especially in emergency shut-down [34].

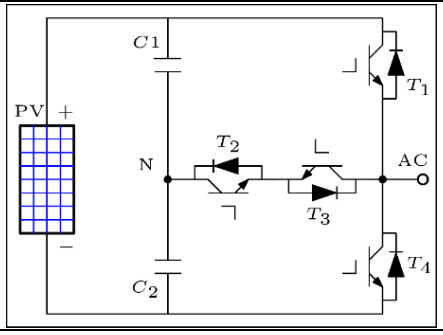

Figure I.15: A leg of three-level T-NPC inverter.

I.3.PV systems control strategies

The PV system is generally consists of two stages, the DC/DC boosting stage and the alternative stage using a single or three phase inverter, and each side needs a specified control technique to well ensure the functioning of the PV conversion chain. The control of PV systems is subdivided into:

- The control of DC/DC converter to ensure the MPPT functioning and the output voltage boosting.
- The DC link voltage regulation.
- The phase locked loop (PLL).
- The DC/AC inverter control.

I.3.1. MPPT functioning

The MPPT is an indispensable part from the control of the DC/DC converter in PV systems; it leads to the extraction of the maximum available power form PV panels whatever the climatic conditions. There are efficient classical methods that proved high performances via the published papers and in commercial systems. We investigate below the most used methods.

- **Perturb and Observe algorithm (P&O)**

The P&O is one of the commonly used techniques due to its simplicity of implementation and efficacy. Its principle is based on the perturbation of the PV voltage by adding or subtracting a small voltage step, and observing the behavior of the output power. This technique is used in [35]. The major drawback of the method is that the used fixed step affect the rapidity of the algorithm by decreasing the efficiency of the system (the system still oscillating around the MPP). For that reason, many research are made in the context of improving the performance of the algorithm by using a variable step size such as in [36].

- **Incremental of Conductance algorithm (Inc-Cond)**

The Inc-Cond MPPT algorithm is proposed in view to enhance the behavior of the P&O and to avoid its drawbacks. This technique is the recent and efficient one between the classical MPPT algorithms. Its principle is based on the perturbation of the voltage, then the current, and observation of the incremental conductance if it is equal to the instantaneous one in order to reach the MPP [37]. The method is subject to several modifications to eliminate its drawbacks

and to enhance the efficiency of the system such as in [38]. In addition, this algorithm is combined with several advanced method to create hybrid MPPT, such as, the fuzzy logic controller, the artificial intelligence controller, and model predictive control [39].

- **Model predictive control based MPPT algorithm**

Model predictive control (MPC) is an advanced control technique well suited for power converters. It takes in consideration the discrete time model of the system and the possible switching states of the converter to make an optimal control decision. MPC is widely applied in PV systems as an MPPT control technique thanks to its flexibility and robustness. In [39], the MPC is combined with the Inc-Cond MPPT algorithm to make a hybrid one. The method is based on the use of the reference current generated by the classical Inc-cond and the predicted current of the MPC, and then a minimization process is done to apply the optimal action to the DC/DC converter. This hybrid algorithm proved better performance over the classical methods. A dual-discrete MPC based MPPT is proposed in [40], this technique is proposed to overcome the problem of the confusion during fast changes of the irradiance known in the classical methods. The MPC-MPPT based on the Inc-Cond is used in this dissertation, where the current and voltage errors are taken as predicted values.

I.3.2. Inverter control

The control strategy of the inverters has a crucial role in improving the DC/AC power converter performance and increasing the efficiency of the system making it more reliable.

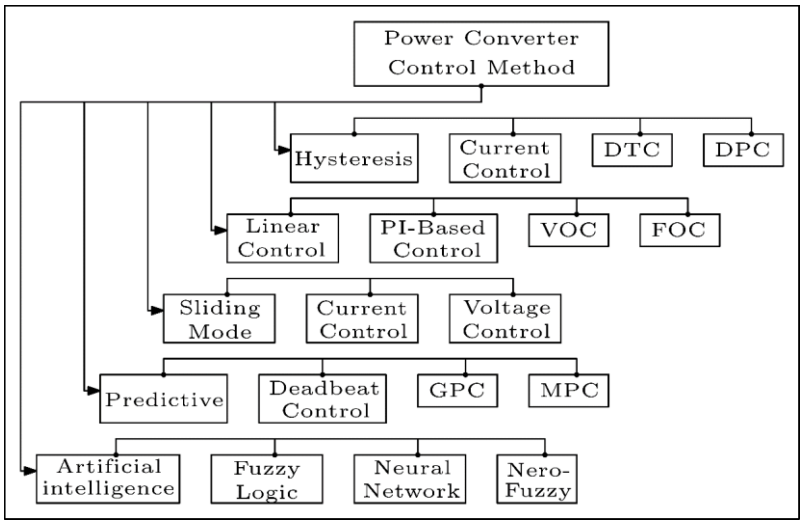

Figure I.16: Control methods of power converters and drives [41].

In literature, several power converter control methods are investigated and developed. Fig.I.16 summarizes these control technics. The development of fast and powerful microprocessors and microcontrollers has helped the invention and implementation of new advanced control methods, such as sliding mode control, neuro-fuzzy control, and predictive control.

I.3.2.1. Classical control methods

- **Hysteresis**

Considered as the most used modulation technique, its principle is to compare the measured values to their desired values within an hysteresis band, in order to select the switching state. This method has a variable switching frequency, which could be an undesired characteristic in some applications, but it is applied in such application for current control, direct torque control, and direct power control as shown in Fig.I.16 [41].

- **Linear controller**

The PWM modulation needs the proportional integral (PI) controller in order to generate the control signals after comparing a sinewave reference with a carrier saw-tooth signal. In addition, voltage oriented control (VOC) is applied for power converters used in grid-tied systems. For implementation of these linear controllers in digital platforms such as DSPs and dSpaces, a sampled data process is required using an approximation of the continuous time model of the system [41]. To achieve acceptable performances, it is recommended to respect the design steps and considerations imposed by the linear controllers. In fact, these controllers suffer from the incapability to consider and include constraints, for that reason, predictive control is highly preferred over linear controllers due to the simple inclusion of the constraints.

I.3.2.2. Advanced methods based on predictive control

Nowadays, finite set model predictive control is well known as the preferred control technique for power electronic converters due to the limited switching states of the power converter. Moreover, MPC is a numerical method that is well suited for direct implementation on digital platforms such as model knowledge based and discrete time implementation [41].

Since the appearance of the MPC control methods, in the seventies, many methods have merged, developed, and can be divided nowadays into several predictive control methods, where Fig.I.17 describes the main technics.

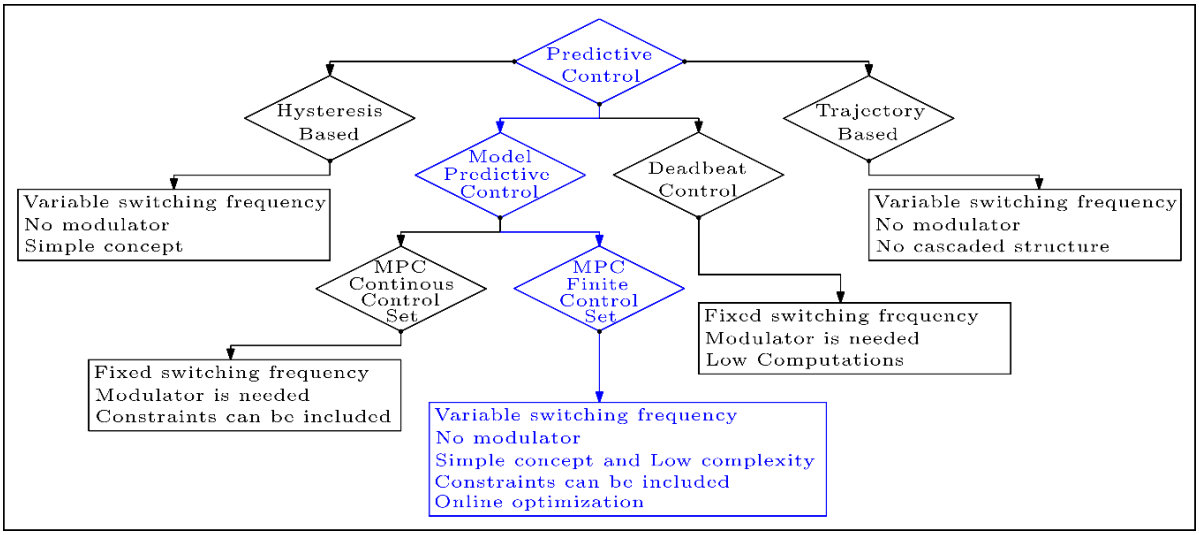

Figure I.17: The main predictive control methods.

The hysteresis-based predictive control is developed in [42]; the technique is based on the so-called bang-bang control, which has the same characteristics as the predictive control such as the variable switching frequency without modulation stage. This method determines the optimal control action by keeping the desired control variable in the hysteresis area, and then the control signal is directly applied with a variable switching frequency as in the trajectory-based control [42]. In this last, the control variables are forced to track the pre-defined trajectories, where the method is applied as a direct self-controller (DSC), and the algorithm is well investigated in [43].

The deadbeat control is the predictive control method that reduces the error down to zero, then the control actions is applied using a modulator. This technique is widely used in the control of power converters such as predictive current control in [44].

As it is illustrated in Fig.I.17, the model predictive control is subdivided into continuous control set and finite control set, and the main difference between them that the first one has a fixed switching frequency using a modulator before the control of the converter. This method proved the best performance compared to linear controllers, deadbeat-based control, or trajectory-based control, but the need for the modulator is a constraint that makes the method in need of fast control platform.

The focus of this dissertation is the finite set model predictive control; this method is the simple and best one in predictive control. Its concept is based on the predicted model of the system and the finite numbers of the converter switching states and then an online optimization process is running before sending the optimal actions to the converter. The method is applied without the need of the modulator, and it has a variable switching frequency. In this dissertation, an optimal control set is proposed based on the cascaded control of the converters using in PV systems. The system is treated as one converter and the predicted models of the converters are used in the algorithm, then a single online optimization process is running for the whole system and the optimal switching states are applied.

I.4. Conclusion

The power converter interfaces are the essential element in the DERs and the control of these interface play a key role in improving the performance of the system, where it directly affect the system reliability and efficacy. For that, we investigate in this chapter the most used power converters in the interface devices, and their control technics. From this investigation, we can conclude that the FS-MPC is the most efficient technic destined to stand-alone and grid connected systems, and it is the primary objective of this dissertation.

In the following chapters, we will investigate the application of the FS-MPC on PV systems, and we will propose an optimal predictive control based on the use of a predictive emulator to well illustrate the correctness and the effectiveness of the proposed algorithms.

I.5. References

[1] « IEA – International Energy Agency ». https://www.iea.org/ (consulté le mai 01, 2021).

[2] J. Zeng, W. Lin, D. Cen, et J. Liu, « Novel K-Type Multilevel Inverter With Reduced Components and Self-Balance », *IEEE J. Emerg. Sel. Topics Power Electron.*, vol. 8, nº 4, p. 4343‑4354, déc. 2020, doi: 10.1109/JESTPE.2019.2939562.

[3] S. Maurya, D. Mishra, K. Singh, A. K. Mishra, et Y. Pandey, « An Efficient Technique to reduce Total Harmonics Distortion in Cascaded H- Bridge Multilevel Inverter », in *2019 IEEE International Conference on Electrical, Computer and Communication Technologies (ICECCT)*, Coimbatore, India, févr. 2019, p. 1‑5, doi: 10.1109/ICECCT.2019.8869424.

[4] E. Z. Bighash, S. M. Sadeghzadeh, E. Ebrahimzadeh, Y. Yang, et F. Blaabjerg, « A novel model predictive control for single-phase grid-connected photovoltaic inverters », in *2017 IEEE Energy*

Conversion Congress and Exposition (ECCE), Cincinnati, OH, oct. 2017, p. 461‑467, doi: 10.1109/ECCE.2017.8095819.

[5] M. Azab, « A finite control set model predictive control scheme for single-phase grid-connected inverters », *Renewable and Sustainable Energy Reviews*, vol. 135, p. 110131, janv. 2021, doi: 10.1016/j.rser.2020.110131.

[6] R. E. Perez-Guzmen, M. Rivera, J. A. Riveros, F. Herrera, et P. W. Wheeler, « Model Predictive Control Applied to the Three-Phase Neutral Point Clamped Inverter », in *2020 IEEE International Conference on Industrial Technology (ICIT)*, Buenos Aires, Argentina, févr. 2020, p. 493‑498, doi: 10.1109/ICIT45562.2020.9067298.

[7] T. Hausberger, A. Kugi, A. Eder, et W. Kemmetmüller, « High-speed nonlinear model predictive control of an interleaved switching DC/DC-converter », *Control Engineering Practice*, vol. 103, p. 104576, oct. 2020, doi: 10.1016/j.conengprac.2020.104576.

[8] A. Bakeer, M. A. Ismeil, A. Kouzou, et M. Orabi, « Development of MPC algorithm for quasi Z-source inverter (qZSI) », in *2015 3rd International Conference on Control, Engineering & Information Technology (CEIT)*, Tlemcen, Algeria, mai 2015, p. 1‑6, doi: 10.1109/CEIT.2015.7233135.

[9] D. Shen, C.-C. Lim, et P. Shi, « Robust fuzzy model predictive control for energy management systems in fuel cell vehicles », *Control Engineering Practice*, vol. 98, p. 104364, mai 2020, doi: 10.1016/j.conengprac.2020.104364.

[10] S. Yu, D. Lin, Z. Sun, et D. He, « Efficient model predictive control for REAL-TIME energy optimization of BATTERY-SUPERCAPACITORS in electric vehicles », *Int J Energy Res*, vol. 44, nº 9, p. 7495‑7506, juill. 2020, doi: 10.1002/er.5473.

[11] S. C. Bhatia, *Advanced renewable energy systems*. New Delhi: Woodhead, 2014.

[12] S. E. Babaa, G. E. Murr, F. Mohamed, et S. Pamuri, « Overview of Boost Converters for Photovoltaic Systems », *JPEE*, vol. 06, nº 04, p. 16‑31, 2018, doi: 10.4236/jpee.2018.64002.

[13] S. Ozdemir, N. Altin, et I. Sefa, « Fuzzy logic based MPPT controller for high conversion ratio quadratic boost converter », *International Journal of Hydrogen Energy*, vol. 42, nº 28, p. 17748‑17759, juill. 2017, doi: 10.1016/j.ijhydene.2017.02.191.

[14] S. El Islam Remache et K. Barra, « Performance comparison among boost and multi level boost converters for photovoltaic grid connected system using finite set model predictive control », in *2018 9th International Renewable Energy Congress (IREC)*, Hammamet, mars 2018, p. 1‑6, doi: 10.1109/IREC.2018.8362483.

[15] M. Shadmand, R. S. Balog, et H. Abu Rub, « Maximum Power Point Tracking using Model Predictive Control of a flyback converter for photovoltaic applications », in *2014 Power and Energy*

Conference at Illinois (PECI), Champaign, IL, USA, févr. 2014, p. 1‑5, doi: 10.1109/PECI.2014.6804540.

[16] S. Arab Ansari et J. Shokrollahi Moghani, « Soft switching flyback inverter for photovoltaic AC module applications », *IET Renewable Power Generation*, vol. 13, nº 13, p. 2347‑2355, oct. 2019, doi: 10.1049/iet-rpg.2019.0365.

[17] M. M. Haji-Esmaeili, E. Babaei, et M. Sabahi, « High Step-Up Quasi-Z Source DC–DC Converter », *IEEE Trans. Power Electron.*, vol. 33, nº 12, p. 10563‑10571, déc. 2018, doi: 10.1109/TPEL.2018.2810884.

[18] M. S. Kumar, J. Vishnupriyan, et N. M. Kumar, « Model Predictive Control Strategy-Based Voltage Sensing of Quasi Z-Source Cascaded Multi-Level PV Inverter with Distributed MPPT Algorithm », p. 10, 2020.

[19] L. Ashok Kumar, S. Albert Alexander, et M. Rajendran, « Inverter topologies for solar PV », in *Power Electronic Converters for Solar Photovoltaic Systems*, Elsevier, 2021, p. 1‑39.

[20] M. A. M. Mosa, « Model Predictive Control Technique of Multilevel Inverter for PV Applications », Thesis, 2018.

[21] K. K. Gupta, A. Ranjan, P. Bhatnagar, L. K. Sahu, et S. Jain, « Multilevel Inverter Topologies With Reduced Device Count: A Review », *IEEE Trans. Power Electron.*, vol. 31, nº 1, p. 135‑151, janv. 2016, doi: 10.1109/TPEL.2015.2405012.

[22] Y. Yang, E. Koutroulis, A. Sangwongwanich, et F. Blaabjerg, « Minimizing the levelized cost of energy in single-phase photovoltaic systems with an absolute active power control », in *2015 IEEE Energy Conversion Congress and Exposition (ECCE)*, Montreal, QC, Canada, sept. 2015, p. 28‑34, doi: 10.1109/ECCE.2015.7309665.

[23] A. Sangwongwanich, Y. Yang, D. Sera, et F. Blaabjerg, « Lifetime Evaluation of Grid-Connected PV Inverters Considering Panel Degradation Rates and Installation Sites », *IEEE Trans. Power Electron.*, vol. 33, nº 2, p. 1225‑1236, févr. 2018, doi: 10.1109/TPEL.2017.2678169.

[24] G. Bettenwort, R. Juchem, M. Victor, et T. Müller, « Method for activating a multi-string inverter for photovoltaic plants », US8212409B2, juill. 03, 2012.

[25] J. Seuss, M. J. Reno, M. Lave, R. J. Broderick, et S. Grijalva, « Advanced inverter controls to dispatch distributed PV systems », in *2016 IEEE 43rd Photovoltaic Specialists Conference (PVSC)*, Portland, OR, USA, juin 2016, p. 1387‑1392, doi: 10.1109/PVSC.2016.7749842.

[26] L. Ashok Kumar, S. Albert Alexander, et M. Rajendran, « Multilevel inverter topologies for solar PV », in *Power Electronic Converters for Solar Photovoltaic Systems*, Elsevier, 2021, p. 41‑109.

[27] A. Bughneda, M. Salem, A. Richelli, D. Ishak, et S. Alatai, « Review of Multilevel Inverters for PV Energy System Applications », *Energies*, vol. 14, nº 6, p. 1585, mars 2021, doi: 10.3390/en14061585.

[28] S. Jain et V. Sonti, « A Highly Efficient and Reliable Inverter Configuration Based Cascaded Multilevel Inverter for PV Systems », *IEEE Trans. Ind. Electron.*, vol. 64, nº 4, p. 2865‑2875, avr. 2017, doi: 10.1109/TIE.2016.2633537.

[29] B. Xiao, L. Hang, J. Mei, C. Riley, L. M. Tolbert, et B. Ozpineci, « Modular Cascaded H-Bridge Multilevel PV Inverter With Distributed MPPT for Grid-Connected Applications », *IEEE Trans. on Ind. Applicat.*, vol. 51, nº 2, p. 1722‑1731, mars 2015, doi: 10.1109/TIA.2014.2354396.

[30] V. G. Agelidis, D. M. Baker, W. B. Lawrance, et C. V. Nayar, « A multilevel PWM inverter topology for photovoltaic applications », in *ISIE '97 Proceeding of the IEEE International Symposium on Industrial Electronics*, Guimaraes, Portugal, 1997, vol. 2, p. 589‑594, doi: 10.1109/ISIE.1997.649027.

[31] V. Dargahi, A. K. Sadigh, M. Abarzadeh, S. Eskandari, et K. A. Corzine, « A New Family of Modular Multilevel Converter Based on Modified Flying-Capacitor Multicell Converters », *IEEE Trans. Power Electron.*, vol. 30, nº 1, p. 138‑147, janv. 2015, doi: 10.1109/TPEL.2014.2304964.

[32] M. Abarzadeh et K. Al-Haddad, « An Improved Active-Neutral-Point-Clamped Converter With New Modulation Method for Ground Power Unit Application », *IEEE Trans. Ind. Electron.*, vol. 66, nº 1, p. 203‑214, janv. 2019, doi: 10.1109/TIE.2018.2826484.

[33] S. S. Lee, Y. Yang, et K.-B. Lee, « A Five-Level Common-Ground-T-Type Inverter for Solar Photovoltaic Applications », in *IECON 2020 The 46th Annual Conference of the IEEE Industrial Electronics Society*, Singapore, Singapore, oct. 2020, p. 1160‑1164, doi: 10.1109/IECON43393.2020.9255097.

[34] I. Staudt, « Application Note », p. 12.

[35] M. I. Munir, T. Aldhanhani, et K. H. Al Hosani, « Control of Grid Connected PV Array Using P&O MPPT Algorithm », in *2017 Ninth Annual IEEE Green Technologies Conference (GreenTech)*, Denver, CO, USA, mars 2017, p. 52‑58, doi: 10.1109/GreenTech.2017.14.

[36] A. Harrag et S. Messalti, « Variable step size modified P&O MPPT algorithm using GA-based hybrid offline/online PID controller », *Renewable and Sustainable Energy Reviews*, vol. 49, p. 1247‑1260, sept. 2015, doi: 10.1016/j.rser.2015.05.003.

[37] P. K. Vineeth Kumar et K. Manjunath, « Analysis, design and implementation for control of non-inverted zeta converter using incremental conductance MPPT algorithm for SPV applications », in *2017*

International Conference on Inventive Systems and Control (ICISC), Coimbatore, India, janv. 2017, p. 1‑5, doi: 10.1109/ICISC.2017.8068662.

[38] Kok Soon Tey et S. Mekhilef, « Modified Incremental Conductance Algorithm for Photovoltaic System Under Partial Shading Conditions and Load Variation », *IEEE Trans. Ind. Electron.*, vol. 61, nº 10, p. 5384‑5392, oct. 2014, doi: 10.1109/TIE.2014.2304921.

[39] H. Wang et O. Abdel-Rahim, « A New High Gain DC-DC Converter With Model-Predictive-Control Based MPPT Technique for Photovoltaic Systems », *CPSS TPEA*, vol. 5, nº 2, p. 191‑200, juin 2020, doi: 10.24295/CPSSTPEA.2020.00016.

[40] A. Lashab, D. Sera, et J. M. Guerrero, « A Dual-Discrete Model Predictive Control-Based MPPT for PV Systems », *IEEE Trans. Power Electron.*, vol. 34, nº 10, p. 9686‑9697, oct. 2019, doi: 10.1109/TPEL.2019.2892809.

[41] S. B. Mohammad, « Model Predictive Control techniques with application to photovoltaic, DC Microgrid, and a multi-sourced hybrid energy system », Ph. D. Dissertation, Texas A&M University, 2015.

[42] P. Eichenberger et M. Junger, « Predictive vector control of the stator voltages for an induction machine drive with current source inverter », in *PESC97. Record 28th Annual IEEE Power Electronics Specialists Conference. Formerly Power Conditioning Specialists Conference 1970-71. Power Processing and Electronic Specialists Conference 1972*, St. Louis, MO, USA, 1997, vol. 2, p. 1295‑1301. doi: 10.1109/PESC.1997.616936.

[43] M. Depenbrock, « Direct self-control (DSC) of inverter-fed induction machine », *IEEE Trans. Power Electron.*, vol. 3, nº 4, p. 420‑429, oct. 1988, doi: 10.1109/63.17963.

[44] S. Saggini, W. Stefanutti, E. Tedeschi, et P. Mattavelli, « Digital Deadbeat Control Tuning for dc-dc Converters Using Error Correlation », *IEEE Trans. Power Electron.*, vol. 22, nº 4, p. 1566‑1570, juill. 2007, doi: 10.1109/TPEL.2007.902262.

Chapter II

Finite Set Model Predictive Control Applied To Photovoltaic Systems

II. Finite set model predictive control applied to photovoltaic systems

II.1. Introduction

In the late seventies, researchers proposed Model Predictive Control (MPC) as a powerful control strategy and a paradigm of an extensive range of control methods. Based on the predictive process model, it gives optimal control signals by minimizing an objective function. Since then, the MPC was developed appreciably in several domains by applying different algorithms on diverse applications from the process industry such as drying towers and cement industry going to robots [1] and clinical anesthesia [2]. From these applications, MPC proved high performance over linear controllers by achieving excellent and efficient control systems by working a long time without any intervention [3]. Therefore, many advantages of MPC cited in [3]; among them, it has a straightforward concept; it can be adapted to a large variety of processes even with multivariable cases. In addition, it is easy to implement, and it will be more efficient when future reference is defined before. Whereas, the disadvantage of the MPC is the significant computational burden caused by the weak calculators and microprocessors that existed previously.

During the eighties, MPC became an attractive solution for processes control and particularly for chemical domain due to the simplicity of the algorithm and the no need for powerful calculators, where several MPC applications in the petrochemical sector were summarized in [4]. In the late eighties, Clarke et al developed the Generalized Predictive Control (GPC) [5] that appears with the context of adaptive control using mono-variable processes (Input-Output Model) [6] and Extended Horizon Adaptive Control (EHAC) [7]. In addition, GPC tried to provide the next output more closely to the reference without solving a Diophantine equation but by using a suboptimal predictor [8]. Therefore, GPC became a contender for general self-tuning applications [3]. MPC has been extended to treat complex tasks by formulating their generalization in the state-space model, where it became able to solve nonlinear processes, stochastic disturbance considerations of the systems and multivariable cases [9]. By giving this flexibility to the GPC, many scientific research papers were proved on system stability and robustness improvement that were appeared in the nineties, where they worked on how to stabilize the process before the objective function minimization [3].

Actually, with the integration of MPC in several domains and industry processes, researchers proved that it could be a control for power electronic converters [10]. Thanks to the fast development of calculators and microprocessors in the last three decades, where MPC can be easily implemented in the standard hardware that exists lastly [11]. MPC had become a desirable solution for control tasks of power converters that need a quick dynamic response (tens to hundreds of microseconds) due to the high performances of the electronic switches. Consequently, MPC is the first control technique that dominates the literature of power converters and electrical drives controls and especially in the last decade [11].

Recently, there are many published papers that summarize the contributions of the MPC applied to four main categories of applications for power electronic converters that can be found in the IEEE explorer in the range of years (from 2007 to 2012) [12]. This helpful statistical study comprises a variety of applications such as Inverters with RL output load (In_RL), Grid-connected converters (GCC), Electric drives (ED) and Inverters with output LC filters (In_LC). When taping the keywords "predictive" and "power converters" in the search rubric of the IEEE platform, it gives more than 200 papers between journals and conferences of the four applications mentioned above, where GCC and ED got from researches more attention than In_LC or In_RL. This means that they found the MPC is a well-suited control for GCC and ED systems [12].

Nowadays, photovoltaic energy applications using MPC have been penetrating Distributed Energy Resources (DER). When sometimes it became the primary source of energy in the system due to the enormous demands of customers like buildings, electrical vehicle chargers, public lighting or factories [13-14]. Two reasons may cause this; the first is for increasing the efficiency of photovoltaic panels, unlike their costs, which have decreased in recent years compared to before, where the second is for the simplicity of the MPC algorithm applied to this kind of processes. For that, an analytical study is done by searching for the published conferences and journal papers in the range of years from 2007 to 2018 in IEEE explore platform when taping the words " model predictive control" and "photovoltaic". This analysis is performed explicitly for two kinds of categories: Grid Connected System with AC Micro Grids (Pv_GCS & AC-MGs) and Standalone System with islanded Micro Grids (Pv_SAS & DC-Mgs). The search gives more than 300 published papers for the studied classes, and there are two figures set to accompany this study. Fig.II.1 provides information about the distribution regarding applications and year of publication, where it is easy to see that the researchers have

given attention to (Pv_GCS & AC-MGs) more than (Pv_SAS & DC-MGs). Fig.II.2 shows a cumulative analysis for each application category, where it can be seen that for the two studied groups, the increasing trends are positive and the published papers have increased in a quasi-exponential way.

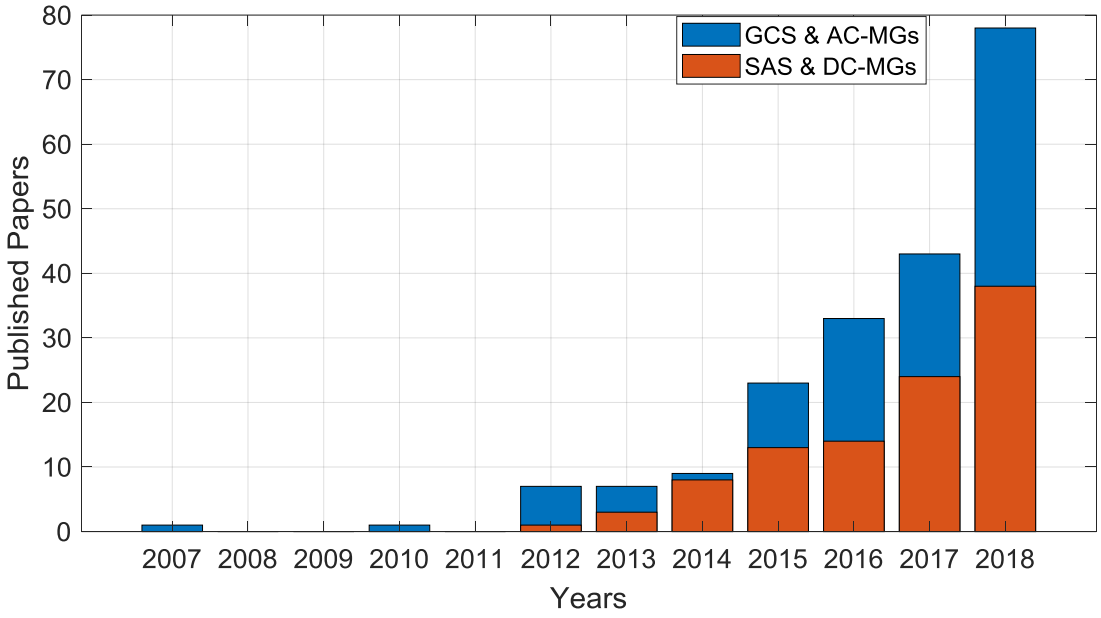

Figure II.1: Research papers of MPC for photovoltaic systems published in IEEE conferences and journals from 2007 to 2018: distribution regarding applications and year of publication.

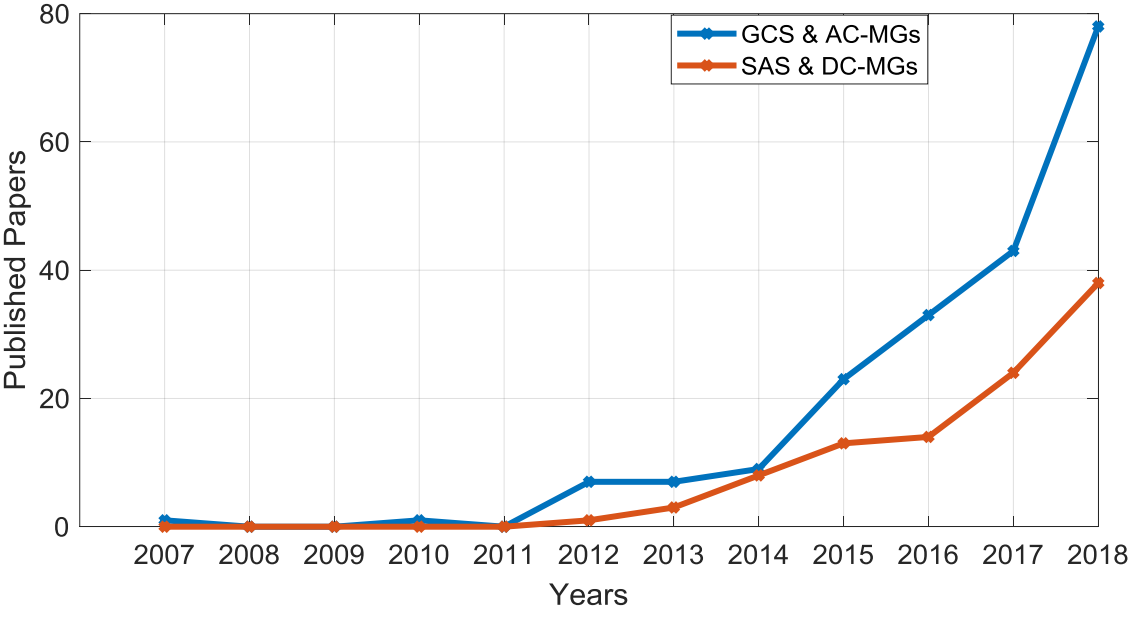

Figure II.2: Research papers of MPC for photovoltaic systems published in IEEE conferences and journals from 2007 to 2018: cumulative analysis for each application category.

II.2. Basic principle of model predictive control

The reason that led MPC to achieve considerable interest of researchers is the simplicity of their algorithms, which have applied in several applications and industrial processes. MPC appeared under various names such as moving horizon control, dynamic matrix control, model algorithmic control, rolling horizon planning, dynamic linear programming, and generalized predictive control [15]. These techniques have been grouped in the same idea of control or the same operating principle, where they all have the ability to make predictions of the variables (until a predefined horizon in time) that influence the system behavior, and take optimal control actions after minimization of the objective function [16]. This underlying idea has several advantages cited in [17], among them:

- It has a straightforward principle and easy to implement.
- It is suitable for a large variety of processes.
- It can treat multivariable cases also nonlinear systems.
- It has the ability to compensate dead time.
- Constraints can be treated easily.

Therefore, as all control techniques, the MPC has also some disadvantages, where the more frequent are:

- It needs a large computational burden, unlike linear controllers.
- It directly based on the system model and that is not suitable when the system parameters change in time. Therefore, estimation algorithms have to integrate with MPC to be a more robust one.

In a discrete-time domain, MPC allows the variables of a system to change their values in each sampling interval, and it can observe the future behavior of the system based on predictions of their dominant variables. The basic principle of the MPC can be summarized in Fig.II.3, where x^* is a reference, which has a value in time k and that to be achieved by the variable x until a predefined horizon in time $k+N$. In each sampling time, MPC predicts the error between x^* and x and try to minimize it to offer excellent control to the system and makes it more robust [15]. The following points demonstrate well the working principle of the MPC:

➢ Model discretization and prediction

To obtain the best control with MPC, a specific discrete model of the system is needed which is obtained from an exact continuous-time model of the system. The passage from continuous-time domain to discrete one is often based on discrete mathematics or discretization methods [15].

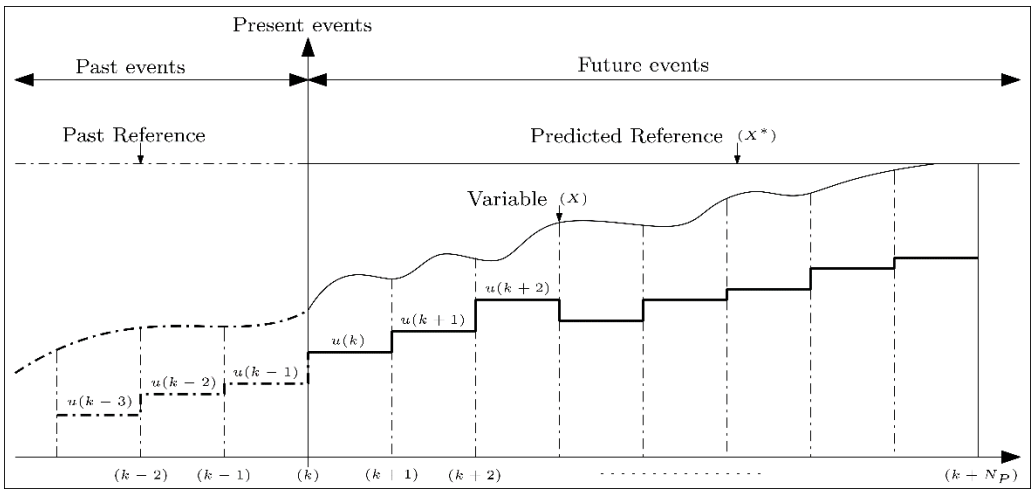

Figure II.3: Operating principle of MPC (N_p = Prediction horizon) [15].

As an example, the continuous-time model of a power conversion system given by (II.1):

$$\frac{dx(t)}{dt} = \dot{x}(t) = Ax(t) + Bu(t) \qquad (II.1)$$

Where, A and B are the parameters of the converter in a continuous time equation. $x(t)$ is the state of vector to be controlled and $u(t)$ is the input vector. This model depends on states of A and B in time, by means, if A and B do not change in time, the system is a Linear Time-Invariant (LTI); else it is a Linear Time-Variant (LTV) system.

For discretization, there are two methods; the first is an exact method using the matrix exponential or, as it is so-called zero-order hold (ZOH), this method is intended for LTV systems. Where the second one is the approximate methods as forward Euler, backward Euler, bilinear transformation and truncated Taylor series, these methods are intended for LTI systems.

The model of the system described by a first order nature of the state equation given by (II.1) and it is considered as a model for a LTI system, for that a discretization could be obtained by Euler forward approximation:

$$\left\{\frac{dx(t)}{dt}\right\}_{t=k} \approx \frac{x(k+1)-x(k)}{T_s} \quad \text{(II.2)}$$

Where, k is the present sample $(k+1)$ is the future sample in one-step ahead, and T_s is the sampling time.

By applying (II.2) into (II.1), a discrete-time model is obtained and (II.3) gives it:

$$\frac{x(k+1)-x(k)}{T_s} = Ax(t) + Bu(t) \quad \text{(II.3)}$$

By simplifying (II.3), we get:

$$x(k+1) = \Phi x(k) + \Upsilon u(k) \quad \text{(II.4)}$$

With,

$$\Phi \approx I + AT_s, \quad \Upsilon \approx BT_s \quad \text{(II.5)}$$

Where, I is a unitary matrix that has the same dimension as the state matrix A.

The discretization methods for MPC of power conversion systems are reported in chapter 7 of [15], where a detailed discussion is given for exact, approximate, and quasi-exact discretization approaches for MPC, along with example problems.

MPC predicts the behavior of the system in horizon of time N_P based on a predictive model as the one given by (II.4) and the measured variables in each sampling interval. Then, an online optimization is done [15].

➢ Optimization process

After predictions of the variables to be controlled, a cost function g(k) is defined based on references, future states, and future actuations. The cost function g(k) is given by:

$$g(k) = f[x^*(k), \dots, x^*(k+N_P), x(k), u(k), \dots, u(k+N_P)] \quad \text{(II.6)}$$

As it is considered that MPC is an optimization task, it consists of a minimization of the defined cost function g(k) given by (II.6), then, the input control sequence that minimizes it will be selected as the optimal actuation to be applied.

$$u^{op}(k) = \arg \underbrace{\min}_{u} g(k) \tag{II.7}$$

➢ Receding horizon strategy

At each sampling interval, the optimization problem is solved again based on the predictive model and new measured variables, and then new optimal actuations are selected. This operation called the receding horizon strategy.

Supposing, the discrete time model given in (II.4), the control objective of the MPC is to minimize the error between x and its reference x^* and to maintain it to zero. This is done by choosing u as a steering variable:

$$\hat{x}^*(k+1) - x(k+1) = 0 \;\rightarrow \underbrace{\hat{x}^*(k+1)}_{\text{Set Point}} - \underbrace{\Phi\, x(k)}_{\text{Feedback}} - \underbrace{\Upsilon\, u(k)}_{\text{Steering}} \tag{II.8}$$

During the sampling interval, the value of $u(k)$ is steered optimally, to keep the state variable at its set-point value, and this is doing despite slight changes in Φ and Υ. This procedure leads MPC to give robustness for the system against parameter uncertainties and modeling errors.

II.3. Finite set model predictive control as a flexible control for power converters

As mentioned previously, MPC appeared in the 1970s, and it was applied for chemical and industrial processes. The fast development of microcontrollers in the last two decades has allowed MPC to integrate with the control of power electronic converters and power conversion systems.

Some published papers that implement MPC for power converters and electrical drives [13-18] appeared with the context of solving the optimization problems analytically by considering the studied systems as linear ones using a modulator without any consideration of constraints, by means using an explicit control law [17]. The explicit MPC treats the optimization problem offline, including the system model and objectives in a look-up table that contains the optimal action as a function of the state of the studied system. However, this method does not take into account the discrete nature of the power converters. For more explication, here some researches that applied the explicit MPC for DC-DC converters and three-phase inverters [17-19].

The Finite Set Model Predictive Control (FS-MPC) proposed mainly to solve the optimization problem for power converters by using their discrete nature and possible switching states. It is able to calculate the optimal actuation based on the evaluation of the behavior of the system with the predicted variables to be controlled and possible switching states of the power converter, and that allows for more flexibility in the control scheme and simplicity in the implementation in real-time. FS-MPC has been widely used in the control of advanced power converters and power conversion systems, including wind and photovoltaic energies [15]. These applications provide several features and challenges that will be analyzed in the next subsection.

II.3.1. Principal features of FS-MPC

FS-MPC got some features from its application to several systems. The main features grouped in Fig.II.4 and presented below [15]:

1. Straightforward concept

Its principle is simple and easy to understand. It uses four subsystems that will be presented in details in the following subsections.

2. Compatible with digital controllers

It takes into consideration the discrete nature of the power converter. It works under the discrete-time domain, and it uses a fixed sampling time. Its algorithm is simple for implementation in simulation and real-time processes without any constraints of time, and that provides flexibility to the system control.

3. Online optimization for a finite number

According to the number of possible switching states $s(k)$ of the power converter (for example $s(k) = 2$ for boost converter, and $s(k) = 8$ for 2L-VSI), the optimization process is simplified and it performs a set of calculations in each sampling period. This makes the implementation of the FS-MPC algorithm possible and simple in real time.

4. Elimination of the modulation stage and linear controllers

FS-MPC can predict the behavior of the controlled variables in a discrete-time domain for all possible switching states of the power converter. A cost function is formulated which needs

online optimization by evaluating all possible combinations of the system variables and possible actuations. After the minimization of the cost function, the optimal sequence is applied to the converter. This nonlinear method provides the best control for power converters without any hysteresis regulators, linear controllers (PI) nor modulation stages.

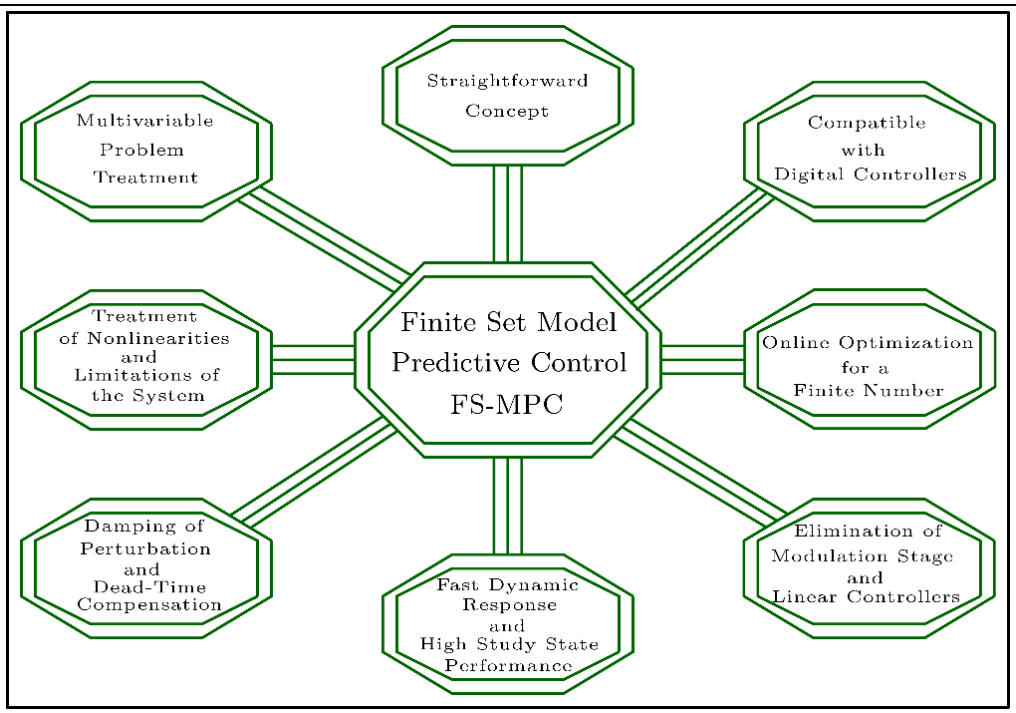

Figure II.4: Principal features of FS-MPC [15].

5. Fast dynamic response and high steady state performance

At a lower switching frequency, FS-MPC has become an attractive strategy for the control of power converters because it takes into consideration their nonlinear nature, unlike the Field Oriented Control (FOC) and Voltage Oriented Control (VOC). FS-MPC provides the best control for power conversion systems and power converters over linear controllers by giving a fast dynamic response, high performance and good reference tracking for both transient and steady state.

6. Damping of perturbation and dead-time compensation

FS-MPC is able to compensate the dead time, the perturbation of the power conversion system, also the on-state voltage drop of power converter switch. It provides the best actuation each sampling time after the minimization of the cost function and influences better on DC-link voltage oscillations.

7. Treatment of nonlinearities and limitations of the system

One of the best features of FS-MPC is that it tries to make the model of power converter more closed to real behavior by taking its nonlinearities. In addition, it has a flexible concept in the cost function. Where it can resolve several system problems and challenges, by means, it includes switching frequency minimization, spectrum shaping, common-mode voltage mitigation, power losses reduction, THD and boundary limits...etc.

8. Multivariable problem treatment

FS-MPC can easily take into consideration multivariable tasks in the same cost function. For example, it handles at the same time, the electrical and mechanical control variables of the electrochemical system.

II.3.2.FS-MPC big challenges

As most controllers have benefits and disadvantages, the FS-MPC also has several challenges that was cited in some researches, from them:

1. Large computational burden

Before the fast development of calculators and microprocessors, FS-MPC could not be applied for power converters and power conversion systems because of their nonlinearities and a large number of calculations that required for resolving these kinds of processes. The number of switching states of converters is always increasing with the development of new topologies of multilevel and matrix converters, which is a significant obstacle for the implementation of FS-MPC in real-time.

2. Variable switching frequency

The variable switching frequency is a significant drawback that confronts the FS-MPC for improving its skills over a linear controller in such applications as grid-tied systems, including renewable energies. However, the average switching frequency can be kept to quasi-constant value by an online optimization of weighting factors [20].

3. Heuristic selection method of weighting factors

More than one predicted error (error of power, voltage or current …etc) can be added in the cost function of the FS-MPC and the importance of one term over the others can be performed through a selection of the weighting factors. The variety of the controlled variables included in the cost function makes the selection process of the weighting factor more complex and tedious. For that reason, more researches have been published in this context [21], and some theoretical methods are discussed in [22].

4. Accurate system model and parameter uncertainties

The accurate model of the system can improve the system performance, and especially when using the FS-MPC because it is directly based on it. In power converters, the continuous-time model of their topologies is available. Nevertheless, when using the FS-MPC method, a discrete-time model is required, where it has been a matter of research subject in the control domain. It is impossible to determine an exact discrete-time model for a linear-time varying system, where many methods to extract an approximate model with high precision are developed to improve the system performance [23].

II.3.3.FS-MPC design procedure

A current control using FS-MPC for a three-phase grid-tied photovoltaic system is presented here in this subsection, where Fig.II.5 describes well the steps of the control procedure. The used power converter for grid connection is a Two Level Voltage Source Inverter (2L-VSI), and to simplify the analysis, the natural (abc) reference frame is taken in this demonstration. The FS-MPC scheme is realized through five steps: (1) determination of reference current, (2) extrapolation of reference currents, (3) combinations of possible switching states, (4) discrete-time predictive model and (5) minimization of the cost function [15]. These steps have to force the grid current to be more close to its reference and minimize the error between them to give a suitable control for the power conversion system. Fig.II.5 illustrates well how to implement the FS-MPC for this kind of system in real-time.

- **Step 1: Measurement of the system dominant variables**

The main variables that influence the system behavior and the variables to be controlled are measured and interfaced to the calculator through current and voltage sensors and analog to

digital converters. For the case of Fig.II.5, a current sensor for the PV panel current (I_{PV}), two current sensors for the grid currents i_a and i_b, where the current i_c is deduced, the DC link voltage V_C which is the same as the PV panel voltage V_{PV} is measured, and two voltage sensors for the grid voltages for phases a and b (V_{ga}, V_{gb}) are used, where the voltage V_{gc} is deduced. Therefore, three current sensors and three voltage sensors are sufficient to implement a three-phase grid-connected PV system in real-time.

- **Step 2: Determination of reference currents**

The reference currents for the grid-side are determined through the DC link voltage regulation, which gives the reference current magnitude. The phase-locked loop block is used to determine the grid phase and allows a safe injection of currents. In the case of a grid-tied PV system, an extra block of maximum power point tracking is used to take part in shaping the grid reference currents and to allow the panel to provide its maximum power whatever the atmospheric conditions. This configuration is the simplest of the grid-tied PV systems.

- **Step 3: Extrapolation of reference currents**

The error can occur in the (k+1) sampling time when the reference current is calculated. The reference currents are extrapolated from the instant (k) to the next sampling instant $(k+1)$ using a third-order Lagrange extrapolation, (it uses the present current value and the three past samples). This method gives the future reference currents by the following equation [15]:

$$\hat{\imath}^*(k+1) = 4\,i^*(k) - 6\,i^*(k-1) + 4\,i^*(k-2) - i^*(k-3) \qquad \text{(II.9)}$$

- **Step 4: Variable predictions**

The prediction of the variables is divided into some sub-steps as described below:

- The continuous-time model of the configuration given in Fig.II.5 is obtained as follows:

$$\frac{di(t)}{dt} = \frac{1}{L}\left[-R\,i(t) + [v(t) - V_g(t)]\right] \qquad \text{(II.10)}$$

Note that, each configuration of power conversion has its proper continuous-time equation.

- The discrete-time model of the configuration of Fig.II.5 is obtained by applying Euler approximation given by (II.2) to the continuous-time model given by (II.10) and it is given by the following equation:

$$i^{P}(k+1) = \underbrace{\left(1 - \frac{RT_s}{L}\right)}_{\Phi} i(k) + \underbrace{\left(\frac{T_s}{L}\right)}_{\Upsilon}\left[v^{P}(k) - V_g(k)\right] \quad \text{(II.11)}$$

Where, T_s is the sampling time, and the superscription (p) denotes the predicted variable.

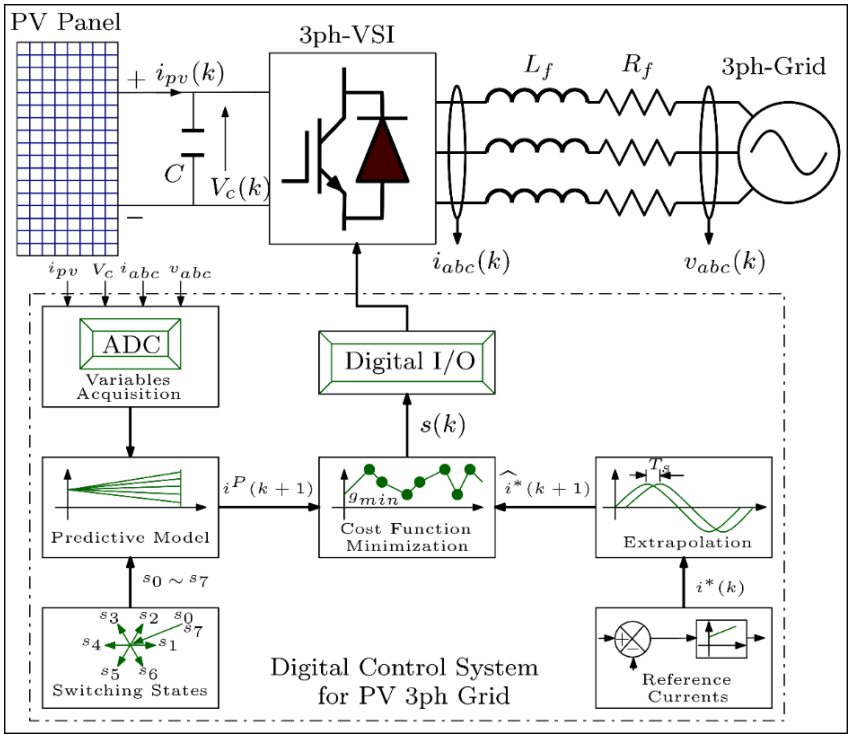

Figure II.5: Model predictive current control for grid connected PV system.

- The discrete-time parameters Φ and Υ have fixed values and they are treated as inputs to the predictive model.
- The predicted grid current is based on the inputs, the previous value, the grid voltage and the voltage of the converter v(k), which is directly based on the possible switching states of the 2L-VSI and the DC link voltage as given by:

$$v(k) = [v_a v_b v_c]^T = S(k) * V_C(k) \quad \text{(II.12)}$$

Where, $S(k) = [S_a S_b S_c]^T$ is the possible switching state of the converter.

The 2L-VSI has eight possible switching states, and the voltage of the converter is based on these combinations as follows:

$$v^{P}(k) = \begin{bmatrix} v_a^P \\ v_b^P \\ v_c^P \end{bmatrix} = \frac{1}{3} V_C(k) \begin{bmatrix} 2 & -1 & -1 \\ -1 & 2 & -1 \\ -1 & -1 & 2 \end{bmatrix} \begin{bmatrix} S_a(k) \\ S_b(k) \\ S_c(k) \end{bmatrix} \quad \text{(II.13)}$$

With the finite number of combinations, the FS-MPC predicts eight possible voltages and currents that simplifies the number of iterations.

- **Step 5: Minimization of the cost function**

In this last step and for a 2L-VSI, a cost function g(k) is formulated; it evaluates the absolute value of eight predicted errors between the predicted currents $i^P(k+1)$ and their references $i^*(k+1)$:

$$g(k) = |\hat{i}^*(k+1) - i^P(k+1)| \quad \text{(II.14)}$$

This cost function is subject to a minimization process, by means the smallest absolute error that minimizes g(k) is selected as the optimal one based on the combination of the switching state. For that, the optimal actuation is chosen to be applied on the converter switch triggers. The optimization process is done during the instant (k), where the optimal switching state is applied at the next sampling time $(k+1)$. This procedure allows a swift control without any PI controller or modulation stage.

II.3.4.Flexibility of the cost function

The simplicity of the FS-MPC applied to power conversion systems takes shape in the flexibility of the cost function. This last fulfils several control requirements by handling multivariable tasks using different physical natures, frequencies, magnitudes, and phase angles as control variables. The cost function design was highlighted in literature by several published scientific works [12-24] and it is presented in this subsection according to [15]. Its flexibility and design are divided into two-control objectives. The primary one deals with the reference tracking and the error between the predictive variables and their references, where the second one treats safety constraints, technical requirements, and nonlinearities through weighting factors. Fig.II.6 well demonstrates this cost function presentation.

In Fig.II.6, the given structures of the cost function are presented by $\{\hat{x}^* - x^P\}$, which represent the following functions:

$$g(k) = |\hat{x}^*(k+1) - x^P(k+1)|$$

$$\epsilon \begin{cases} |\hat{x}^*(k+1) - x^P(k+1)| & \text{(Absolute cost function)} \\ [\hat{x}^*(k+1) - x^P(k+1)]^2 & \text{(Quadratic cost function)} \\ \exp|\hat{x}^*(k+1) - x^P(k+1)| & \text{(Exponential cost function)} \\ \frac{|\hat{x}^*(k) - x^P(k)| + |\hat{x}^*(k+1) - x^P(k+1)|}{2} & \text{(Integral cost function)} \end{cases} \quad \text{(II.15)}$$

Where, x^P and $\hat{x}^*$ are the predicted value and the extrapolated reference value, respectively.

The absolute cost function evaluates the error between the predicted value and its reference and gives a positive value. The quadratic cost function produces the square of the predicted error value. The exponential cost function provides an over-proportionate error value. The integral cost function minimizes the error of the instant value and the predicted one and gives an average value between these errors [25]. This last cost function gives a good reference tracking with less error in the steady state, but is not well recommendable because it incurs large number of calculations.

The absolute and the quadratic cost functions are most commonly used in FS-MPC for power converters and electrical drives, where the second one provides the best performance when the sub-cost functions are considered simultaneously because of the small quadratic error value since it is easily detected among the control variables [18]. For that reason, only the absolute and quadratic cost functions are considered for the rest of this study.

➢ Primary control objectives

The primary control objectives presentation of the FS-MPC focuses only on the objectives used for the control of stand-alone or grid-tied photovoltaic conversion systems. The considered notations are x^P and $\hat{x}^*$ instead of $x^P(k+1)$ and $\hat{x}^*(k+1)$.

- **Current control:** For the control of power conversion systems, the predictive current control (PCC) is often used in the inner control loop, whatever the converter topology. The formulated cost function treats the errors of the currents in the natural, stationary, or synchronous frames in a decoupled way as it is given by the following equation [15]:

$$g_i(k) = \{\hat{i}^* - i^P\}$$

$$\epsilon \begin{cases} \{\hat{i}_a^* - i_a^P\} + \{\hat{i}_b^* - i_b^P\} + \{\hat{i}_c^* - i_c^P\} & \text{(Natural frame)} \\ \{\hat{i}_\alpha^* - i_\alpha^P\} + \{\hat{i}_\beta^* - i_\beta^P\} & \text{(Stationary frame)} \\ \{\hat{i}_d^* - i_d^P\} + \{\hat{i}_q^* - i_q^P\} & \text{(Synchronous frame)} \end{cases} \quad \text{(II.16)}$$

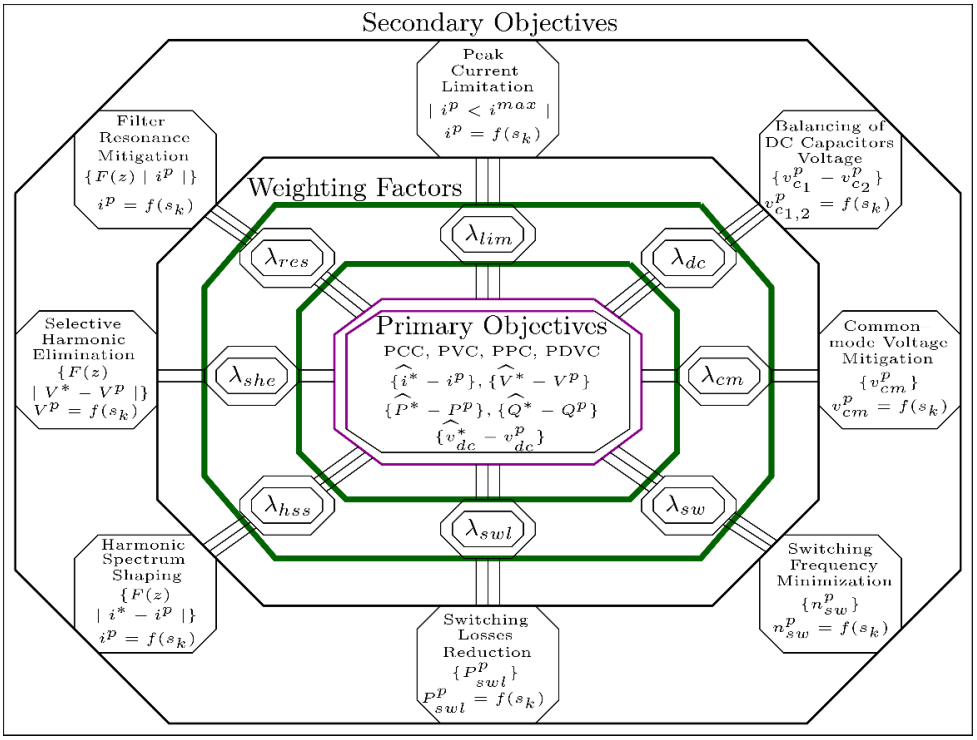

Figure II.6: Cost function with several primary and secondary control objectives [15].

- **Voltage control:** As in the case of PCC, the power conversion systems also use the predictive voltage control to allow the power converter to give high-quality sinusoidal voltages, and can be defined in the three frames. The presented cost function (II.17) treats the predicted errors in the natural frame [15]:

$$g_v(k) = \{\hat{v}^* - v^P\} = \{\widehat{v_a^*} - v_a^P\} + \{\widehat{v_b^*} - v_b^P\} + \{\widehat{v_c^*} - v_c^P\} \quad \text{(II.17)}$$

- **Decoupled power control:** The grid-tied PV systems in many research papers use the predictive power control (PPC) in a decoupled way similar to the conventional direct power control (DPC). This control is also used to control wind turbines and electric drives. The defined cost function is formulated as follows [15]:

$$g_{PQ}(k) = \{\widehat{P}^* - P^P\} + \{\widehat{Q}^* - Q^P\} \quad \text{(II.18)}$$

- **DC link voltage control:** The PCC and PPC are giving more flexibility to the power conversion systems control by eliminating the internal current PI controllers, the modulation stage, and the hysteresis as regulators. However, the DC link voltage stilled regulating by an outer control loop using a linear PI controller since researchers in [26] proposed a flexible DC-bus voltage regulation by integrating the predicted error of the V_C^P and its reference V_C^* in the PCC/PPC cost functions. This proposed control approach

is called as predictive DC-bus voltage control (PDVC). The cost function of this technique is given by:

$$g_{vc}(k) = \{V_C^* - V_C^P\}$$

$$\in \begin{cases} \{\widetilde{V_C^*} - V_C^P\} + \lambda_{id}\{\widehat{i_d^*} - i_d^P\} + \lambda_{iq}\{\widehat{i_q^*} - i_q^P\} & \text{(PDVC with PCC)} \\ \{\widetilde{V_C^*} - V_C^P\} + \lambda_P\{\widehat{P}^* - P^P\} + \lambda_Q\{\widehat{Q}^* - Q^P\} & \text{(PDVC with PCC)} \end{cases} \quad \text{(II.19)}$$

Where, $\widetilde{V_C^*}$ is the filtered reference of the DC-bus voltage. λ_{id}, λ_{iq} , λ_P , and λ_Q are the weighting factors for the internal PCC and PPC schemes. This technique proved high dynamic response and less oscillation around the reference over the outer PI control loop in simulations and experimental tests [26]. However, this technique modeling is complex and its steady-state performance is based directly on the modeling error [15].

➢ Secondary control objectives

The flexibility of FS-MPC also appears in the control goals of power converter systems, where this technique treats many constraints, fixes secondary control objectives and allows the system to provide the best skills.

- **Limitation of peak current:** The feedback current dynamics have been ignored in the previous predictive controls cited above (PCC, PPC, and PDVC), where the classical controls treated these issues by employing saturation blocks. In the transient interval, the feedback current can exceed the maximum threshold limit (i^{max}), thus, it is dangerous for some system components. Therefore, FS-MPC fulfills this lack by defining a sub-cost function that should be with the main one and it is given as [15]:

$$g_{lim}(k) = \{|i^P| < i^{max}\} = \begin{cases} \infty & \text{if } |i^P| > i^{max} \\ 0 & \text{if } |i^P| \leq i^{max} \end{cases} \quad \text{(II.20)}$$

- **DC link capacitors voltage balancing:** The capacitors voltages in a neutral point clamped (NPC) inverter should be kept equal to each other. This equilibrium minimizes the stress of the converter devices and allows for reliable functioning. The cost function that deals with this issues is given by:

$$g_{dc}(k) = \{v_{c1}^P - v_{c2}^P\} \quad \text{(II.21)}$$

Where, v_{c1}^{P} and v_{c2}^{P} are the predicted values of the capacitors voltages of an NPC converter. This cost function is suitable for other kind of three level inverters such as diode-clamped and floating capacitor converters [15].

- **Common-mode voltage mitigation:** The common-mode voltage (CMV) should be mitigated in the control scheme of the converter because it causes severe voltage stress, malfunctioning of ground fault protection system, and electromagnetic interference [15]. The minimization of the CMV is realized by this cost function (II.22):

$$g_{cm}(k) = \{v_{cm}^{P}\} = \left\{\frac{v_{aN}^{P}+v_{bN}^{P}+v_{cN}^{P}}{3}\right\} \quad \text{(II.22)}$$

Where, v_{aN}^{P}, v_{bN}^{P} and v_{cN}^{P} are the predicted values of the converter output voltages.

- **Minimization of the switching frequency:** This sub-objective aims to minimize the number of commutations for each converter switch between two sampling instants, thus, reduces the average switching frequency of the system and increases the global efficiency. For a three-phase power converter with N_s the number of the switching devices per phase, the cost function is given as:

$$g_{sw}(k) = \{n_{sw}^{P}\} = \left\{\sum_{j=1}^{N_s}\sum_{x=a,b,c}\left|s_{xj}^{P}(k) - s_{xj}(k-1)\right|\right\} \quad \text{(II.23)}$$

Where, $s_{xj}^{P}(k)$ and $s_{xj}(k-1)$ are the predicted values of the optimal combination between two sampling instants of a j^{th} device.

- **Reduction of the switching losses:** The improvement of the system efficiency and reduce the cooling efforts, the switching losses reduction method is used as a sub-objective by including the switching losses formula directly in the cost function as given below [27] :

$$g_{swl}(k) = \{P_{swl}^{P}\} = \left\{\sum_{j=1}^{N_s}\Delta i_{c,j}^{P} . \Delta v_{ce,j}^{P}\right\} \quad \text{(II.24)}$$

Where, $\Delta i_{c,j}^{P}$ is predicted changes in the collector current and $\Delta v_{ce,j}^{P}$ is the predicted changes in the collector-emitter voltage of the switching device j^{th}.

- **Harmonic spectrum shaping:** This sub-cost function aims to fulfill the FS-MPC lack that makes the switching frequency of the converter not fixe. This issue causes a harmonic spectrum that spread over a wide range of frequencies and appears in the output current and voltage of the converter. The spread spectrum causes an undesirable harmonic resonance and electromagnetic interferences. For that, a frequency-dependent discrete-time weight function $F(z)$ is used in the principal cost function [28] as:

$$g_{hss}(k) = \{F(z)|i^* - i^P|\}, F(z) = \frac{z^0 + b_1 z^{-1} + \cdots + b_n z^{-n}}{a_0 z^0 + a_1 z^{-1} + \cdots + a_n z^{-n}} \quad \text{(II.25)}$$

Where, $F(z)$ is an n^{th} order filter that enforces a desired harmonic content on the variables to be controlled. Its coefficients a_0 to a_n and b_0 to b_n are set according to the required filter function [15].

- **Selective harmonic elimination:** Selective Harmonic Elimination (SHE) is used as a modulation technique for high power converter to improve grid power quality and to minimize switching losses by eliminating some low-order harmonics. This method can easily be integrated with FS-MPC, and it is based on the good tracking reference of the voltage V to its predefined voltage reference V^* such that the low-order harmonics are removed, and a small number of commutations are implicated. The used cost function for this approach is formulated by using the Sliding Discrete Fourier Transform (SDFT) given in [29]:

$$g_{she}(k) = \{SDFT(z)|V^* - V^P|\}$$

$$= \left\{SDFT_{f_1}(z)|V^* - V^P|\right\} + \lambda_f \sum_{i=2}^{n} \left\{SDFT_{f_i}(z)|V^* - V^P|\right\} \quad \text{(II.26)}$$

As it is denoted by (II.26), the first term can minimize the voltage error at the fundamental frequency, where the second one aims to eliminate the few selected harmonics (up to n^{th} order), this second term is affected by a weighting factor λ_f.

- **Mitigation of filter resonance:** LCL filters are often used in the grid-connected photovoltaic systems in view to improve grid side power quality and to minimize low-frequency current harmonics. As it is known for the resonant behavior of this kind of filters and current oscillations caused by current harmonics and step changes of the reference. Active damping methods are used to resolve the resonance problem of frequency ω_1 and ω_2 of the filter components. Also a frequency-dependent cost function is proposed and used [30]:

$$g_{res}(k) = \{F(z)|i^P|\} = \left\{F_1(z)\left|i_1^p\right| + F_2(z)\left|i_2^p\right|\right\} \quad \text{(II.27)}$$

Where $F_1(z)$ and $F_2(z)$ are discrete first-order bandpass filters tuned at ω_1 and ω_2 for the converter and grid-side predicted currents (i_1^p and i_2^p, respectively).

II.3.5. Weighting factor selection methods

The flexibility in FS-MPC leads to include several targets and constraints with variables of different natures in a single cost function where the main advantage of this suppleness is that they are simultaneously controlled. However, each term in this hybrid cost function is accompanied by a weighting factor, and this last should be appropriately designed to reach the optimal control [15-17]. The design stage of this factor plays a crucial role in improving MPC performances, for that many selection methods showed by Fig.II.7 and discussed below:

- **Heuristic selection**

The method is an empirical approach that is commonly used to select the appropriate weighting factor (λ) for each variable error in the global cost function and it is based on a trial-and-error procedure. In other words, for a global cost function, that contains secondary objectives besides the primary objectives and that should be regulated to ensure the system functioning, then the trial-and-error method to select λ starts from high to low value. In the same way, for secondary objectives that have only an effect on improving FS-MPC performances, the trial-and-error procedure begins with a low value. (For more details, see chapter 4 in [15]).

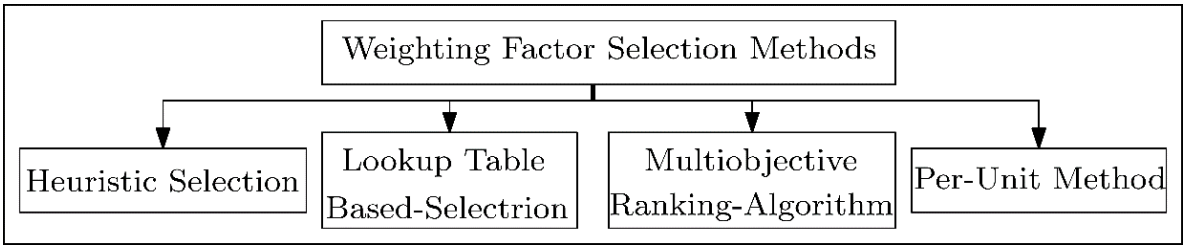

Figure II.7: Descriptive flowchart of weighting factor selection methods.

- **Lookup table based-selection**

This procedure gives the optimal weighting factors based on the reference control variable such as current control, active and reactive power control, torque and flux control, or CMV mitigation, ...etc. In such cases, it bases on values determined by the empirical procedure and stored in a lookup table that is destined for FS-MPC online uses [15].

- **Multiobjective ranking algorithm**

This approach was proposed to give the optimal switching state after ranking each objective's variable errors by giving the lower rankings for the smaller errors and the higher rankings for the larger errors, then the average ranking is computed and the appropriate combination is selected. In other words, this method can eliminate the need for a weighting factor, and at the same time minimizes the global cost function to select the optimal control action [15].

- **Per-unit method**

Thanks to the researchers and their effort to collect and improve knowledge on converters and their controls, an analytical procedure was proposed to design the global cost function's weighting factors. The principle of this method employs per-unit values for variable errors. In other words, for a global cost function that contains a current error and DC link capacitors voltage error, the first term is divided by the rated reference current, and the rated DC link voltage divides the second one. The overall cost function is multiplied by the rated reference current (the reference of the primary control objective) [15].

II.4. Stand-alone and grid-tied photovoltaic systems using finite set model predictive control

Nowadays, our planet can be destroyed by burning the hydrocarbons from fossil energy for human needs. Therefore, it is time to replace the traditional energy with one that is suitable and its natural renewable is fast enough to be considered as inexhaustible. Concerning renewable and clean energies, solar energy, despite a very rapid development for the last years, still relatively marginal at the global level, far behind wind energy, biomass, and especially hydraulic energy [31]. Solar energy is the clean and renewable energy which owns the highest margin of progression for decades to come and the highest potential to become the first source of energy for humanity before the middle of this century [31]. Solar energy is divided into thermal energy and photovoltaic (PV) energy, the studied system is interested in the latest one, which allows us to deliver electrical power to loads, such as domestic lighting, appliances, electric vehicles..., and it can be stored in batteries, these applications are grouped in so-called stand-alone systems [32, 33]. Furthermore, grid-connected systems are realized using this kind of clean energy [33].

PV energy applications need adaptation stages to deliver electric power to loads or to the grid. Generally, for stand-alone systems, a DC-DC converter was used to increase the output voltage of the PV panel. Moreover, an inversion stage is implemented by using a single-phase or three-phase inverter that are the second stage for grid-connected systems [34]. Despite this adaptation, the conversion chain remains incomplete and the PV panel is still in need of excitation to operate at the Maximum Power Point (MPP). Therefore, the tracking algorithm of MPP is required for attacking the controllable switch trigger of the DC-DC converter and allows the PV panel to offer its maximum power under different environmental changes such as temperature and irradiance [35]. In recent years, several Maximum Power Point Tracking (MPPT) algorithms are suggested, and many of them are discussed in [35], in this section, the Incremental Conductance algorithm (Inc-Con) is chosen to be implemented with the FS-MPC.

Recently, several advanced topologies of power electronic converters have been proposed by researchers for different applications such as multilevel inverter, multilevel boost and quasi-ZS inverter [33-34, 36-37]. Due to this progression, considerations have been taking into account for the control of these complex converters [38] that required effective techniques to deal with it, so, there are and there will be more and more advanced methods in the future [36].

Finite Set Model Predictive Control (FS-MPC) is a recent control method for several applications such as step-up converters, inverters, and motor drives… [37]. It has been considered as a paradigm of control in power electronics due to its robustness, simplicity, and its fast response. This technique is based on the model of the system and the possible switching states of the power converters (2 states for boost and multilevel boost, 7 states for two levels inverter) and it uses them to predict the behavior of the dominant variables for each switching state, then a cost function should be defined and evaluated for the predicted values on each sampling interval then the optimal switching state is selected to apply during the next sampling interval [33].

II.4.1. Model predictive control of DC/DC converters

The two compared converters are shown in Fig.II.8 and Fig.II.9 [39, 40] for boost and multilevel boost converters respectively, the first is a basic model and it is still the platform that relies on it to create other topologies, it has two simple and known working operations corresponding to its switch states, with an easy control procedure [39], its output voltage V_{C1} is related to the PV panel voltage V_{PV} and the duty cycle D by [41]:

$$V_{C1} = \frac{1}{1-D} \times V_{PV} \quad \text{(II.28)}$$

The second structure is one of the recent topologies of boost converters. It is a two-level boost converter (MLB), as it seems in Fig.II.9. The MLB has one controllable switch, its operation has three sequences corresponding to its switch states, the first sequence is done when the switch is 'ON', then the second and the third sequences are done when the switch is 'OFF'. The procedure of control is easier than other topologies such as in [41-42]. The output voltage V_{C1} of the MLB is proportional to the number of the DC output voltage levels (N = 2) and it given as [41]:

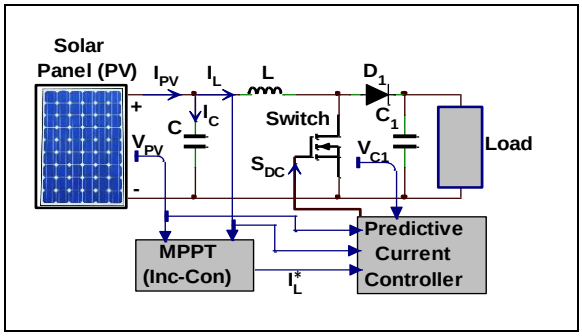

Figure II.8: Conventional boost converter.

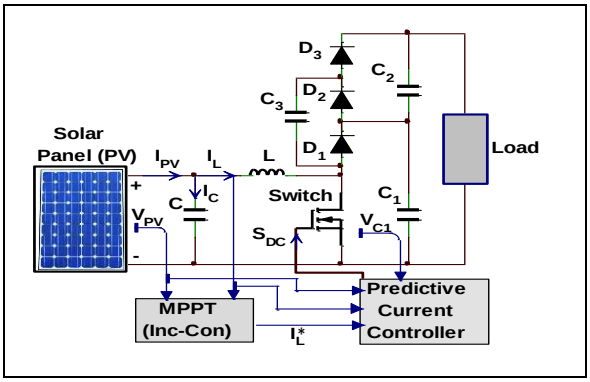

Figure II.9: Two level boost converter.

$$V_{C1} = N \times \frac{1+D}{1-D} \times V_{PV} \quad \text{(II.29)}$$

While there is only one controllable switch for each converter, a common model predictive control is given for them. The dominant variables that describe the system and that need a discrete-time model are the inductor current and PV panel voltage. The discrete-time model is given as [40]:

When the switch is ON ($\zeta = 1$):

$$I_L(k+1) = I_L(k) + V_{pv}(k) \times \frac{T_s}{L} \quad \text{(II.30)}$$

$$V_{PV}(k+1) = V_{PV}(k) + [I_{PV}(k) - I_L(k)] \times \frac{T_s}{L} \quad \text{(II.31)}$$

Then, when it is OFF ($\zeta = 0$):

$$I_L(k+1) = I_L(k) + [V_{pv}(k) - V_{C1}(k)] \times \frac{T_s}{L} \quad \text{(II.32)}$$

$$V_{PV}(k+1) = V_{PV}(k) + [I_{PV}(k) - I_L(k)] \times \frac{T_s}{L} \quad \text{(II.33)}$$

As it seems from (II.30)-(II.33), there are four variables to measure V_{PV}, I_{PV}, I_L and V_{C1}. To decrease the number of input variables, the equations (II.31) and (II.33) can be rearranged [40]. The new representation is as follows:

$$I_L(k+1) = I_L(k) + [V_{pv}(k) - V_{C1}(k) \times (1-\zeta)] \times \frac{T_s}{L} \quad \text{(II.34)}$$

$$V_{PV}(k+1) = 2V_{PV}(k) - V_{PV}(k-1) \quad \text{(II.35)}$$

The derived equations can be represented in matrix form by (II.36) corresponding to the switch states (ζ) as follows:

$$\begin{bmatrix} I_L(k+1) \\ V_{PV}(k+1) \end{bmatrix} = \begin{bmatrix} 1 & \frac{T_s}{L} & -(1-\zeta)\frac{T_s}{L} \\ 0 & 2 & 0 \end{bmatrix} \times \begin{bmatrix} I_L(k) \\ V_{PV}(k) \\ V_{C1}(k) \end{bmatrix} + \begin{bmatrix} 0 \\ -1 \end{bmatrix} \times V_{PV}(k-1) \quad \text{(II.36)}$$

The performances of the two converter topologies of Fig.II.8 and Fig.II.9 for a standalone application are revealed under a Finite Set Model Predictive Control MPC-MPPT technique given in [40]. Relation (II.36) will be used to predict the values of I_L and V_{PV} for one-step ahead prediction. Note that the used load is a simple resistance. The used parameters in simulation are listed in Table II.1.

Table II.1: Simulation parameters of the stand-alone systems.

Parameter	Value	Unit
PV power at 1000 W/m²	50	W
Voltage at maximum power (V_{MP})	17.44	V
Current at maximum power (I_{MP})	2.86	A
Input capacitor C	3	mF
Inductor (L_{Boost})	0.4	mH
Inductor (L_{MLB})	0.2	mH
DC link capacitor ($C1_{Boost}$)	10	µF
DC link capacitor ($C1_{MLBoost}$, C2, C3)	80	µF
Sampling Time (T_s)	50	µs

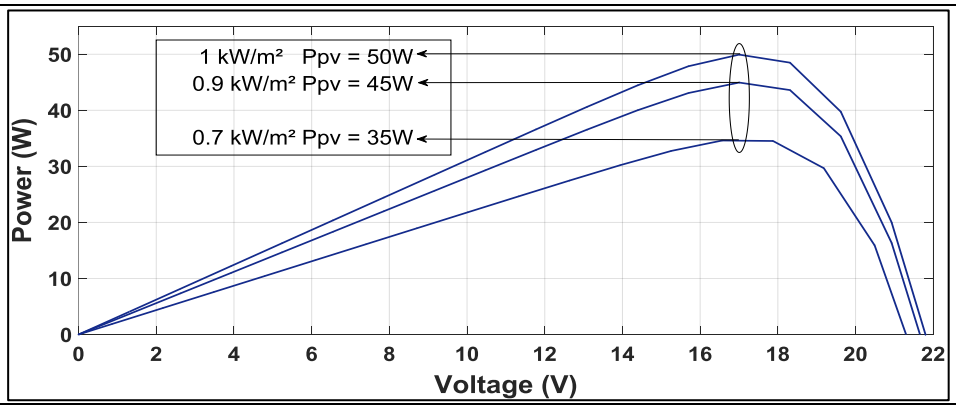

Figure II.10: MPP of the used PV panel for different changes in the irradiance.

II.4.2. Maximum power point tracking using model predictive control

In PV systems, the conversion rate of light into electricity is a key factor in terms of development and profitability, but unfortunately, it is a significant hindrance to their growth [36], at the moment, Maximum Power Point Tracking (MPPT) is the only effective solution for the PV panel to avoid its disadvantage and to provide its maximum power for the system. There are many methods of MPPT discussed in the few past years, and each one has certain advantages and disadvantages for PV system applications [40], among these methods, the Incremental of Conductance algorithm (Inc-Con) illustrated in Fig.II.11 has been applied for determining the reference current for the MPC which determines the switching state that will be applied [40].

The schemes of PV applications and their control procedure are shown in Fig.II.8 and Fig.II.9. The characteristics of the used PV panel are shown in Table II.1 and the MPP is shown in Fig.II.10 for different changes in irradiance. The principle of the MPC-MPPT procedure is to take the model that was calculated in section I in (II.36), and the reference current that was calculated by the Inc-Con algorithm, then a cost function is formulated containing the predicted error of the inductor current subject to minimization as shown in Fig.II.11 by:

$$g = \left| I_L^p - I_L^* \right| \tag{II.37}$$

After the minimization of (II.37), the optimal switching state should be applied at the next sampling time as shown in Fig.II.11.

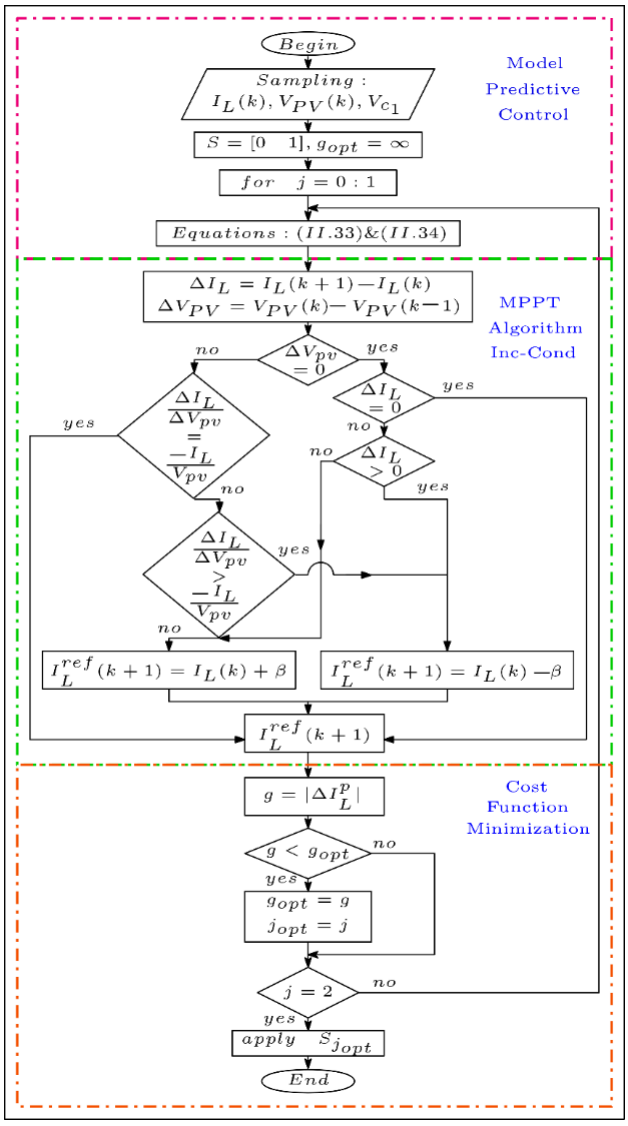

Figure II.11: Flowchart of the MPC-MPPT procedure.

II.4.3. Cascaded converters in grid connected systems using model predictive control

Basically, for a grid-connected system (GCS), a two level voltage source inverter (2L-VSI) is mostly used in cascade with an MPPT DC chopper but separately controlled. The proposed predictive control of Fig.II.13 aims to:

- Including the MPPT algorithm in the presented control.
- Minimization of a single cost function for both converters.
- Control both the cascaded converters at the same time as a matrix converter instead of controlling each converter separately. The global control system is widely reduced.

The three legs switching states of the 2L-VSI can be determined by gating signals and are given by a vector shape as:

$$S = \frac{2}{3}(S_a + aS_b + a^2S_c) \quad \text{(II.38)}$$

Where $a = e^{j\frac{2\pi}{3}}$.

The load voltage vector v is related to the DC link voltage V_{C1} and the switching state vector S by:

$$v = V_{C1}S \quad \text{(II.39)}$$

The predictive control of 2L-VSI required a discrete time model of the grid that can be defined from the following continuous time equation:

$$v = R_f I_{in} + L_f \frac{dI_{in}}{dt} + V_G \quad \text{(II.40)}$$

Where v is the voltage generated by the two level inverter, I_{in} the grid current, R_f, L_f are the grid filter resistance and the grid filter inductance per phase respectively. V_G is the balanced three-phase grid voltage vector and it is assumed sinusoidal with constant frequency and constant amplitude.

Table II.2: Simulation parameters of the grid connected systems.

Parameter	Value	Unit
PV power at 1000 W/m²	305	W
PVG power at 1000 W/m² (2x2)	1221	W
Voltage at maximum power (V_{MP})	54.7	V
Current at maximum power (I_{MP})	5.58	A
Input capacitor C	3	mF
Inductor (L_{Boost})	0.4	mH
Inductor (L_{MLB})	0.4	mH
DC link capacitor ($C1_{Boost}$)	0.1	mF
DC link capacitor ($C1_{MLBoost}$, C2, C3)	0.1	mF
DC link voltage	440	V
Sampling Time (T_s)	50	µs

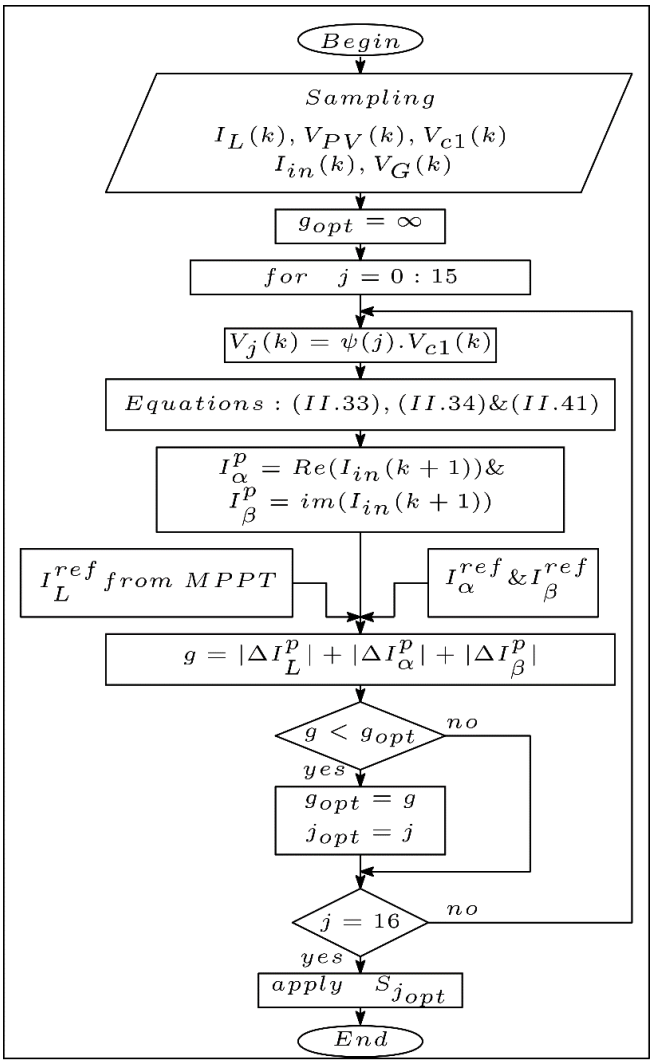

Figure II.12: Flowchart of control of the global chain.

A discrete time model equation of the grid current I_{in} for the sampling time T_S indicated in Table II.2 can be used to predict the grid current in one-step ahead by using Euler method, and the derivative $\frac{dI_{in}}{dt}$ approximation given by:

$$\frac{dI_{in}}{dt} = \frac{I_{in}(k+1) - I_{in}(k)}{T_S} \tag{II.41}$$

Then the predicted grid current is as follows:

$$I_{in}(k+1) = (1 - R_f \frac{T_S}{L_f})\, I_{in}(k) + \frac{T_S}{L_f}(v(k) - V_G(k)) \tag{II.42}$$

The predicted grid currents I_α^p and I_β^p indicated in Fig. II.12 was found by a α-β coordinate's transformation of their real values given by:

$$I_{in}(k+1) = I_{\alpha}^{p} + jI_{\beta}^{p} \quad \text{(II.43)}$$

The reference currents I_{α}^{*} and I_{β}^{*} have sinusoidal forms, and are obtained by a classical phase locked loop (PLL), their amplitudes are obtained from the DC link voltage regulation loop, which was done by a simple PI regulator. Then, a cost function is defined to control the input inductance current for the MPPT in the PV panel side and the grid currents in the AC side by:

$$g = \left|I_{L}^{p} - I_{L}^{*}\right| + \left|I_{\alpha}^{p} - I_{\alpha}^{*}\right| + \left|I_{\beta}^{p} - I_{\beta}^{*}\right| \quad \text{(II.44)}$$

The flowchart of the proposed predictive control is illustrated by Fig.II.12 according to the 14 switching states of the cascaded converters structure (2 states for the chopper and 7 states for the inverter). For each sampling time, the cost function (II.44) is then minimized for all the 16 output voltage vectors of the matrix converter topology. The optimal voltage vector is selected to be applied in the next sampling time interval.

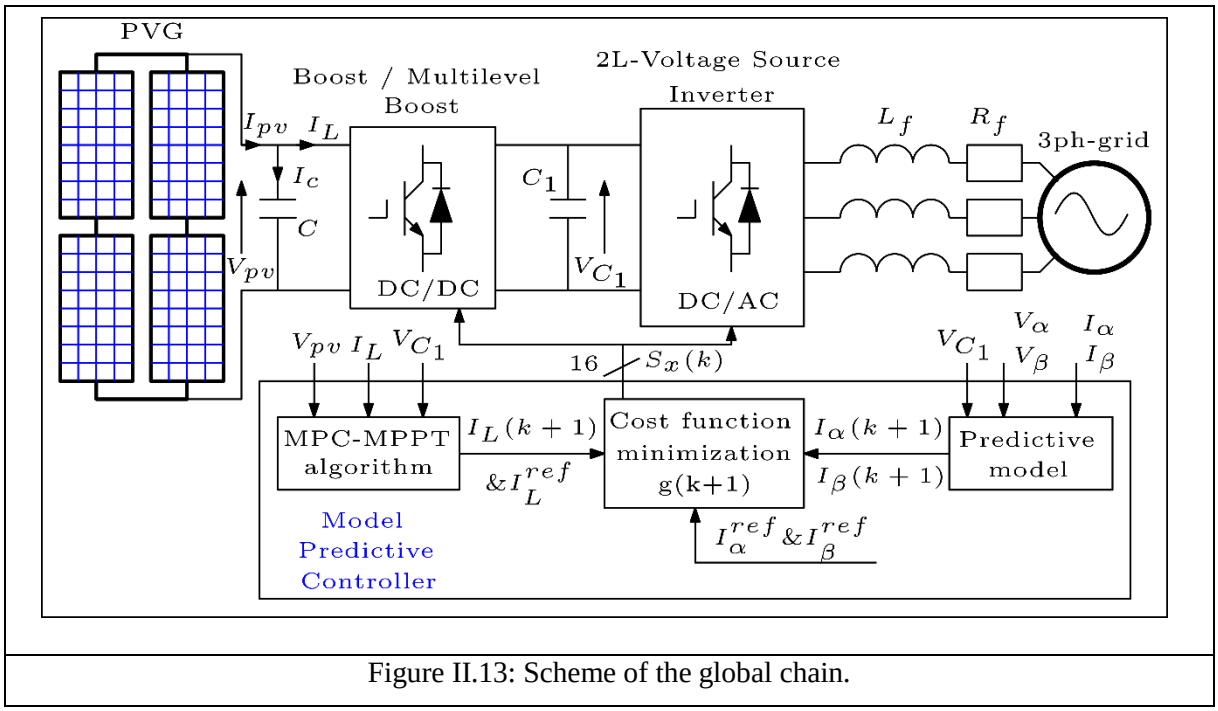

Figure II.13: Scheme of the global chain.

II.4.4. Simulation results

The stand-alone systems (SAS) and the grid-connected systems (GCS) are investigated in MATLAB/SIMULINK software under sudden changes of solar radiation as shown in Fig.II.14. Simulations of the control system given by Fig.II.13 are done for both Boost and Multilevel Boost (MLB) converters for each system, firstly when the system uses a boost converter, secondly when the system is connected to the MLB converter. The comparison is done based

on efficiency, transient dynamics, harmonic distortion level, oscillation around MPP, and switching number in order to quantify the commutation losses.

Table II.3: Switching table.

Output Voltage	S_{DC}	S_a	S_b	S_c
$V_0 = 0$	0	0	0	0
$V_1 = 0$	1	0	0	0
$V_2 = \frac{2}{3}.V_{C1}$	0	1	0	0
$V_3 = \frac{2}{3}.V_{C1}$	1	1	0	0
$V_4 = V_{C1}.(\frac{1}{3} + j.\frac{\sqrt{3}}{3})$	0	1	1	0
$V_5 = V_{C1}.(\frac{1}{3} + j.\frac{\sqrt{3}}{3})$	1	1	1	0
$V_6 = V_{C1}.(-\frac{1}{3} + j.\frac{\sqrt{3}}{3})$	0	0	1	0
$V_7 = V_{C1}.(-\frac{1}{3} + j.\frac{\sqrt{3}}{3})$	1	0	1	0
$V_8 = -\frac{2}{3}.V_{C1}$	0	0	1	1
$V_9 = -\frac{2}{3}.V_{C1}$	1	0	1	1
$V_{10} = V_{C1}.(-\frac{1}{3} - j.\frac{\sqrt{3}}{3})$	0	0	0	1
$V_{11} = V_{C1}.(-\frac{1}{3} - j.\frac{\sqrt{3}}{3})$	1	0	0	1
$V_{12} = V_{C1}.(\frac{1}{3} - j.\frac{\sqrt{3}}{3})$	0	1	0	1
$V_{13} = V_{C1}.(\frac{1}{3} - j.\frac{\sqrt{3}}{3})$	1	1	0	1

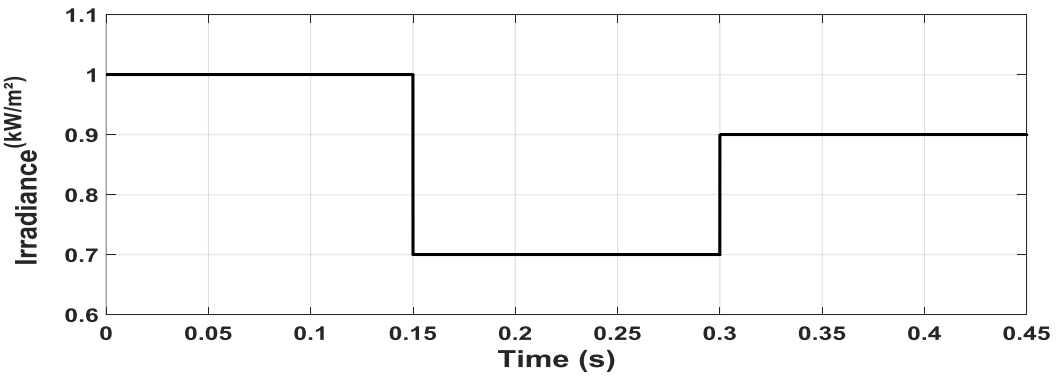

Figure II.14: Profile of irradiance variations.

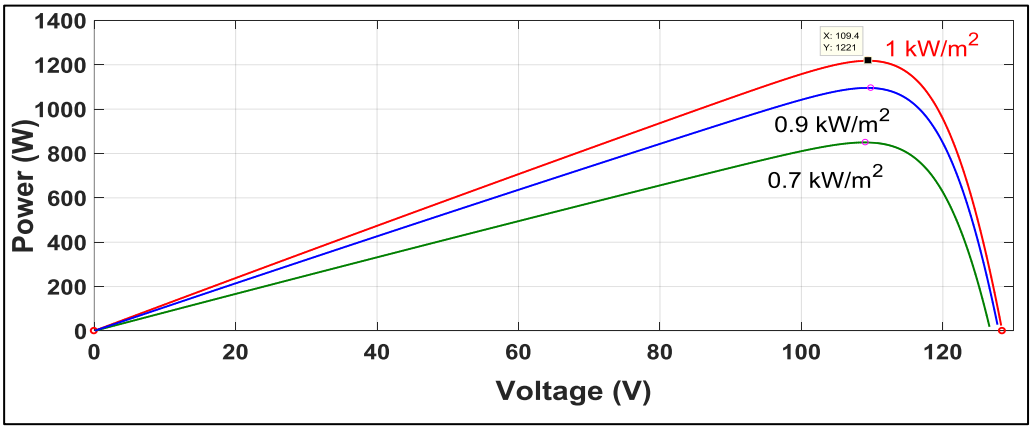

Figure II.15: MPP of the PVG under different changes of irradiance.

Simulation parameters of the stand-alone (SAS) systems of Fig.II.8 and Fig.II.9 are listed in Table II.1, the P-V curves of the PV panel are shown in Fig.II.10 under different changes of irradiance. “Fig.II.16,” illustrates the PV panel power when it is connected to the Boost converter then to MLboost converters, it can be seen that the power ripples for the PV-Boost system are less than for the PV-MLboost system, also, the convergence towards the MPP in the first system is done in less than 55 ms while for the second system, the convergence towards the MPP is done in less than 75 ms. In addition, when the radiation changes abruptly, the response time is always better for the PV Boost system. “Fig.II.17,” illustrates the output power for the two converters, it seems that the power losses for the first system are less than for the PV-MLboost, so the efficiency of the first system is always better than the second system as is shown in Fig.II.18 (about 95.26 % for the first system and 93.26 % for the second).

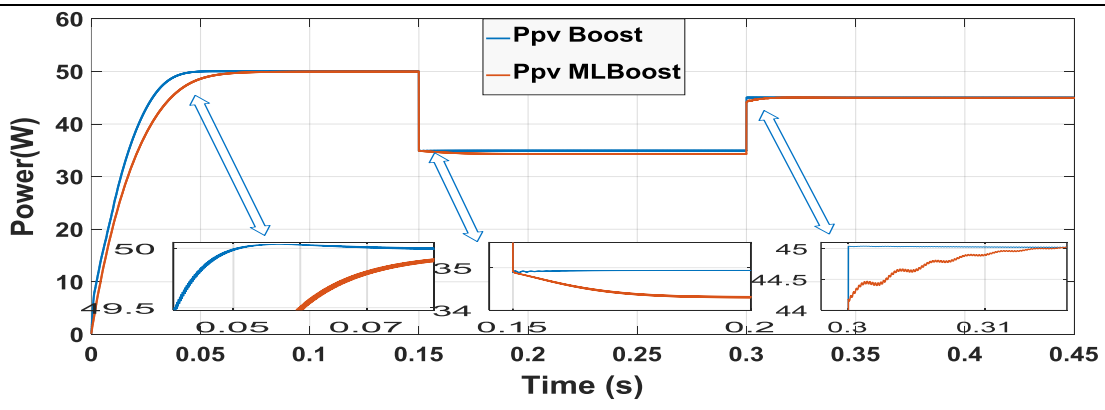

Figure II.16: Comparison of PV power of the two systems.

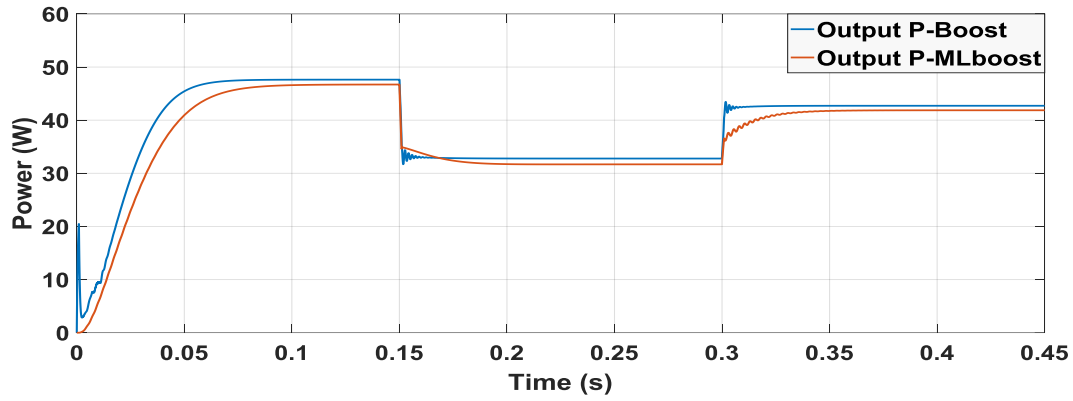

Figure II.17: Output powers of the boost and MLboost converters.

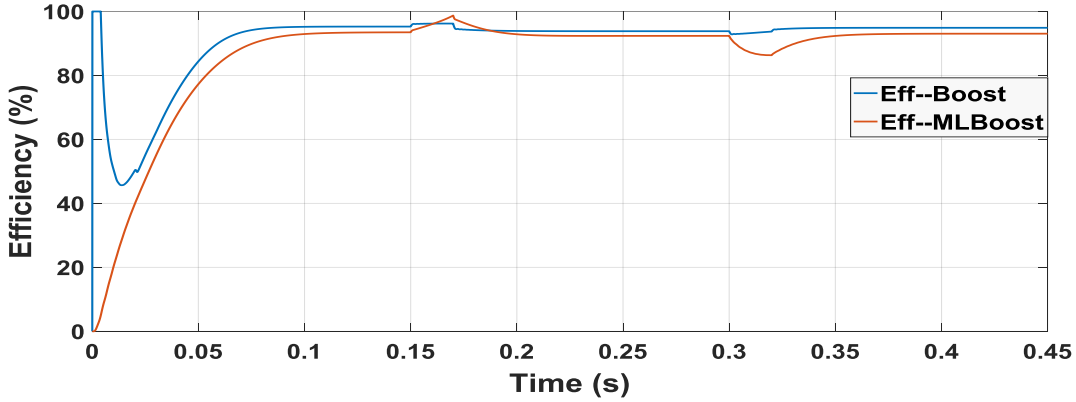

Figure II.18: Efficiency of the two step-up converters.

For the grid-connected system applications (GCS), simulation parameters are indicated in Table II.2 and the possible switching states of the cascaded converters are indicated in Table II.3, the P-V curves of the GPV are shown in Fig.II.15 under different changes of irradiance. “Fig.II.19,” illustrates the GPV power for both boost and MLboost converters, it can be observed that the GPV power ripples are the least when the system is connected to the boost converter. “Fig.II.20,” represents the transmitted powers from the two step-up converters to the inverter where it is clear to see that the power losses are the least with the GPV-Boost system. Fig.II.21 and Fig.II.22 show the grid currents with their references in phase with the grid voltages where it can be seen that there are more ripples in the grid current for GPV-MLboost system than for the GPV-Boost system due to more ripples of the DC Link voltage for the MLBoost topology shown in Fig.II.23.

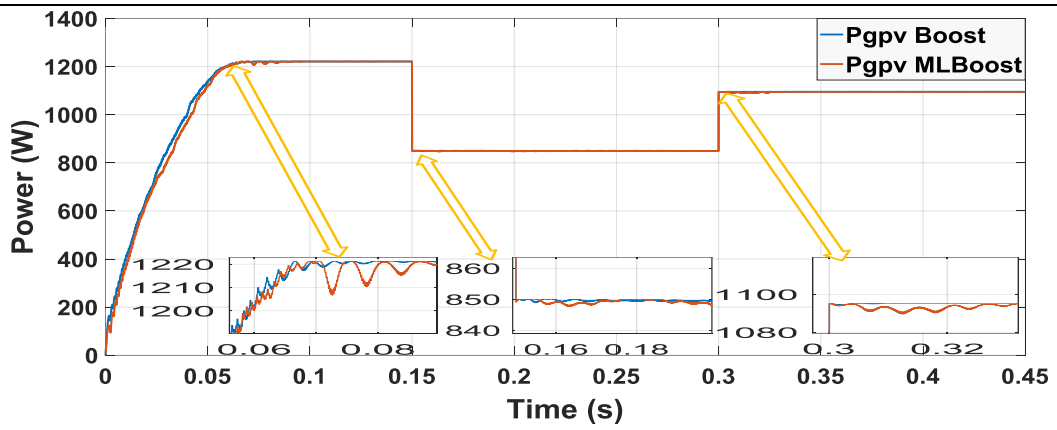

Figure II.19: PVG power comparison.

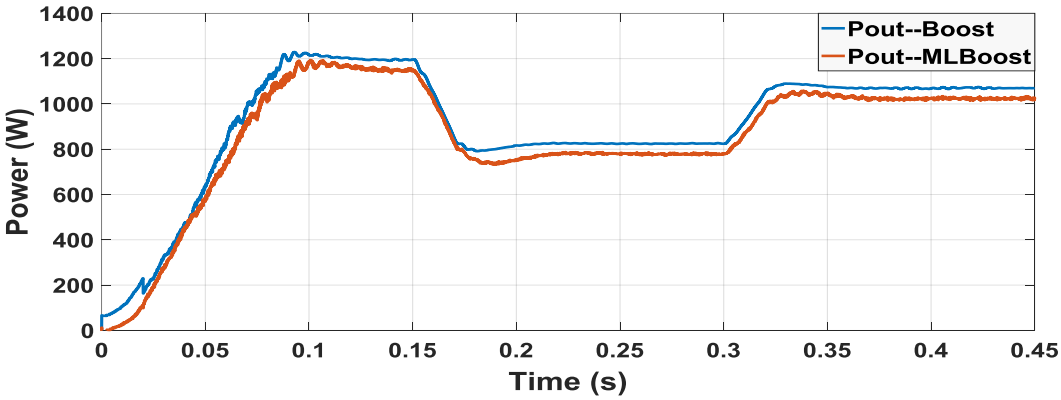

Figure II.20: Transmitted powers from DC/DC converters to the VSI.

"Fig.II.24," shows the switching numbers per period of the two-cascaded converters where it is observed that the switching numbers are smaller in the GPV-Boost system meaning that the topology based Boost converter is more efficient than MLB topology. "Fig.II.25," illustrates the THD evolution for the whole cycle for both topology where it is easy to see that the THD with boost converter presents low values than MLBoost (about 2.57 % for the boost-based system and 4.7 % for the MLBoost at 1000 W/m²). The power conservation from GPV to the grid is done with less losses and with a small reactive power when the system is connected to boost converter as shown in Fig.II.26, so the efficiency of the chain based boost converter is better than for the system based MLBoost as can be seen by Fig.II.27 (97.26 % for the boost based system and 92.2 % for the MLboost based system).

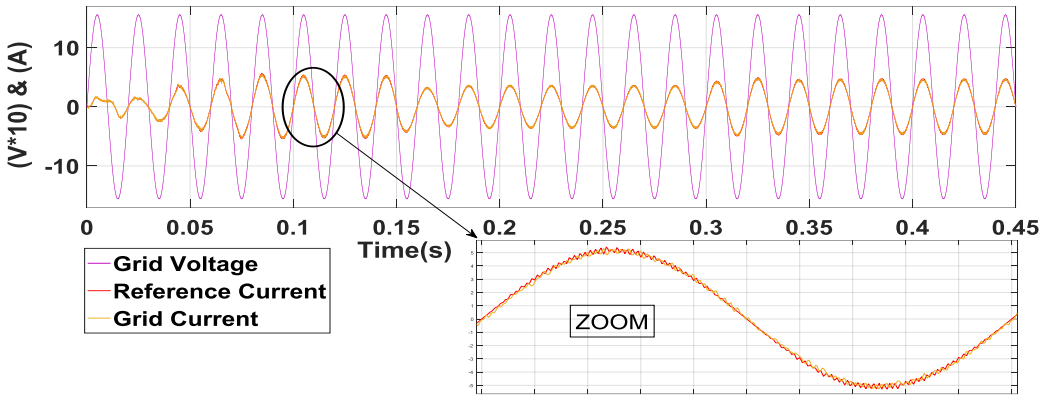

Figure II.21: Grid current and voltage using boost converter.

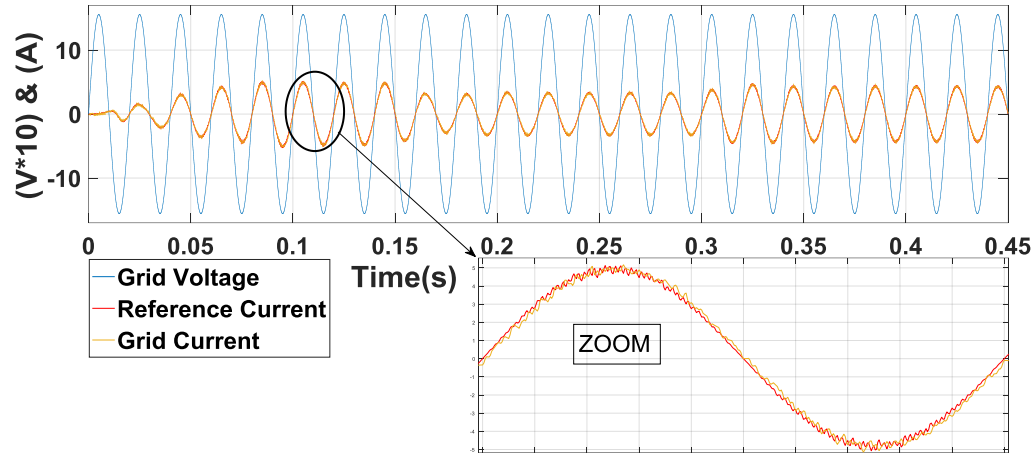

Figure II.22: Grid current and voltage using MLboost converter.

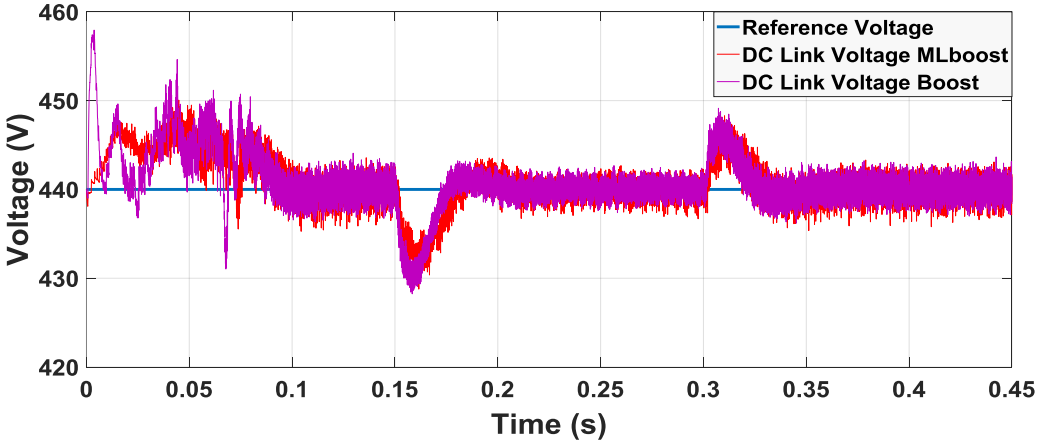

Figure II.23: DC link voltage comparison.

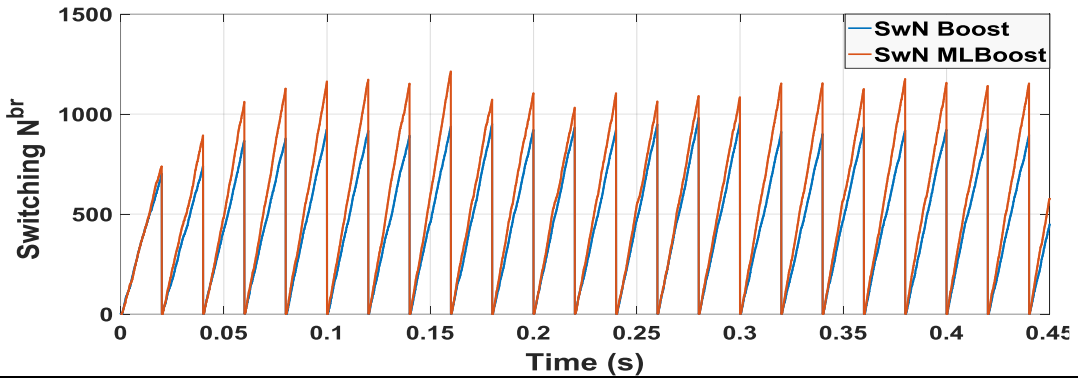

Figure II.24: comparison of the switching's number of the cascaded converters.

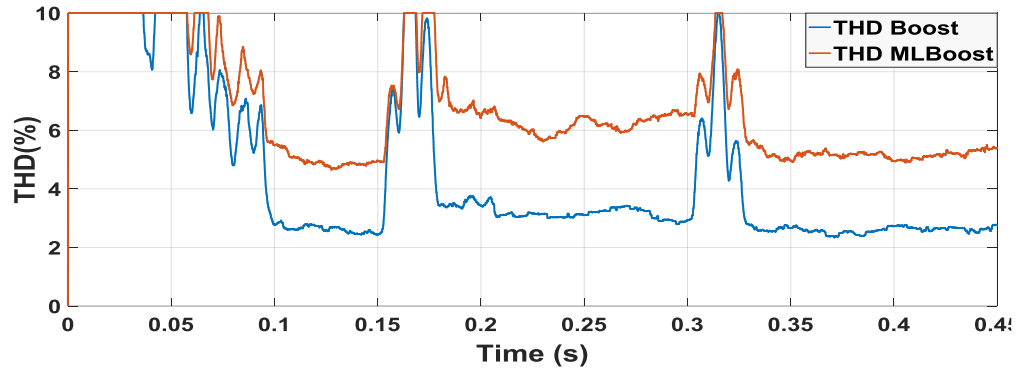

Figure II.25: Comparison of the grid current THD.

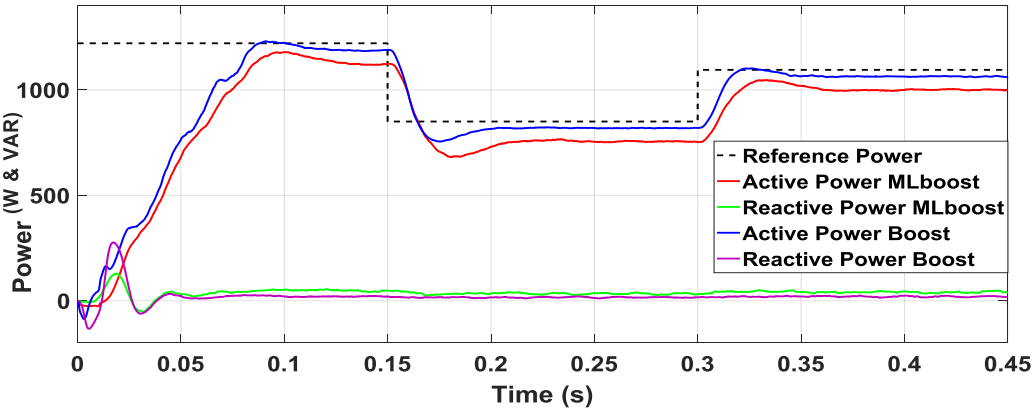

Figure II.26: Active and reactive grid powers of the two compared systems.

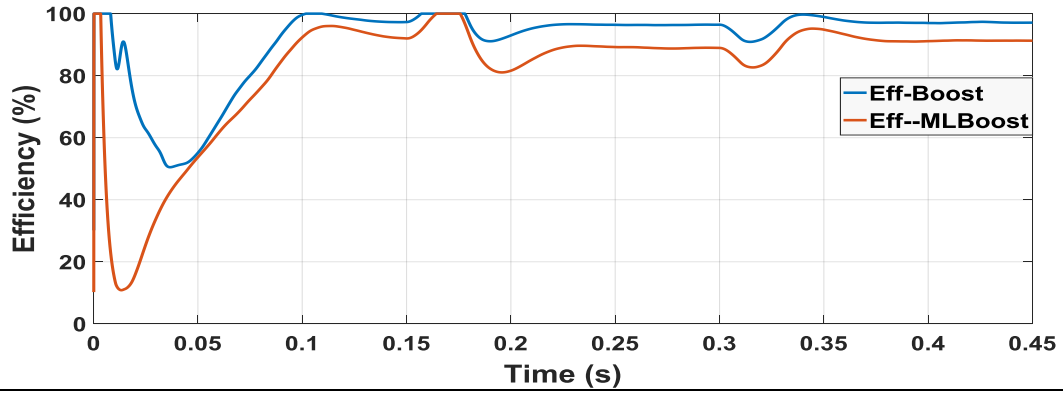

Figure II.27: Efficiencies of the grid–tied systems using the two step-up converters.

II.5. Conclusion

This chapter gives at first an overview about the finite set model predictive control (FS-MPC), its principle, and the most important features when it is applied on power converters.

At the second, we investigates the use of the FS-MPC on photovoltaic systems and its benefits. For that, a flexible FS-MPC method is presented and applied on stand-alone PV systems and grid connected PV systems, where, the used MPPT is a hybrid one based on the incremental conductance (Inc-Cond) and the MPC. Besides, in grid-tied PV systems the presented method controls the two-cascaded converters at the same time as a matrix converter instead to control each converter separately. Consequently, the global control system is extremely reduced.

A comparative study between the boost and multilevel boost converters is done under FS-MPC control for two kinds of systems, namely, the stand-alone system and the grid connected system. Over the different simulation results, it is easy to conclude that the performances of the PV system based boost converter are better than those obtained with MLboost converter in terms of efficiency, low grid current THD, dynamics and low ripples.

In addition, we can conclude that the FS-MPC is a preferred control for power converters and PV systems, where it opens many challenges and research axes in the way of improving system behaviors and efficiencies.

II.6. References

[1] J. G. Ortega et E. F. Camacho, « Mobile robot navigation in a partially structured static environment, using neural predictive control », *Control Engineering Practice*, vol. 4, nº 12, p. 1669-1679, déc. 1996, doi: 10.1016/S0967-0661(96)00184-0.

[2] L. Ljung, « System Identification », in *Signal Analysis and Prediction*, A. Procházka, J. Uhlíř, P. W. J. Rayner, et N. G. Kingsbury, Éd. Boston, MA: Birkhäuser, 1998, p. 163-173.

[3] E. F. Camacho et C. Bordons, *Model predictive control*. London ; New York: Springer, 2004.

[4] C. E. García, D. M. Prett, et M. Morari, « Model predictive control: Theory and practice—A survey », *Automatica*, vol. 25, nº 3, p. 335-348, mai 1989, doi: 10.1016/0005-1098(89)90002-2.

[5] D. W. Clarke, C. Mohtadi, et P. S. Tuffs, « Generalized predictive control—Part I. The basic algorithm », *Automatica*, vol. 23, nº 2, p. 137-148, mars 1987, doi: 10.1016/0005-1098(87)90087-2.

[6] V. Peterka, « Predictor-based self-tuning control », *Automatica*, vol. 20, nº 1, p. 39-50, janv. 1984, doi: 10.1016/0005-1098(84)90063-3.

[7] B. E. Ydstie, « Extended Horizon Adaptive Control », *IFAC Proceedings Volumes*, vol. 17, nº 2, p. 911-915, juill. 1984, doi: 10.1016/S1474-6670(17)61089-9.

[8] R. M. C. De Keyser et A. R. Van Cauwenberghe, « Extended Prediction Self-Adaptive Control », *IFAC Proceedings Volumes*, vol. 18, nº 5, p. 1255-1260, juill. 1985, doi: 10.1016/S1474-6670(17)60736-5.

[9] M. Morari, « Model Predictive Control: Multivariable Control Technique of Choice in the 1990s? », in *In Advances in Model-based Predictive Control*, 1990, p. 22–37.

[10] P. Eichenberger et M. Junger, « Predictive vector control of the stator voltages for an induction machine drive with current source inverter », in *PESC97. Record 28th Annual IEEE Power Electronics Specialists Conference. Formerly Power Conditioning Specialists Conference 1970-71. Power Processing and Electronic Specialists Conference 1972*, St. Louis, MO, USA, 1997, vol. 2, p. 1295-1301, doi: 10.1109/PESC.1997.616936.

[11] S. Vazquez, J. Rodriguez, M. Rivera, L. G. Franquelo, et M. Norambuena, « Model Predictive Control for Power Converters and Drives: Advances and Trends », *IEEE Transactions on Industrial Electronics*, vol. 64, nº 2, p. 935-947, févr. 2017, doi: 10.1109/TIE.2016.2625238.

[12] S. Vazquez *et al.*, « Model Predictive Control: A Review of Its Applications in Power Electronics », *IEEE Industrial Electronics Magazine*, vol. 8, nº 1, p. 16-31, mars 2014, doi: 10.1109/MIE.2013.2290138.

[13] S. E. I. Remache, A. Y. Cherif, et K. Barra, « Optimal cascaded predictive control for photovoltaic systems: application based on predictive emulator », *IET Renewable Power Generation*, vol. 13, nº 15, p. 2740-2751, nov. 2019, doi: 10.1049/iet-rpg.2019.0068.

[14] S. E. I. Remache, S. Remache, A. Y. Cherif, K. Barra, et A. Reama, « Stand-alone Photovoltaic System with integrated Energy Storage using Cascaded Predictive Direct Power Control », in *2019 1st International Conference on Sustainable Renewable Energy Systems and Applications (ICSRESA)*, Tebessa, Algeria, déc. 2019, p. 1‑6, doi: 10.1109/ICSRESA49121.2019.9182315.

[15] V. Yaramasu et B. Wu, *Model Predictive Control of Wind Energy Conversion Systems*. Hoboken, NJ, USA: John Wiley & Sons, Inc., 2017.

[16] A. M. A. Almaktoof, « MULTILEVEL INVERTERS USING FINITE SET- MODEL PREDICTIVE CURRENT CONTROL FOR RENEWABLE ENERGY SYSTEMS APPLICATIONS », p. 199.

[17] J. Rodriguez et P. Cortes, *Predictive Control of Power Converters and Electrical Drives: Rodriguez/Predictive Control of Power Converters and Electrical Drives*. Chichester, UK: John Wiley & Sons, Ltd, 2012.

[18] S. Kouro, P. Cortes, R. Vargas, U. Ammann, et J. Rodriguez, « Model Predictive Control—A Simple and Powerful Method to Control Power Converters », *IEEE Trans. Ind. Electron.*, vol. 56, nº 6, p. 1826‑1838, juin 2009, doi: 10.1109/TIE.2008.2008349.

[19] P. Cortes, M. P. Kazmierkowski, R. M. Kennel, D. E. Quevedo, et J. Rodriguez, « Predictive Control in Power Electronics and Drives », *IEEE Trans. Ind. Electron.*, vol. 55, nº 12, p. 4312‑4324, déc. 2008, doi: 10.1109/TIE.2008.2007480.

[20] V. Yaramasu, B. Wu, et J. Chen, « Model-Predictive Control of Grid-Tied Four-Level Diode-Clamped Inverters for High-Power Wind Energy Conversion Systems », *IEEE Trans. Power Electron.*, vol. 29, nº 6, p. 2861‑2873, juin 2014, doi: 10.1109/TPEL.2013.2276120.

[21] P. Cortes *et al.*, « Guidelines for weighting factors design in Model Predictive Control of power converters and drives », in *2009 IEEE International Conference on Industrial Technology*, Churchill, Victoria, Australia, févr. 2009, p. 1‑7, doi: 10.1109/ICIT.2009.4939742.

[22] R. E. Perez-Guzman et M. Rivera, « Weighting Factor Selection in Power Converters Based on Model Predictive Control », in *2020 Congreso Estudiantil de Electrónica y Electricidad (INGELECTRA)*, Santiago, Chile, avr. 2020, p. 1‑6, doi: 10.1109/INGELECTRA50225.2020.246963.

[23] H. Miranda, P. Cortes, J. I. Yuz, et J. Rodriguez, « Predictive Torque Control of Induction Machines Based on State-Space Models », *IEEE Trans. Ind. Electron.*, vol. 56, nº 6, p. 1916‑1924, juin 2009, doi: 10.1109/TIE.2009.2014904.

[24] T. Orłowska-Kowalska, F. Blaabjerg, et J. Rodríguez, Éd., *Advanced and Intelligent Control in Power Electronics and Drives*, vol. 531. Cham: Springer International Publishing, 2014.

[25] R. P. Aguilera, P. Lezana, et D. E. Quevedo, « Finite-Control-Set Model Predictive Control With Improved Steady-State Performance », *IEEE Trans. Ind. Inf.*, vol. 9, nº 2, p. 658‑667, mai 2013, doi: 10.1109/TII.2012.2211027.

[26] D. E. Quevedo, R. P. Aguilera, M. A. Perez, P. Cortes, et R. Lizana, « Model Predictive Control of an AFE Rectifier With Dynamic References », *IEEE Trans. Power Electron.*, vol. 27, nº 7, p. 3128‑3136, juill. 2012, doi: 10.1109/TPEL.2011.2179672.

[27] R. Vargas, U. Ammann, et J. Rodriguez, « Predictive Approach to Increase Efficiency and Reduce Switching Losses on Matrix Converters », *IEEE Trans. Power Electron.*, vol. 24, nº 4, p. 894‑902, avr. 2009, doi: 10.1109/TPEL.2008.2011907.

[28] P. Cortes, J. Rodriguez, D. E. Quevedo, et C. Silva, « Predictive Current Control Strategy With Imposed Load Current Spectrum », *IEEE Trans. Power Electron.*, vol. 23, nº 2, p. 612‑618, mars 2008, doi: 10.1109/TPEL.2007.915605.

[29] H. Aggrawal, J. I. Leon, L. G. Franquelo, S. Kouro, P. Garg, et J. Rodriguez, « Model predictive control based selective harmonic mitigation technique for multilevel cascaded H-bridge converters », in *IECON 2011 - 37th Annual Conference of the IEEE Industrial Electronics Society*, Melbourne, Vic, Australia, nov. 2011, p. 4427‑4432, doi: 10.1109/IECON.2011.6120037.

[30] H. Miranda, R. Teodorescu, P. Rodriguez, et L. Helle, « Model predictive current control for high-power grid-connected converters with output LCL filter », in *2009 35th Annual Conference of IEEE Industrial Electronics*, Porto, Portugal, nov. 2009, p. 633‑638, doi: 10.1109/IECON.2009.5414994.

[31] « L'énergie solaire pourrait dominer les énergies renouvelables en 2030 ». https://www.notre-planete.info/actualites/4177-energie-solaire-evolution (consulté le mai 01, 2021).

[32] P. E. Kakosimos et A. G. Kladas, « Implementation of photovoltaic array MPPT through fixed step predictive control technique », *Renewable Energy*, vol. 36, nº 9, p. 2508‑2514, sept. 2011, doi: 10.1016/j.renene.2011.02.021.

[33] K. Barra et D. Rahem, « Predictive direct power control for photovoltaic grid connected system: An approach based on multilevel converters », *Energy Conversion and Management*, vol. 78, p. 825‑834, févr. 2014, doi: 10.1016/j.enconman.2013.06.064.

[34] M. Ismeil, *High Performance Finite Control Set-Model Predictive Controller Algorithm for Quasi Z-Source Inverter*. 2015.

[35] T. Esram et P. L. Chapman, « Comparison of Photovoltaic Array Maximum Power Point Tracking Techniques », *IEEE Trans. On Energy Conversion*, vol. 22, nº 2, p. 439‑449, juin 2007, doi: 10.1109/TEC.2006.874230.

[36] H. Mahmoudi, P. Moamaei, M. Aleenejad, et R. Ahmadi, « A new maximum power point tracking method for photovoltaic applications based on finite control set model predictive control », in *2017 IEEE Applied Power Electronics Conference and Exposition (APEC)*, Tampa, FL, USA, mars 2017, p. 1111‑1115, doi: 10.1109/APEC.2017.7930834.

[37] M. Aleenejad, H. Mahmoudi, R. Ahmadi, et H. Iman-Eini, « A New High-Switching-Frequency Modulation Technique to Improve the DC-Link Voltage Utilization in Multilevel Converters », *IEEE Trans. Ind. Electron.*, vol. 64, nº 3, p. 1807‑1817, mars 2017, doi: 10.1109/TIE.2016.2623256.

[38] M. Aleenejad, H. Mahmoudi, et R. Ahmadi, « A Fault-Tolerant Strategy Based on Fundamental Phase-Shift Compensation for Three-Phase Multilevel Converters With Quasi-Z-Source Networks With Discontinuous Input Current », *IEEE Trans. Power Electron.*, vol. 31, nº 11, p. 7480‑7488, nov. 2016, doi: 10.1109/TPEL.2016.2520884.7480-7488, 2016.

[39] S. Bououden, O. Hazil, S. Filali, et M. Chadli, « Modelling and model predictive control of a DC-DC Boost converter », in *2014 15th International Conference on Sciences and Techniques of Automatic Control and Computer Engineering (STA)*, Hammamet, Tunisia, déc. 2014, p. 643‑648, doi: 10.1109/STA.2014.7086663.

[40] M. B. Shadmand, M. Mosa, R. S. Balog, et H. A. Rub, « An improved MPPT technique for high gain DC-DC converter using model predictive control for photovoltaic applications », in *2014 IEEE Applied Power Electronics Conference and Exposition - APEC 2014*, Fort Worth, TX, USA, mars 2014, p. 2993‑2999, doi: 10.1109/APEC.2014.6803730.

[41] M. Mousa, M. E. Ahmed, et M. Orabi, « New converter circuitry for high v applications using Switched Inductor Multilevel Converter », in *2011 IEEE 33rd International Telecommunications Energy Conference (INTELEC)*, Amsterdam, Netherlands, oct. 2011, p. 1‑8, doi: 10.1109/INTLEC.2011.6099811.

[42] O. Abdel-Rahim, M. Orabi, et M. E. Ahmed, « High gain single-stage inverter for photovoltaic AC modules », in *2011 Twenty-Sixth Annual IEEE Applied Power Electronics Conference and Exposition (APEC)*, Fort Worth, TX, USA, mars 2011, p. 1961‑1967, doi: 10.1109/APEC.2011.5744865.

Chapter III

Optimal Cascaded Predictive Control for Photovoltaic Systems: application based on predictive emulator

III. Optimal cascaded predictive control for photovoltaic systems : application based on predictive emulator

III.1. Introduction:

The increase in global consumption of energy has made a big step towards the installation of smart grid, micro-grid and smart homes. The photovoltaic (PV) solar panels depend primarily on climatic conditions such as temperature and irradiance, where they provide limited output power with low efficiency because of their non-linear characteristics [1, 2]. For this, a maximum power point tracking (MPPT) block is always connected between the PV solar panels and the load, thus playing a pivotal role in extracting the maximum power [3, 4]. Several MPPT algorithms are suggested in recently specialized literature, and most of the theme are discussed in [5]. These MPPT control methods differ from each other in terms of dynamic convergence, oscillation around the maximum power point, simplicity of implementation, sensor requirements, energy efficiency, cost and parametric sensitivity.

The effectiveness of these algorithms is rigorously tested in real conditions, and it is necessary to change the irradiation and temperature under predefined profiles. For example, the profile of the irradiance can be changed using a controllable light-emitting diode (LED) or a halogen lamp, which is fed by a controllable stabilized power supply, where it requires a high power to create the irradiance variations. Despite that, these procedures cannot make a sudden profile to test the dynamic response of the MPPT algorithms properly. Therefore, these methods are not recommendable since temperature manipulation is not manageable [6]. The importance of these algorithms and their tests have allowed researchers to invent equivalent to PV panel called PV emulators considered as a useful tool for testing the performance of MPPT power converters under hard climatic conditions.

The PV emulator can imitate the non-linear characteristics of the PV panel based on a non-linear direct current (DC) source [6]. The basic idea of emulating PV characteristics was firstly introduced with the single diode-based approximation techniques, then, modified using the double diode model, more accurate at the expense of the model complexity. Based on these two essential models, researchers have tested the irradiance and temperature variations on MPPT algorithms and proved that these techniques imitate exactly the I-V and P-V curves [1].

Generally, PV emulator system is composed of three essential parts: the PV model part, producing the reference signal to the control stage. The second part is the control strategy, and at last, the power converter part. Basic topologies of power converters such as boost, buck and z-source are highly integrated into photovoltaic applications, due to their suitability, robustness, reliability and efficiency [7]. As it is well known that the performance of the PV emulators depends mostly on the accuracy, realization cost, level of complexity, sensitivity to climatic conditions, hardware implementation and efficiency, the choice of the control and modulation technique is an essential task to fulfil the requirements of PV emulators. Many structures of PV emulators have been reported in [1] and [6] such as the resistance comparison method [8], Lambert ω based method [9], the hybrid-mode controlled method [10] and the direct referencing method [11]. Usually, these methods based on primary linear controllers, are commonly used in PV emulators because of their simplicity but characterized by the inadequate dynamic response, sensitivity to climatic conditions and lack of precision since significant error values are detected mainly in the open-circuit and short-circuit operating zones and are therefore rarely used [1]. To overcome these limitations, advanced control techniques such as Finite Set Model Predictive Control (FS-MPC) which is also considered as a powerful control technique well suited for power converters, appears recently as a robust control method that can fulfil the requirements of PV emulators.

Finite Set Model Predictive Control (FS-MPC) has practically dominated the control of power converters and becomes a desirable strategy due to its simplicity, rapidity, flexibility and robustness. Based on the discrete-time model, FS-MPC can predict the behavior of the system using the possible switching states of the power converter. The method uses a cost function for minimization, and the optimal switching state will be applied at the next sampling interval [12]. FS-MPC proved its performance on several applications such as electrical drives [13], wind turbine [14, 15], energy management for smart and micro-grid [16, 17] and photovoltaic applications [18--20].

In this chapter, a new PV emulator based on FS-MPC is proposed (P-PVE) with high performance compared to a conventional one. Then, a flexible cascaded predictive control strategy is presented for two kinds of PV system applications, namely, stand-alone and grid-connected systems. The used cascaded power converters are treated as an indirect matrix converter using only one cost function and then controlled in one stage. Consequently, the global control system is widely reduced.

The chapter is organized as follows; Section 2 presents the topology of the proposed predictive PV emulator (P-PVE). Then, a stand-alone photovoltaic system using the P-PVE is presented in Section 3, whereas, Section 4 is dedicated to the performance of the P-PVE in a grid-connected system using the cascaded predictive control (CPC). Section 5 illustrates the simulation results and discussions. Section 6 shows the experimental test bench of the developed P-PVE and the proposed CPC strategy for both stand-alone and grid-connected systems. Moreover, several experimental results are shown and discussed.

III.2. Photovoltaic emulators design

III.2.1. Brief overview of photovoltaic emulators

As mentioned in [6] and shown in Fig.III.1, PV emulators can be divided into three main parts as:

a- The PV solar panel model considered as the first part providing the referencing signal used to imitate the real PV characteristics after receiving irradiance, temperature and PV voltage as inputs. The PV model is calculated in real-time in order to confer the accuracy for the PV emulator.
b- The second part is the control strategy. This part represents the heart of the PV emulator and considered as the responsible of the obtained tracking performance.
c- At last, the power converter, considered as the executing element of the PV emulator, is able to transform the mathematical model into real and measurable electric parameters.

III.2.2. Modelling of photovoltaic solar panel

In order to assess the behavior of the PV emulator, the mathematical model of the solar panel is a key factor where it gives more accuracy to emulate PV panel characteristics. Many equivalent electrical circuits have been proposed to allow researchers to extract the mathematical model of the PV panel. Among them, there are the ones based on single and double diodes, and additionally, the three diodes model, this last one is less available in the literature [2]. The single diode model is mostly used due to its simplicity and efficacy; for this reason, a single diode model presented in [21] and shown in Fig.III.2, is chosen in this research.

The photon generated current I_{ph} is related to the solar radiation G and temperature T by:

$$I_{ph} = (I_{sc} + K_i(T - 298))\frac{G}{1000} \quad \text{(III.1)}$$

Where I_{sc} is the short-circuit current of the cell at 25°C, K_i is the cell short-circuit current temperature coefficient in A/°C, T is the cell temperature and G is the solar radiation in W/m².

The relationship between the PV output current I_{PV} and voltage V_{PV}, well known as the I-V characteristic of the PV cells, is given by :

$$I_{PV} = I_{ph} - I_s\left(e^{\frac{V_{PV}+I_{PV}R_s}{nN_{se}V_t}} - 1\right) - \frac{V_{PV}+I_{PV}R_s}{R_{sh}} \quad \text{(III.2)}$$

Where, I_s is the dark saturation current, R_s and R_{sh} are the series and shunt resistances of the solar panel respectively, n is the diode quality factor, N_{se} is the number of series-connected PV cells in the PV panel, V_t is the solar cell thermal voltage defined as $V_t = kT/q$. Where k is Boltzmann constant (1.38×10^{-23} J/K), q is the elementary charge (1.6×10^{-19} C), and T is P-N junction temperature in kelvin.

III.2.3. Photovoltaic emulator based on PI controller

In this section, the direct referencing method is used for the PV emulator due to its simplicity, and it is more commonly found in PV emulators using switched-mode power supply system (SMPS), with the V_{PV} as the PV solar panel model input. The control scheme of the buck converter is shown in Fig.III.5.

At first, the output voltage from the buck converter V_{PV} is equal to zero, so, the PV solar panel model generates the reference current signal I_{Le}^{ref}, which is equal to the short circuit current I_{sc} at the given irradiance G and temperature T. Then, when V_{PV} increases, I_{Le}^{ref} begins to decrease smoothly as in the I-V characteristic curve of the PV panel. Down to the optimal point, the PV emulator reaches a stable state when the ratio of the output voltage V_{PV} to the output current I_{Le} corresponds to the output resistive load R [6].

III.2.3.1. Buck converter modelling and control

The buck converter circuit is modeled based on its switch operations and using Kirchhoff's circuit laws. The obtained model of the buck converter is used to derive the transfer function relation between the input current I_{Le} and the output duty cycle D. According to the behavior of the buck converter and by choosing (I_{Le}, V_{PV}) as the state variables of the system, the modelling is divided into two parts when the switch T_1 is ON, then when it is OFF.

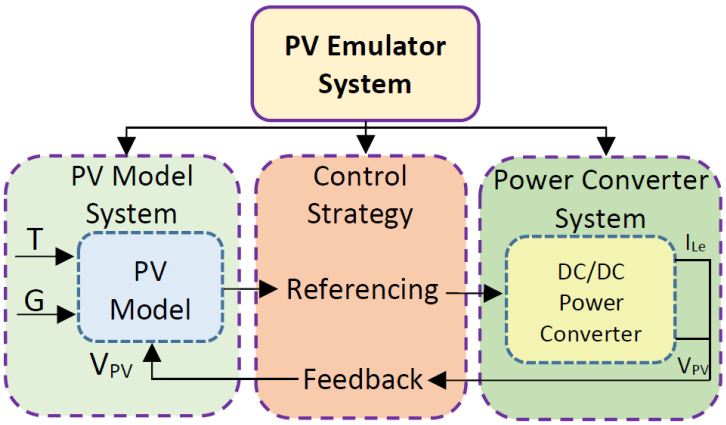

Figure III.1: The three main parts of the PV emulator system [6].

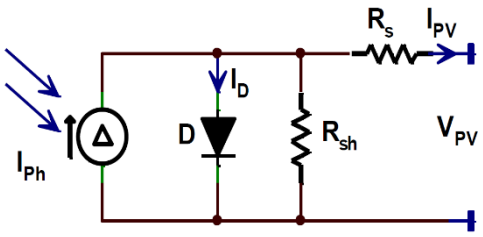

Figure III.2: Equivalent circuit of single-diode solar cell model.

When the switch T_1 is ON, we get the following equation:

$$\begin{cases} \frac{dI_{Le}}{dt} = \frac{V_{C_f}}{L_e} - \frac{V_{PV}}{L_e} \\ \frac{dV_{PV}}{dt} = \frac{I_{Le}}{C} - \frac{V_{PV}}{R.C} \end{cases} \quad \text{(III.3)}$$

Then, when the switch T_1 is turned OFF, we obtain the following equation:

$$\begin{cases} \frac{dI_{Le}}{dt} = -\frac{V_{PV}}{L_e} \\ \frac{dV_{PV}}{dt} = \frac{I_{Le}}{C} - \frac{V_{PV}}{R.C} \end{cases} \quad \text{(III.4)}$$

Now, a common behavior model of the buck converter is given by:

$$\begin{bmatrix} \frac{dI_{Le}}{dt} \\ \frac{dV_{PV}}{dt} \end{bmatrix} = \begin{bmatrix} 0 & -\frac{1}{L_e} \\ \frac{1}{C} & -\frac{1}{R.C} \end{bmatrix} \times \begin{bmatrix} I_{Le} \\ V_{PV} \end{bmatrix} + \begin{bmatrix} \frac{V_{C_f}}{L_e} \\ 0 \end{bmatrix} \times D \quad \text{(III.5)}$$

As the output current is the variable to be regulated, the transfer function $G_p(s)$ of the converter is derived as follows:

$$G_p(s) = \frac{I_{Le}(s)}{D(s)} = \frac{V_{C_f}}{R} \times \frac{1}{\left(1+s\frac{L_e}{R}+s^2 L_e C_1\right)} \quad \text{(III.6)}$$

The PI controller transfer function $G_c(s)$ is given by:

$$G_c(s) = \frac{K_P s + K_i}{s} \quad \text{(III.7)}$$

Traditionally, the PI controller is designed for PV emulators in order to regulate the converter output current with acceptable stability margins and minimal steady-state error [2]. The Bode plot of both uncompensated and the compensated system are shown in Fig.III.4 where a phase margin of 56.2° is well suited with a crossover frequency at 451 rad/s allowing the design values of the PI regulator $K_p = 0.1483$ and $K_i = 7.7100$.

The values of the designed components of the step-down converter (inductance L_e and capacitorC_1) are chosen according to the switching frequency, the continuous conduction mode and the ripple factor. Their selection procedure is given in [6]. For proper behavior of the PV emulator, the ripple factor must be less than 2%. In addition, the step-down converter must operate in a continuous conduction mode, according to the load values and the switching frequency. For high switching frequencies, a small inductance is required; the opposite case happens for low switching frequencies.

The minimum value of the inductance $L_{e_{min}}$ to preserve the continuous conduction mode for the buck converter is given by:

$$L_{e-min} = \frac{(1-D).R}{2.f} \quad \text{(III.8)}$$

Where, D is the duty cycle, R is the output resistance, and f is the switching frequency.

Furthermore, the capacitor affects ripple factor, when it is large, the ripple factor is small, but conversely, it gives the PV emulator an inadequate dynamic response. The following equation can determine the value of the capacitor as follows:

$$C_1 = \frac{1-D}{8 L_e r_V f^2} \quad \text{(III.9)}$$

Where, L_e is the buck converter inductance, r_v is the output voltage ripple factor $\frac{\Delta V_0}{V_0}$.

Equations (III.8) and (III.9) are used to calculate the component values of the buck converter correctly. For a switching frequency of 10 kHz, the inductance value preserving the continuous conduction mode is chosen to be 10 mH, and the capacitance is settled to 680 µF.

With these values, the PV emulator works properly with voltage ripples of 0.0005 V as it is shown in Fig. III.3. The PV emulator based on PI controller proved acceptable performances in the presence of sudden illumination variations, but still sensible to load variation of the model, making the system in need of different gain values. To avoid this deficiency, researchers developed PV emulators based on advanced controllers such as in [21, 22]. Based on these advanced researches and other recent ones, the P-PVE is proposed.

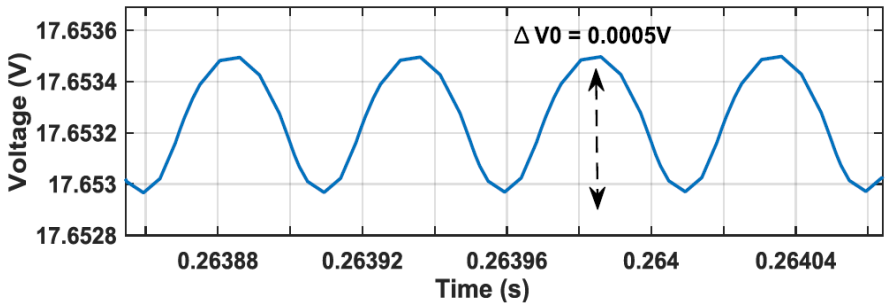

Figure III.3: Output voltage ripples of the buck converter (based on PI controller).

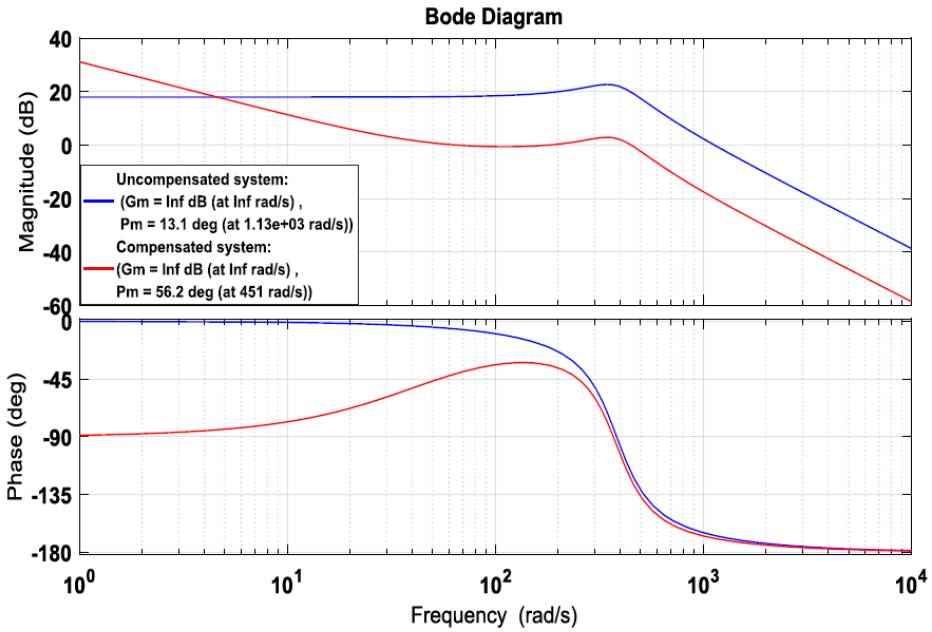

Figure III.4: Bode plot of the uncompensated system with the open-loop system.

III.2.4. Proposed photovoltaic emulator based on FS-MPC

Finite Set Model Predictive Control (FS-MPC) has become the most common control of power electronic converters since it offers high efficiency, low voltage and current ripples and fast dynamic response [12]. Its robustness lies on switching states of power converters by evaluating a cost function subject to minimization in only possible switching states [4]. FS-MPC has been applied in most power converter systems and recently in PV system applications [3, 18]. Despite these investigations, FS-MPC has not been applied for PV emulators.

In this section, a predictive PV emulator named P-PVE is presented and shown in Fig. III.5. The P-PVE is based on the synchronous buck converter mentioned above, sized with the same component values indicated in subsection three and it is modelled using the ON/OFF switch operations.

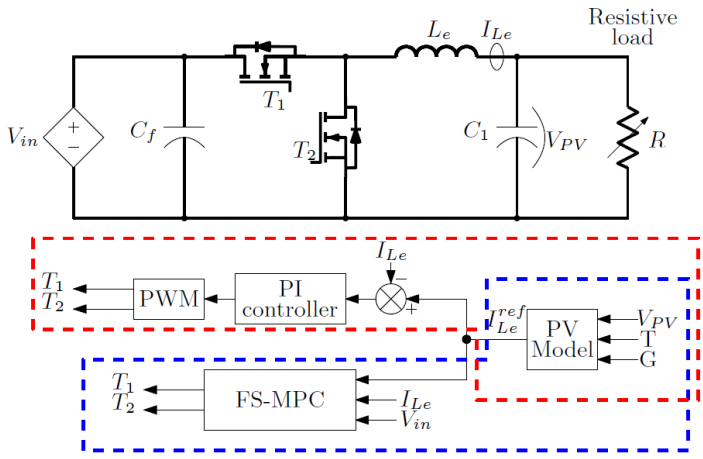

Figure III.5: Scheme of PV emulator with two kinds of controllers (the PI controller in red) and (the FS-MPC in blue).

III.2.4.1. Discrete time model of the buck converter

Taking into account the internal resistor r_{Le} of the inductance $L_e$and using the equations (III.3) when the switch is ON and (III.4) when the switch is OFF, the predicted equations for the two switch states using Euler forward approximation, are as follows:

When the switch is ON:

$$\begin{cases} I_{Le}(k+1) = \left(1 - \left(\frac{T_s}{L_e} * r_{Le}\right)\right) * I_{Le}(k) - \frac{T_s}{L_e} * \left(V_{PV}(k) - V_{C_f}(k)\right) \\ V_{PV}(k+1) = \left(1 - \frac{T_s}{R.C_1}\right) * V_{PV}(k) + \frac{T_s}{C_1} * I_{Le}(k) \end{cases} \quad \text{(III.10)}$$

Then, when the switch is turned OFF:

$$\begin{cases} I_{Le}(k+1) = \left(1 - \left(\frac{T_s}{L_e} * r_{Le}\right)\right) * I_{Le}(k) - \frac{T_s}{L_e} * V_{PV}(k) \\ V_{PV}(k+1) = \left(1 - \frac{T_s}{R.C_1}\right) * V_{PV}(k) + \frac{T_s}{C_1} * I_{Le}(k) \end{cases} \quad \text{(III.11)}$$

These equations are rearranged in a common predictive model and presented by a matrix form corresponding to the switch state S as given by (III.12), then it is used in the proposed predictive algorithm for PV emulators as it is shown in the flowchart of Fig. III.6.

$$\begin{bmatrix} I_{Le}(k+1) \\ V_{PV}(k+1) \end{bmatrix} = \begin{bmatrix} (1 - \frac{r_{Le}}{L_e} T_s) & -\frac{T_s}{L_e} \\ \frac{T_s}{C_1} & (1 - \frac{T_s}{R.C_1}) \end{bmatrix} . \begin{bmatrix} I_{Le}(k) \\ V_{PV}(k) \end{bmatrix} + \begin{bmatrix} \frac{T_s}{L_e} S \\ 0 \end{bmatrix} . V_{C_f}(k) \quad \text{(III.12)}$$

III.2.4.2. Proposed predictive algorithm

In each sampling time, the proposed P-PVE algorithm of Fig. III.6 receives the measures of the input voltage $V_{C_f}(k)$, the inductance current $I_{Le}(k)$ and the output voltage $V_{PV}(k)$. When $V_{C_f}(k)$ supplies the buck converter, as shown in Fig. III.5, the current $I_{Le}(k)$ begins to circulate, and the predicted current model is calculated based on inputs and switch states according to the relationship (III.12). The cost function is formulated that contains two predicted current errors according to S. The cost function g given by (III.13) is subject to minimization, and the optimal switching state is selected to be applied in the next sampling time.

$$g = \left| I_{Le}^{P} - I_{Le}^{ref} \right| \quad \text{(III.13)}$$

Recently, many commercialized emulators have a variable cost according to the used range power from 6000 $ (Elgar ETS60X14C-PVF) to 21.000 $ (Magna Power TSD50050240) [6], the cost of the P-PVE is under evaluation. The performance of the realized P-PVE, in terms of dynamic response, reference tracking, and current oscillations, is compared to the commonly used one based on the PI controller and is given by Table III.1.

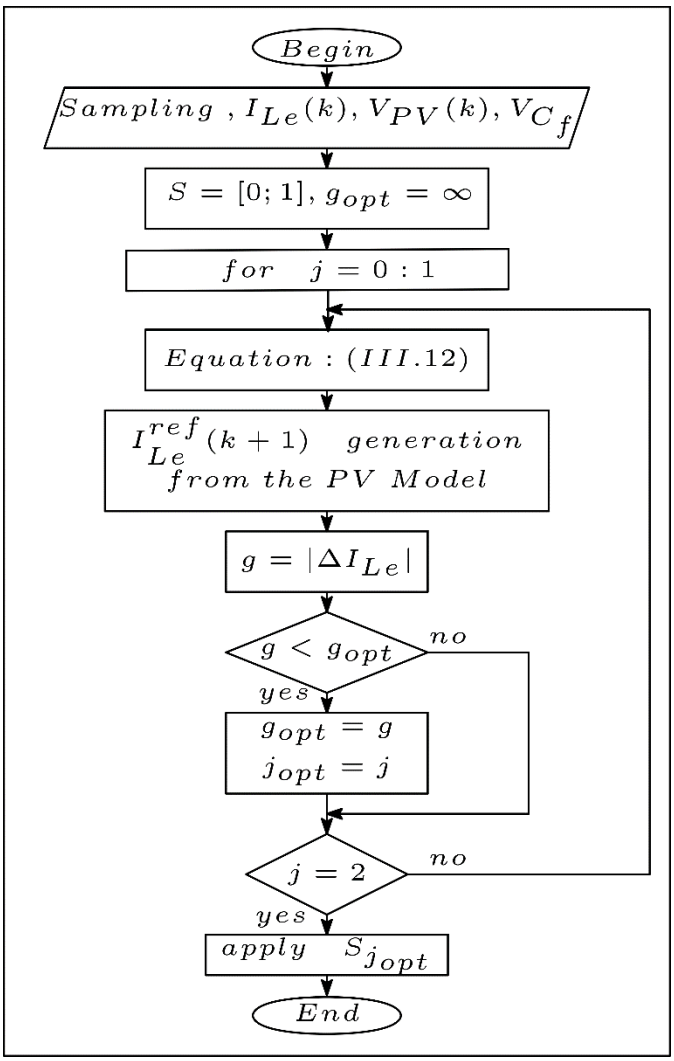

Figure III.6: Flowchart of the proposed P-PVE algorithm.

Table III.1: Performance comparison between the P-PVE and the PI-PVE.

Parameter	P-PVE	Emulator based on PI	Unit
Experimental dynamic response	4	18	ms
Experimental reference tracking	4	10	ms
Experimental oscillations	0.08	0.085	A
Simulated dynamic response	3	5.5	ms
Simulated reference tracking	0.8	5	ms
Simulated oscillations	0.04	0.045	A
Efficiency	High	Medium	-

III.3. Proposed cascaded predictive control for stand-alone systems (SAS)

Generally, PV emulators are mostly used in cascade with the boosting stage in PV applications, where the power system includes two power converters placed in a cascade structure, as shown in Fig. III.7 The control system needs to control each power converter separately, requiring more calculators and more controllers, which is not suited practically.

In this section, a suitable cascaded predictive control called CPC is proposed having the following aims:

a- Treat the system topology as a single power converter by controlling it using a single predictive controller, programmed in the same calculator. Consequently, the global control system is widely reduced.

b- Directly include the MPPT algorithm in the predictive controller.

III.3.1. Discrete time model of the boost converter

A DC-DC boost converter is connected to the PV emulator (considered as a real PV module) in order to supply the resistive load R as shown in Fig. III.7. The predicted model of the buck converter is given in the previous section, and the predicted model of the boost converter is defined according to its switch operations. For more accuracy, the internal resistance r_L of the Boost inductance is taken into account.

The predicted model of the Boost converter when the switch T_3 is ON can be given by (III.14):

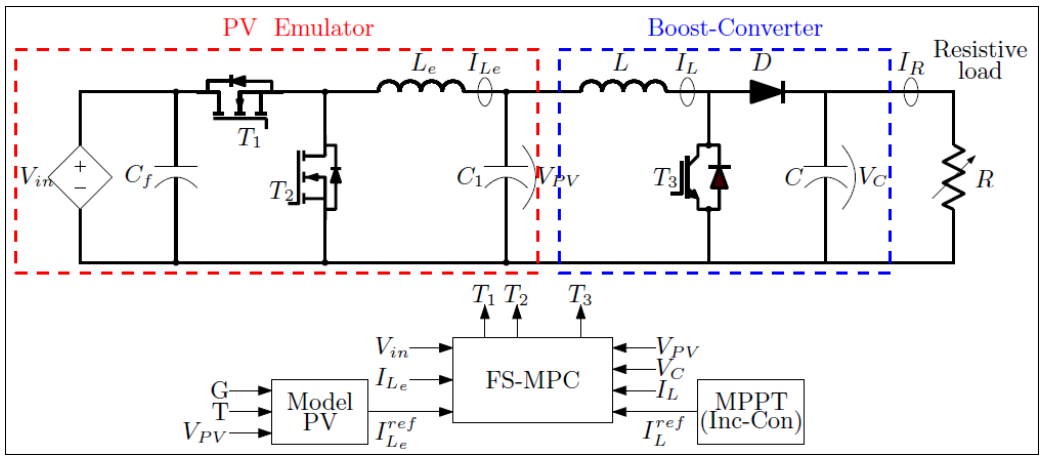

Figure III.7: The stand-alone PV system with the proposed cascaded predictive control.

$$\begin{cases} I_L(k+1) = \left(1 - \left(\frac{T_s}{L} * r_L\right)\right) * I_L(k) - \frac{T_s}{L} * V_{PV}(k) \\ V_{PV}(k+1) = V_{PV}(k) + \frac{T_s}{C_1} * (I_{Le}(k) - I_L(k)) \end{cases} \quad \text{(III.14)}$$

Then, when it is OFF, we get:

$$\begin{cases} I_L(k+1) = \left(1 - \left(\frac{T_s}{L} * r_L\right)\right) * I_L(k) - \frac{T_s}{L} * \left(V_{PV}(k) - V_C(k)\right) \\ V_{PV}(k+1) = V_{PV}(k) + \frac{T_s}{C_1} * (I_{Le}(k) - I_L(k)) \end{cases} \quad \text{(III.15)}$$

The equations (14) and (15) are rearranged in order to decrease the number of input variables by means of reducing current sensor of $I_{Le}(k)$, then they are grouped in a common predictive model corresponding to the switches states, and they are represented in a matrix form by (III.16).

$$\begin{bmatrix} I_L(k+1) \\ V_{PV}(k+1) \end{bmatrix} = \begin{bmatrix} (1 - \frac{r_L}{L} T_s) & \frac{T_s}{L} & -(1-S)\frac{T_s}{L} \\ 0 & 2 & 0 \end{bmatrix} . \begin{bmatrix} I_L(k) \\ V_{PV}(k) \\ V_C(k) \end{bmatrix} + \begin{bmatrix} 0 \\ -1 \end{bmatrix} . V_{PV}(k-1) \quad \text{(III.16)}$$

Where, S represents the four possible working operations of the cascaded converters of Fig. III.7.

The proposed algorithm of Fig. III.8 has three treatment steps before generating control signals, and they can be summarized as follows:

a- Calculate the predicted currents for one step ahead by using inputs and based on the four possible switching states of the two cascaded converters.

b- The hybrid MPPT algorithm is based on the Incremental conductance one that generates the predicted reference current of the boost converter. In contrast, the PV panel model generates the reference current for the buck emulator converter.

c- The cost function g of (III.17) is now formulated, and it contains two predicted current errors, which should be minimized before selecting the optimal switching state.

$$g = \left|I_{Le}^{P} - I_{Le}^{ref}\right| + \left|I_{L}^{P} - I_{L}^{ref}\right| \quad \text{(III.17)}$$

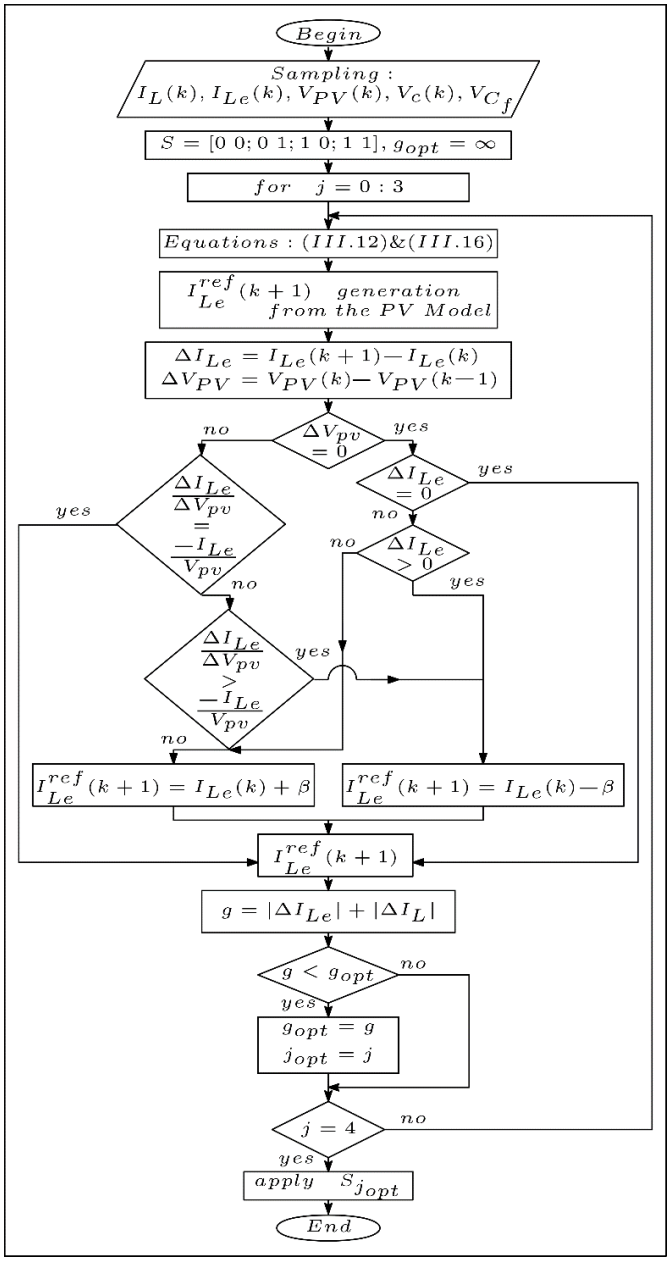

Figure III.8: Flowchart of the proposed control for stand-alone PV systems.

III.4. Proposed cascaded predictive control for grid-connected systems (GCS)

With the huge demands on photovoltaic installations, the PV systems can become even more decentralized, vulnerable with a poor efficiency [23]. Advanced control strategies should be developed and merged into the control system to exploit better the energy potential from a wide scale of PV systems. Besides, advanced testing methods are required for allowing PV grid-connected systems to improve their efficacy by providing good current and voltage waveforms

with fewer ripples and less losses. In this section, the previous P-PVE is now used in a GCS application composed of three cascaded power converters, as given by Fig. III.9.

III.4.1. The Grid-connected system description

The P-PVE and the Boost converter (used for ensuring the MPPT functioning) are now cascaded to a single-phase H-bridge inverter that is used as a configuration for residential PV applications, to thoroughly test a prototype of a grid-tied photovoltaic system as it is shown by Fig. III.9.

The DC link stage is adopted to an appropriate power injection by controlling the AC side, so the DC link voltage V_C is kept to 80V for a 50V/50Hz AC grid system bench. The orthogonal signal generation (OSG) and a phase detection blocks are used for shaping the injected current, which has to be purely sinusoidal and synchronized with the grid voltage. In the normal operation mode of synchronization, a phase-locked loop (PLL) is usually used, such as in [24]. In this paper, the synchronization is done with the use of a trigonometric function, and the value of the reference grid current is obtained using the method mentioned in [25, 26].

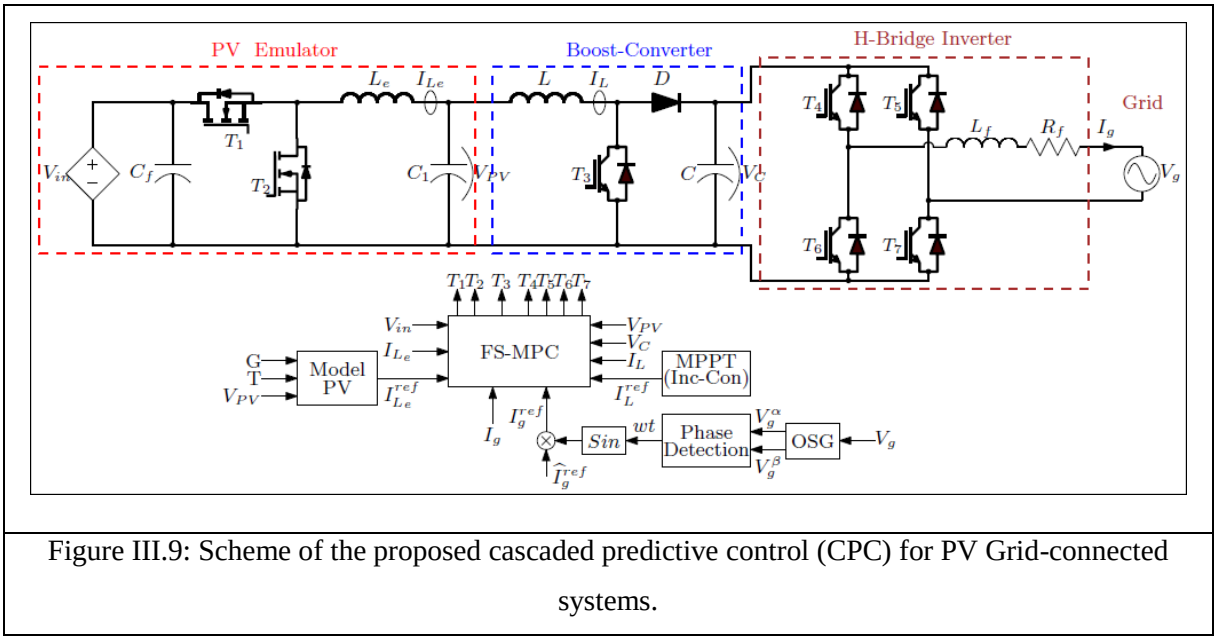

Figure III.9: Scheme of the proposed cascaded predictive control (CPC) for PV Grid-connected systems.

III.4.1.1. DC bus voltage regulation and grid reference current generation

The DC bus voltage must be kept to a constant value by adjusting the available extracted power from the PV emulator and according to the illumination levels [27]. Assuming for

simplification reasons that $P_{PV} = P_{out}$ [25]. The value of the grid reference current can be obtained by using the equation (III.18) that is mentioned in [25, 26] as follows:

$$I_g^{ref_{max}} = K \times \frac{I_{Le}(K+1) \times V_{PV}(K+1)}{V_g} \quad \text{(III.18)}$$

Where, K is a constant value adjusted according to the illumination levels and the efficiency of the system.

After obtaining the magnitude value of the grid reference current by (III.18), an OSG module is used to shape the grid reference current. An extra block is used to detect the grid voltage phase, in order to obtain a pure sinusoidal reference current that is synchronized with the grid voltage [28, 29] as the scheme of Fig. III.9 illustrates it. This method has the advantage that the global control system does not need an outer DC link voltage PI controller.

III.4.1.2. Discrete time model of the H-Bridge inverter

The H-Bridge inverter shown in Fig. III.9 is mostly used for residential PV applications as well as in modular multilevel inverter type, to increase output voltage levels and to provide high power quality [30].

The output voltage vector of the inverter $v(k)$ is related to the DC link voltage $V_C(k)$ by the following equation (III.19) as in [28]:

$$v(k) = \Psi(t) \times V_C(k) \quad \text{(III.19)}$$

Where:

$$\Psi(t) = S_{T4}(t)S_{T7}(t) - S_{T6}(t)S_{T5}(t) \quad \text{(III.20)}$$

The control of the H-Bridge inverter requires a discrete-time model of the grid, which can be defined from the following continuous-time equation (III.21):

$$v(k) = R_f . I_g(k) + L_f \frac{dI_g(k)}{dt} + V_g(k) \quad \text{(III.21)}$$

Where, $I_g(k)$ is the grid current, R_f is the grid filter resistance, L_f is the grid filter inductance, and $V_g(k)$ is the grid voltage vector, and it is assumed to be sinusoidal with constant frequency and constant amplitude.

By applying Euler approximation method to the derivative $\frac{dI_g}{dt}$ as follows:

$$\frac{dI_g}{dt} = \frac{I_g(k+1) - I_g(k)}{T_S} \tag{III.22}$$

The predicted grid current for one-step-ahead can be given as:

$$I_g(k+1) = (1 - R_f \frac{T_S}{L_f})\, I_g(k) + \frac{T_S}{L_f}(v(k) - V_g(k)) \tag{III.23}$$

The error between the predicted grid current and its reference generated, as shown in Fig. III.9 is used in a cost function, which should be minimized to select the optimal switching state that must be applied in the next sampling time.

III.4.2. The proposed cascaded predictive control

The GCSs are considered generally as multiple stage systems, which are related by the DC link stage, and that requires a complex control using two or more controllers. The cascaded predictive control is proposed to facilitate system control by considering the whole system as an indirect matrix converter. The three cascaded converters are controlled by the same predictive controller in one stage using only one cost function that contains the three terms, as shown on the flowchart of Fig. III.10. The formulated cost function is subject to minimize the errors of three currents to their references.

The cost function g is now formulated tacking into account the specifications for the P-PVE, the MPPT control, and the GCS control as:

$$g = \left|I_{Le}^{P} - I_{Le}^{ref}\right| + \left|I_{L}^{P} - I_{L}^{ref}\right| + \left|I_{g}^{P} - I_{g}^{ref}\right| + \lambda . N_s \tag{III.24}$$

The last term $\lambda . N_s$ deals with the minimization of the switching frequency in order to reduce current ripples and to protect converter components by using the following equation:

$$N_S = \sum_{x=1}^{M} \left(S_x(k) - S_x(k-1)\right) \tag{III.25}$$

Where, $M = 4$

The proposed CPC-GCS algorithm generates only 12 active switching states instead of 16 possible ones by eliminating 4 redundant ones, as given in Table III.2.

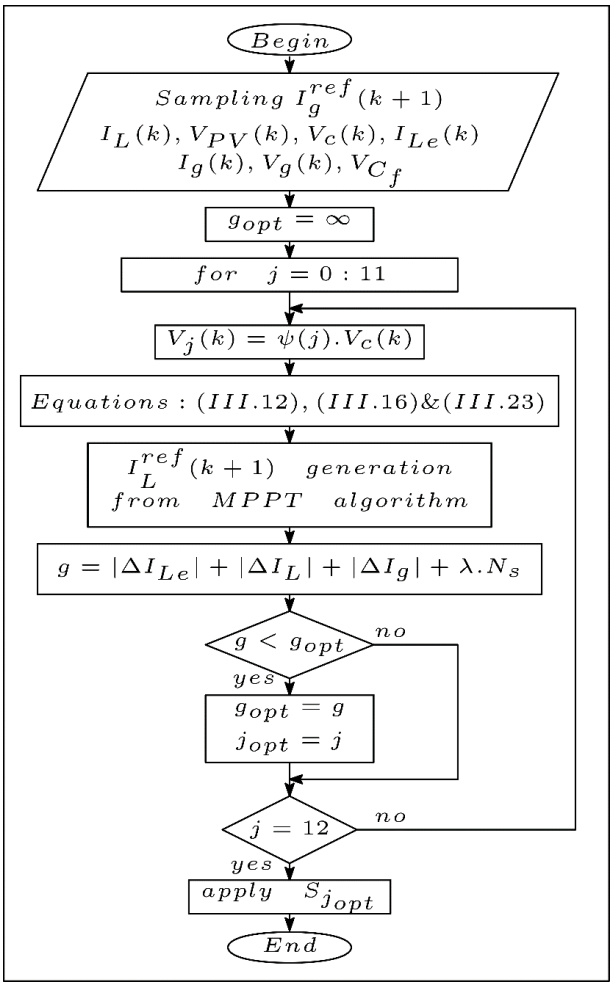

Figure III.10: Flowchart of the proposed cascaded predictive control for grid PV systems.

Table III.2: Active switching states of the CPC-GCS application.

Output Voltage	S_{Emul}	S_{Boost}	S_a	S_b
0	0	0	0	0
$-V_C$	0	0	0	1
V_C	0	0	1	0
0	0	1	0	0
$-V_C$	0	1	0	1
V_C	0	1	1	0
0	1	0	0	0
$-V_C$	1	0	0	1
V_C	1	0	1	0
0	1	1	0	0
$-V_C$	1	1	0	1
V_C	1	1	1	0

III.5. Simulation results and discussions

Detailed simulation results are done under MATLAB/SIMULINK software in order to confirm the high efficacy of the proposed system schemes. Specifications of the used panel model and component values are indicated in Table III.3. The sampling time T_S is set to 10µs for emulator tests and PV-SAS, where it is set to 50µs for PV-GCS. For the PV emulator test, one TE505 panel is used, whereas two panels in series are used for SAS and GCS.

Table III.3: Active switching states of the CPC-GCS application.

Parameter	Symbol	Value	Unit
PV maximum power	P_{MPP}	49.26	W
PV maximum current	I_{MPP}	2.8	A
Short circuit current	I_{SC}	3.1	A
PV maximum voltage	V_{MPP}	17.6	V
Open circuit voltage	V_{OC}	21.7	V
Input voltage	V_{Cf}	60	V
DC Link voltage	V_C	80	V
Grid voltage	V_g	50	V
Filter resistor	R_f	0.2	Ω
Filter inductor	L_f	30	mH
Buck converter capacitor	C_1	0.68	mF
Boost converter capacitor	C	1.1	mF
Input capacitor	C_f	0.68	mF
Buck converter inductor	L_e	10	mH
Boost converter inductor	L	3	mH

III.5.1. Simulation results for PV emulator

To compare the performance of the proposed P-PVE emulator with those of a conventional emulator based on PI controller, a set of simulation results for reference current tracking, oscillations, and dynamic response are made, under several tests of abrupt irradiance variations [1 - 0.5 - 0.8] kW/m² and load changes [6.3 - 9.9 - 6.3] Ω.

From Fig. III.11a, one can see the high dynamic response under a sudden change in the load for the P-PVE emulator compared to the PI-based one. In addition, Fig. III.11b shows a useful

reference current tracking achieved in the transient state with fewer oscillations (see the zoomed zone). This performance is also confirmed in Fig. III.12 when the system is subject to an abrupt change of irradiance.

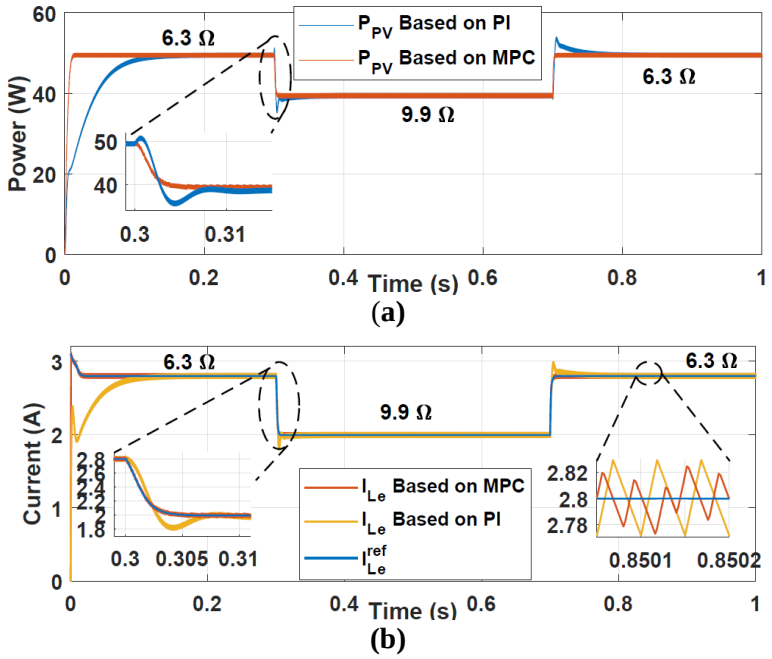

Figure III.11: Performance of PV emulators under load changes:
(a) Powers (P_{PV}) and (b) Currents (I_{Le}).

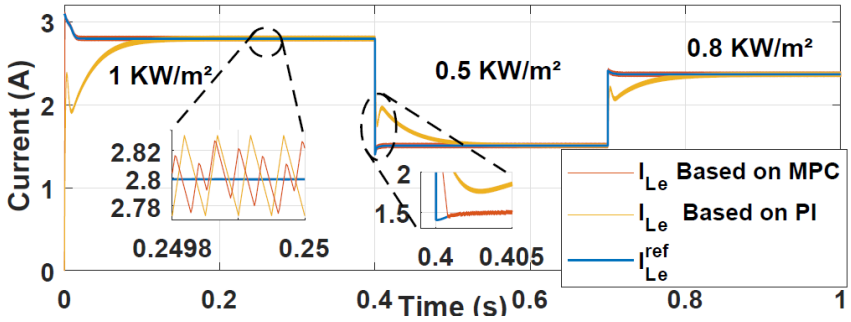

Figure III.12: PV emulator currents and their reference under irradiance changes.

III.5.2. Simulation results for the stand-alone PV system

To illustrate well the efficacy of the CPC algorithm for SAS using the P-PVE. Simulation results are done and depict the dynamic response, reference current tracking and efficiency under both load variations [80- 54- 80] Ω, and solar irradiance changes [1- 0.5- 0.8] kW/m². It can seem from Fig. III.13 that the CPC algorithm with the included MPPT works perfectly at the exact MPP under sudden changes of the load. Also, Fig. III.14 depicts that fast dynamic

response of the reference current track can be achieved under quick changes of irradiance. Fig. III.15 gives the profile of the conversion chain efficiency for the whole cycle. The previous results prove that the proposed CPC algorithm can be a valuable alternative for the control of PV-SAS.

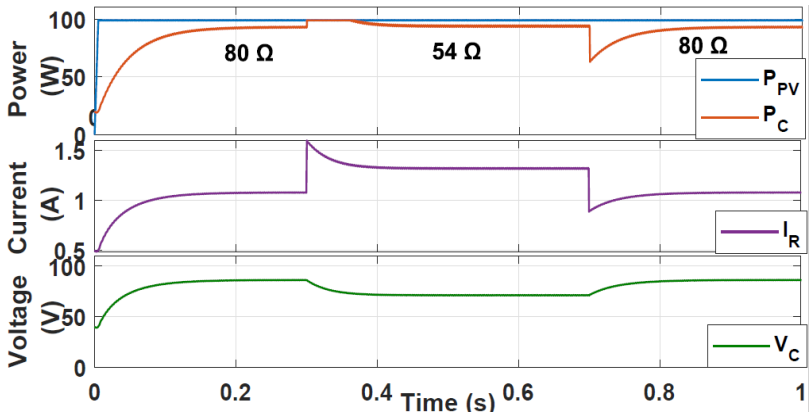

Figure III.13: Performance of the proposed stand-alone system under load changes (P_{PV}, P_C, I_R, and V_C).

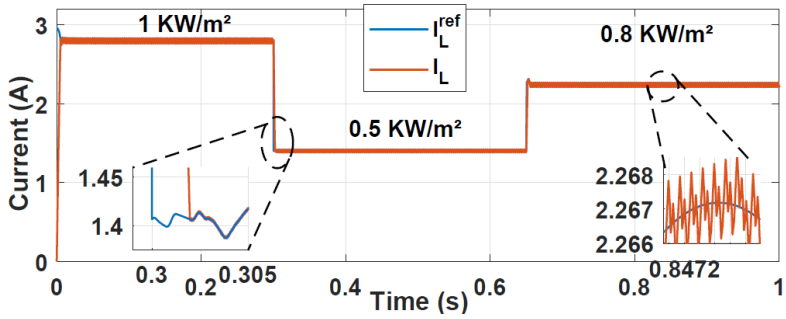

Figure III.14: Boost inductor current and its reference around the MPP using the proposed cascaded predictive algorithm.

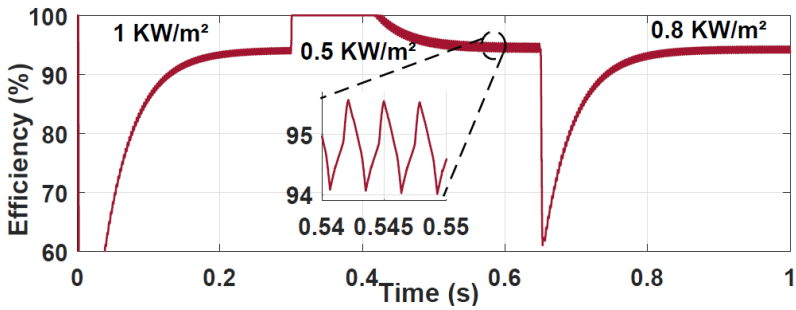

Figure III.15: Efficiency of the stand-alone system under irradiance variations.

III.5.3. Simulation results for the grid-connected system

The next set of simulation results focuses on the application of the CPC algorithm on a GCS shown in Fig. III.9. Fig. III.16 shows the performance of the DC side (P_{PV}, I_L, V_{PV}, and V_C) under irradiance variations where it can be seen that the MPP is well tracked and the previous static and dynamic performances are still conserved.

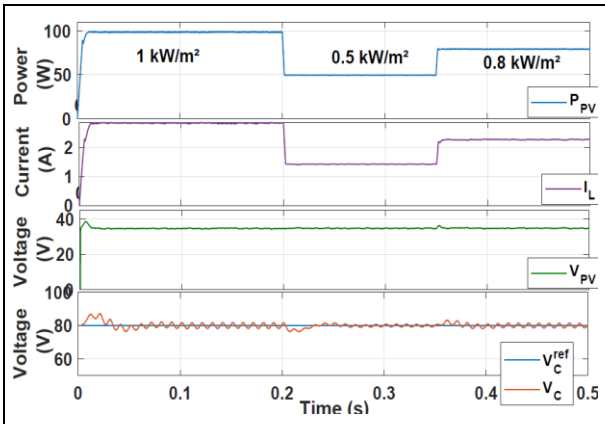

Figure III.16: Performance in the DC side of the grid connected system under irradiance changes (P_{PV}, I_L, V_{PV}, and V_C).

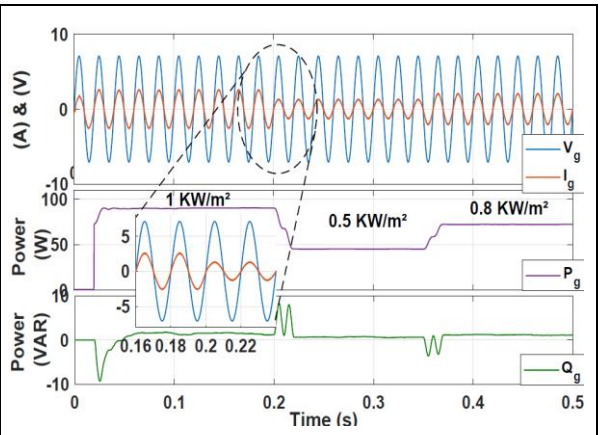

Figure III.17: Performance in the AC side of the grid connected system under irradiance changes (V_g, I_g, P_g, and Q_g).

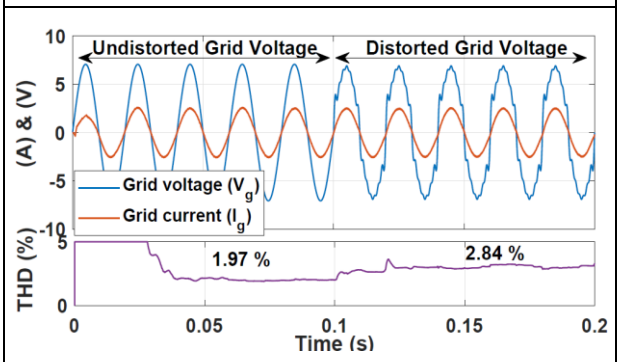

Figure III.18: Performance of the grid current (I_g) under undistorted and distorted grid voltage (V_g).

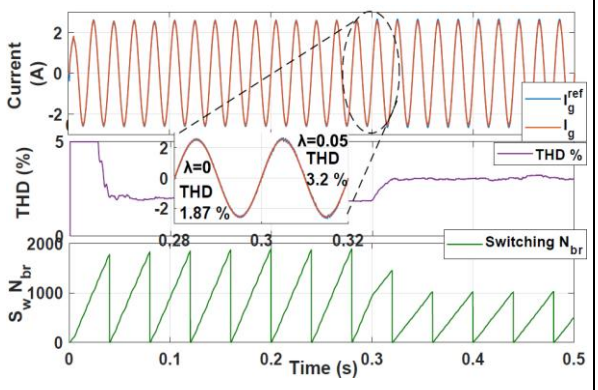

Figure III.19: Performance in the AC side of the grid connected system under minimization of the switching frequency (λ=0, λ=0.05) with 1kW/m².

In the AC side, the grid current and voltage are perfectly sinusoidal and in phase. The injected current follows exactly the irradiance levels, which is confirmed by the profile of the active and reactive powers, as given by Fig. III.17. In addition, the grid current (I_g) is subject to a distorted grid voltage (V_g) test (the thirteenth harmonic), where it proved a robust

performance with low Total Harmonic Distortion (THD) current as it is shown by Fig. III.18, by meaning that the reference generation method given by (III.18) gives an exact current reference value whatever the grid conditions.

Fig. III.19 deals with a minimization of the switching number of all cascaded power converters, which is done to protect converter switches and kept the THD current under acceptable values. By considering the fourth term of the equation (III.24), one can see that it is possible to allow the conversion chain works within adequate switching numbers without affecting the current THD. For the illustrated example, it is observed that when the control system operates without weighting factor (λ=0), the current THD is about 1.87% having 1900 commutations, whereas when the weighting factor is settled to (λ=0.05), the THD current increases to 3.2% with a reduction of the switching number to 1000 commutations.

III.6. Experimental validations

The prototype of the realized PV emulator based on DC-DC synchronous buck converter is shown in Fig. III.20. It contains two MOSFET IRFP460Z (500V/20A) controlled in a complementary form. The used MOSFET driver is an LT1158cn. The current and voltage are measured using LA-25 and LV-25 sensors, respectively. The general experimental bench is built in our laboratory that is shown in Fig. III.21 using a dSPACE 1104 card. The used boost and H-bridge inverter are those of SEMIKRON IGBT (750V/30A).

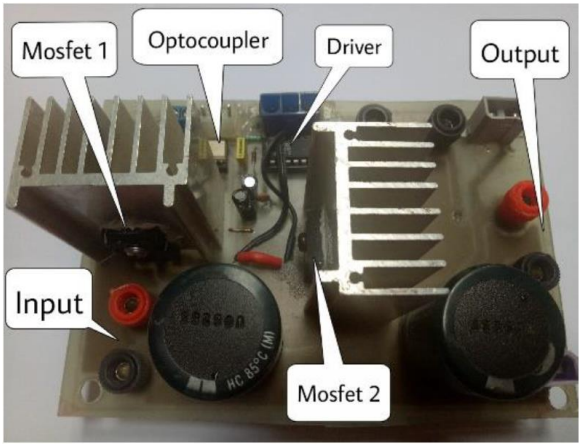

Figure III.20: The DC-DC synchronous buck converter.

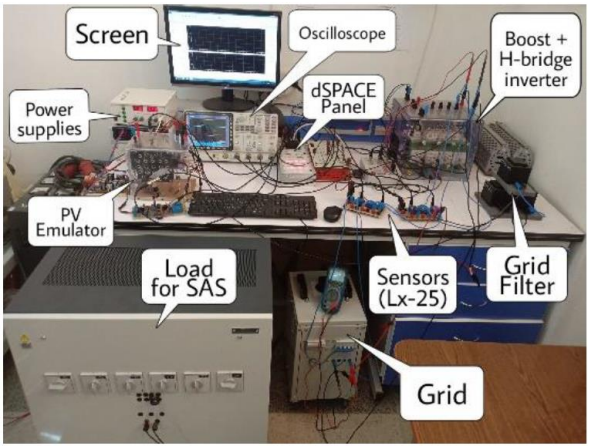

Figure III.21: The used experimental bench.

III.6.1. Experimental results for PV emulator

To illustrate the effectiveness of the proposed P-PVE on other one based on PI controller (PI-PVE). Two tests have been carried out. The first deals with load variations in the range [6.3 - 9.9 - 6.3] Ω, whereas the second is based on abrupt irradiance variations [1 - 0.5 - 0.8] kW/ m². The sampling time T_s is 50µs. Note that both PV emulators are working without MPPT control.

Both of figures (Fig. III.22a and Fig. III.22b) show the high dynamic response of the realized P-PVE compared to the PI-PVE. Under sudden changes in the load, the extracted power (P_{PV}) for the P-PVE takes only 4ms to achieve the new steady-state when the load increases from 6.3Ω to 9.9Ω whereas, it takes 18ms for the PI-PVE as it is shown in the zoomed zones. Figures (Fig. III.23a and Fig. III.23b) illustrate the tracking performance of the P-PVE and the PI-PVE currents, respectively, under abrupt irradiance variations in the range [1 - 0.5 - 0.8] kW/ m². The superiority of the P-PVE on PI-PVE is confirmed since its reference current (I_{Le}^{ref}) is closely tracked, and its duty cycle shows a high dynamic response. The P-V and I-V characteristics of the two compared PV emulators are emulated under different hard climatic conditions of irradiance [1 - 0.5 - 0.8] KW/m² and temperature [25 - 40 - 50] C° to illustrate well their performances. Figures (Fig. III.24a and Fig. III.24b) show that the emulated P-V characteristics for the P-PVE are obtained with low oscillations even under hard conditions compared to the PI-PVE one. Also, the high performance of the P-PVE compared to the PI-PVE one are confirmed by the emulated I-V characteristics (Fig. III.25a for P-PVE and Fig. III.25b for PI-PVE). The performance of the P-PVE compared to those of real PV panels (Two panels in series with bypass diode for each one) under shaded condition, are illustrated by Fig. III.26 when the first panel received 0.901 KW/m² of irradiance under 38 C° of temperature, whereas the second panel received 0.576 KW/m² under 35 C° of irradiance and temperature respectively. One can see from Fig. III.26a that the shaded P-V curves (coloured in blue) for the P-PVE are obtained with the same dynamic response and fewer oscillations of those of real PV panels (coloured in red), meaning that the P-PVE imitates exactly the behaviour of real PV panels under any hard climatic conditions. The shaded I-V curves of Fig. III.26b confirm that.

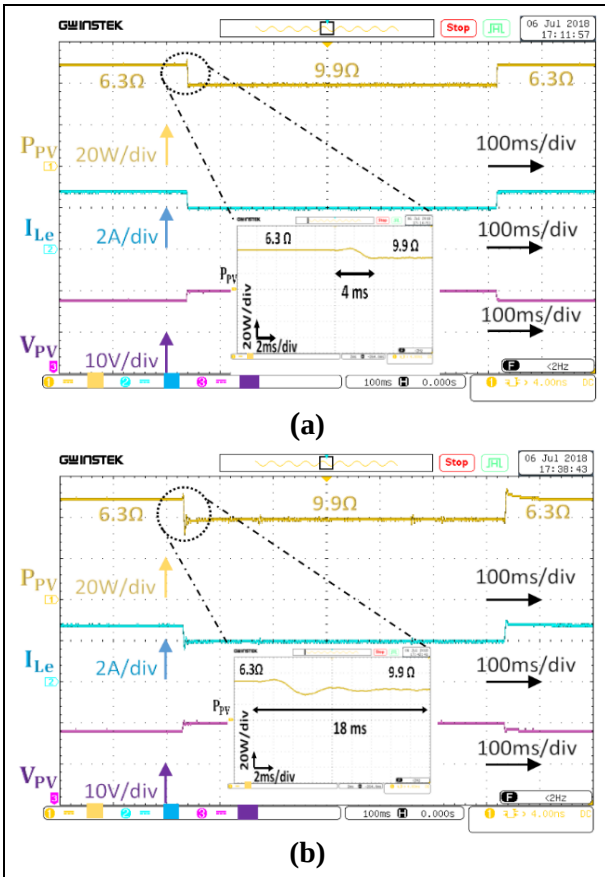

Figure III.22: PV emulator's performance under load variations: (a) for P-PVE, (b) for PI-PVE.

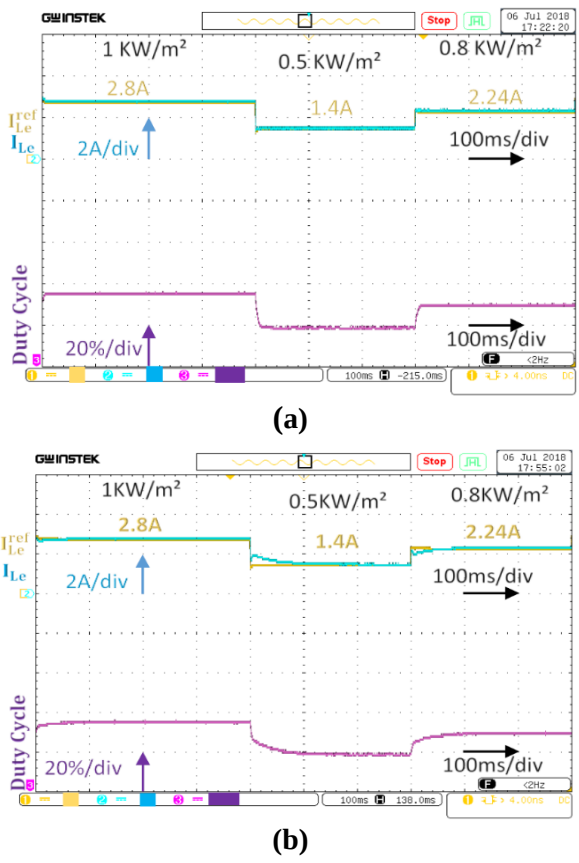

Figure III.23: PV emulator's performance under irradiance variations: (a) for P-PVE, (b) for PI-PVE.

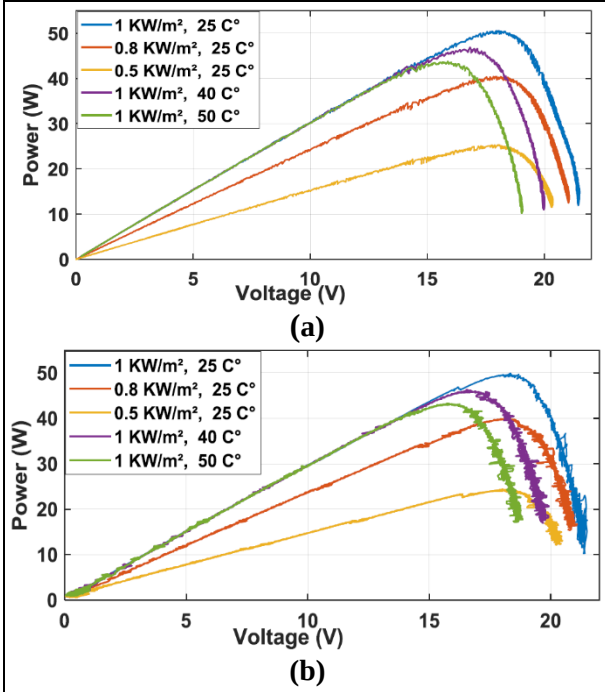

Figure III.24: The experimental P-V characteristics: (a) for P-PVE, (b) for PI-PVE.

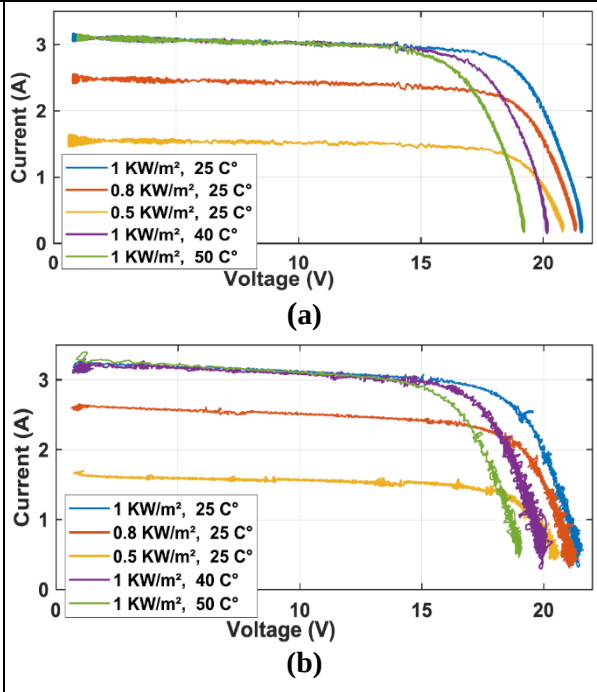

Figure III.25: The experimental I-V characteristics: (a) for P-PVE, (b) for PI-PVE.

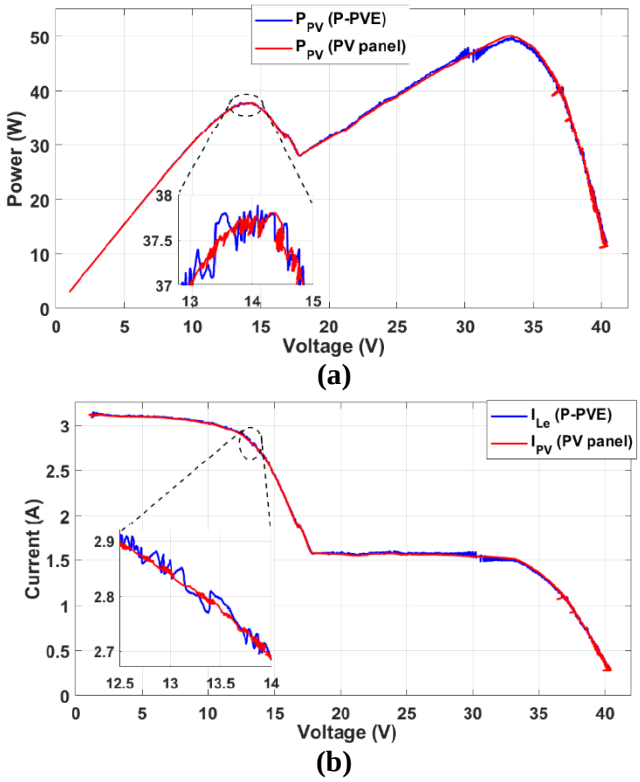

Figure III.26: Experimental performance of the P-PVE under partial shaded condition: (a) P-V curves for both P-PVE and real panels, (b) I-V curves for both P-PVE and real panels.

III.6.2. Experimental results for the stand-alone PV system

Examining now the experimental performance of the P-PVE cascaded to a boost power converter used for MPPT control. The flowchart of the control system is that of Fig. III.8, the first test deals with a constant irradiance of 1kW/m² and a sudden change of the load from 80Ω to 54Ω and then to 80Ω. The output P-PVE power (P_{PV}), the load dissipated power (P_C), the load current (I_R), and the load voltage (P_C) are shown respectively in Fig. III.27. Contrary to Fig. III.22a, where the P-PVE works without MPPT control and the extracted power (P_{PV}) varies according to the load variation, Fig. III.27a shows that the MPPT control works efficiently, whatever the load variation since the (P_{PV}) power is kept constant. The current and voltage load are compensating each other in order to give a quasi-constant output power (P_C). The second test is done with a constant resistive load of 80Ω under the irradiance profile in the range [1 - 0.5 - 0.8] kW/ m². Fig. III.27b illustrates the performances of the CPC. , where the output emulator power (P_{PV}), the inductance current (I_L), and the emulator voltage (V_{PV}) are depicted with high dynamic performance by working at the MPP with fewer ripples, whereas, Fig. III.27c shows the efficiency of the conversion chain considered as the ratio between the load power to the (P_{PV}) about 90% for the full irradiance profile.

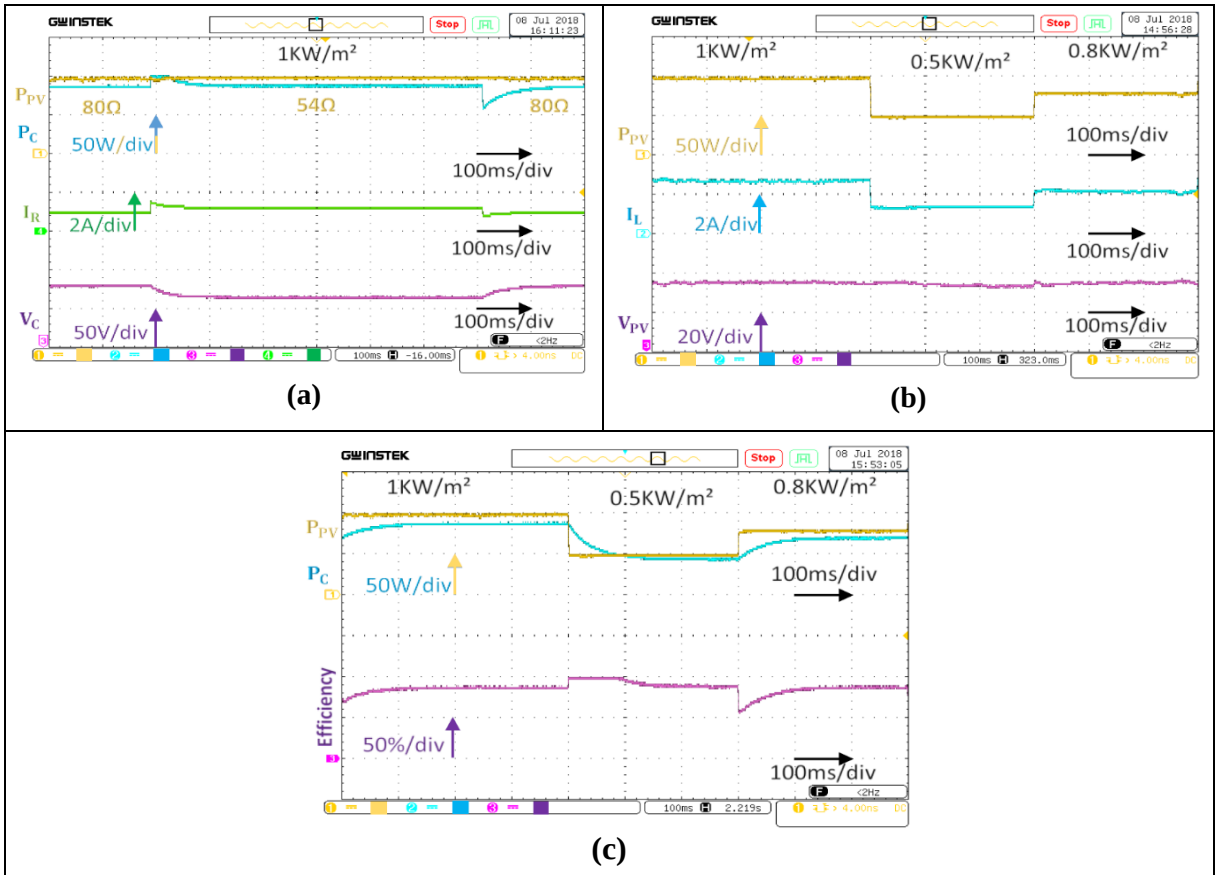

Figure III.27: Performance of the stand-alone system : (a) under load variation, (b) and (c) under irradiance variation.

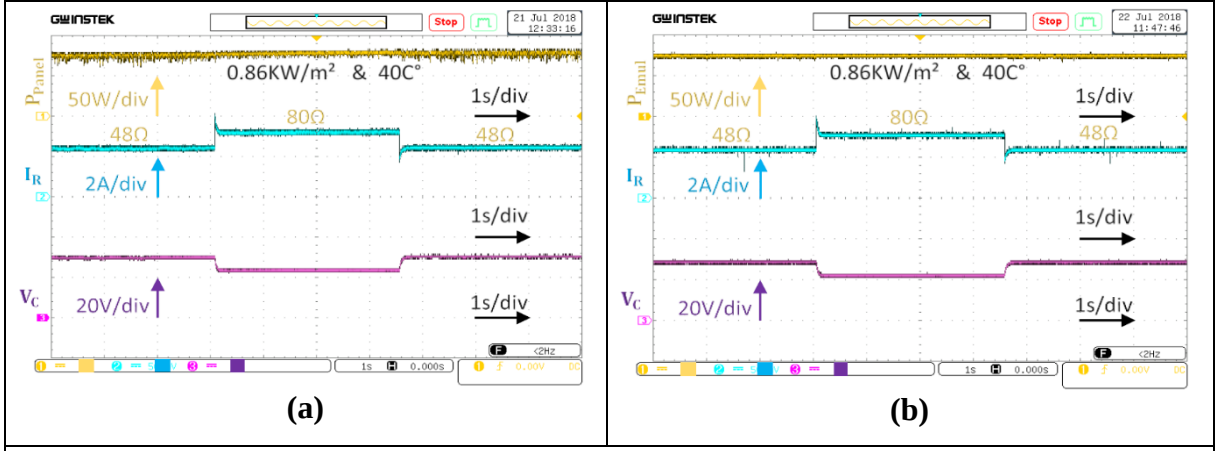

Figure III.28: Performances of the stand-alone PV systems: (a) for real panels, (b) for P-PVE.

To evaluate more the performance of the CPC structure using the P-PVE, experimental results have been compared to those of a stand-alone system based on real PV panels (two TE505 panels connected in series replacing the P-PVE). The figures (Fig. III.28a and Fig. III.28b) show the performance of the two systems under the same climatic conditions (0.86kW/m² and 40C°) when they are subject to a load variation test. As can be seen from these

figures that the proposed emulator provides the best skills than in the case of a system based real PV panels in terms of fewer oscillations with the same dynamic response.

III.6.3. Experimental results for the grid-connected system

The CPC algorithm of Fig. III.10 for a GCS application (Fig. III.9) is now tested experimentally under hard irradiance variations [1 - 0.5 - 0.8] kW/m². The second test deals with the minimization of the switching frequency by keeping the grid current THD with acceptable values. The sampling time is of 95µs.

From Fig. III.29, one can see the high dynamic response of the system under abrupt changes of the irradiance where the PV emulator power (P_{PV}), the voltage (V_{PV}) and the inductor current (I_L) achieve the MPP in less than 2ms as well as the DC link voltage (V_C) having a constant behavior whatever the irradiance level, confirming the well-functioning of the DC side of the proposed topology. In the AC side of the grid-connected system, Fig. III.30 illustrates the grid current having a sinusoidal form in phase with the grid voltage, and its magnitude follows the irradiance level perfectly, by means that the grid reactive-power is very small (about 2VAR at 1kW/m²). Also, the active transmitted power from the PV emulator to the grid is done with fewer ripples and less losses. The grid current THD is about [2.77 - 5.3 - 3.26] % according to the irradiance [1 - 0.5 - 0.8] kW/m² respectively. A fourth term is added to the cost function (III.24) in order to reduce the switching number and, consequently, the commutation losses and to preserve the flexibility of the FS-MPC. From Fig. III.31 one can see that the grid-current form is kept sinusoidal and in phase with the grid voltage, whereas the switching number is reduced from 360 switchings in 0.04s for λ=0 to 280 switchings when λ=1.2. For this test, the current THD increases slightly from 2.77 % to 4.29 %. These experimental results demonstrate the high efficacy of the proposed CPC with the included MPPT for GCSs.

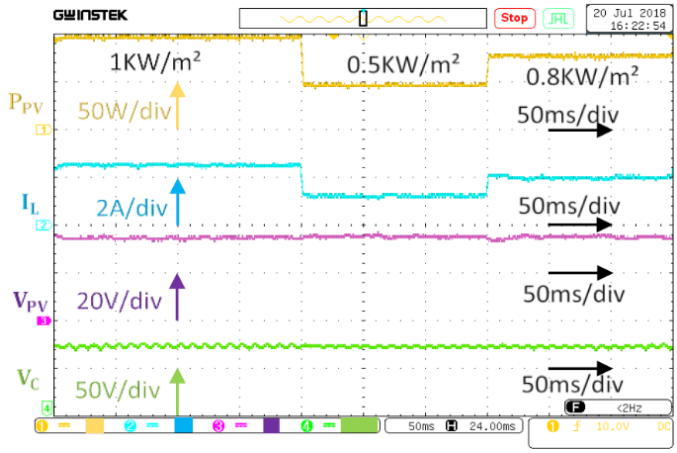

Figure III.29: Performance in the DC side of the grid-connected system under irradiance variations.

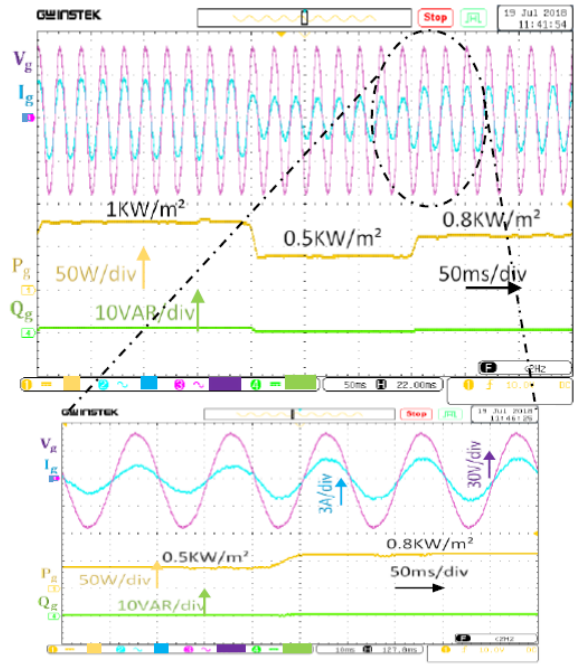

Figure III.30: Performance in the AC side of the grid-connected system under irradiance variations.

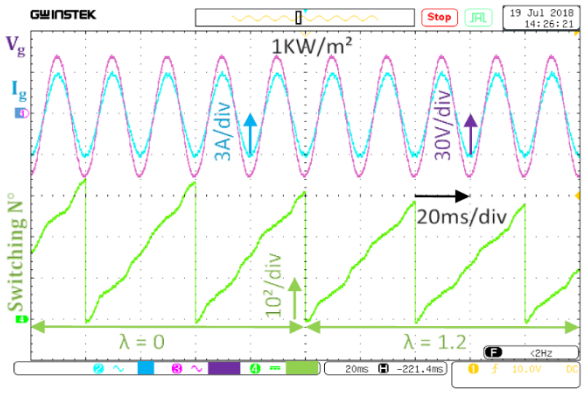

Figure III.31: Minimization of the switching numbers (λ=0 and λ=1.2).

III.7. Conclusion

The present chapter presents a new conception of a PV emulator based on FS-MPC using a synchronous Buck converter by sweeping the three significant steps of the design, namely the PV model, the control strategy, and the power converter. The performance of the presented P-PVE is compared by simulation and experimental studies to that of a commonly used emulator based on a linear PI controller. The high performance of the P-PVE is confirmed in terms of dynamic response in transients, simple implementation, accuracy, efficiency and reference

tracking with more stability of the operating point. The second contribution presented in this chapter is an efficient control methodology based on FS-MPC of many cascaded power converters (CPC) applied on two topologies of PV systems, namely the SAS and the GCS. In both systems, the P-PVE was cascaded to a Boost MPPT converter. The main advantage of the CPC topology is that only one cost function was used for minimization for all cascaded power converters, so their gating signals are delivered at the same time instead of controlling them separately. In addition to the brilliant performance of the FS-MPC control, the CPC structure has added simple controllability to the overall control system. The effectiveness and the correctness of the proposed CPC method have been proved by simulation and experimentally verified under hard climatic conditions as well as distorted grid voltage functioning. Another optimization aspect, such as switching number minimization for all cascaded power converters, has also been verified due to the flexibility of FS-MPC.

III.8. References

[1] J. P. Ram, H. Manghani, D. S. Pillai, T. S. Babu, M. Miyatake, et N. Rajasekar, « Analysis on solar PV emulators: A review », *Renewable and Sustainable Energy Reviews*, vol. 81, p. 149‑160, janv. 2018, doi: 10.1016/j.rser.2017.07.039.

[2] M. Azharuddin, T. S. Babu, N. Bilakanti, et N. Rajasekar, « A Nearly Accurate Solar Photovoltaic Emulator Using a dSPACE Controller for Real-time Control », *Electric Power Components and Systems*, vol. 44, nº 7, p. 774‑782, avr. 2016, doi: 10.1080/15325008.2015.1131763.

[3] S. El Islam Remache et K. Barra, « Performance comparison among boost and multi level boost converters for photovoltaic grid connected system using finite set model predictive control », in *2018 9th International Renewable Energy Congress (IREC)*, Hammamet, mars 2018, p. 1‑6, doi: 10.1109/IREC.2018.8362483.

[4] A. Dehghanzadeh, G. Farahani, H. Vahedi, et K. Al-Haddad, « Model predictive control design for DC-DC converters applied to a photovoltaic system », *International Journal of Electrical Power & Energy Systems*, vol. 103, p. 537‑544, déc. 2018, doi: 10.1016/j.ijepes.2018.05.004.

[5] T. Esram et P. L. Chapman, « Comparison of Photovoltaic Array Maximum Power Point Tracking Techniques », *IEEE Transactions on Energy Conversion*, vol. 22, nº 2, p. 439‑449, juin 2007, doi: 10.1109/TEC.2006.874230.

[6] R. Ayop et C. W. Tan, « A comprehensive review on photovoltaic emulator », *Renewable and Sustainable Energy Reviews*, vol. 80, p. 430‑452, déc. 2017, doi: 10.1016/j.rser.2017.05.217.

[7] M. T. Iqbal, M. Tariq, M. K. Ahmad, et M. S. B. Arif, « Modeling, analysis and control of buck converter and Z-source converter for photo voltaic emulator », in *2016 IEEE 1st International Conference on Power Electronics, Intelligent Control and Energy Systems (ICPEICES)*, Delhi, India, juill. 2016, p. 1‑6, doi: 10.1109/ICPEICES.2016.7853605.

[8] C. H. Balakishan et N. Sandeep, « Development of a Microcontroller Based PV Emulator with Current Controlled DC-DC Buck Converter », p. 7, 2014.

[9] T. Jiang, G. Putrus, S. McDonald, M. Conti, B. Li, et D. Johnston, « Generic Photovoltaic System Emulator Based on Lambert ω Function », p. 5, 2011.

[10] Y. Kim, W. Lee, M. Pedram, et N. Chang, « Dual-mode power regulator for photovoltaic module emulation », *Applied Energy*, vol. 101, p. 730‑739, janv. 2013, doi: 10.1016/j.apenergy.2012.07.025.

[11] A. Koran, T. LaBella, et Jih-Sheng Lai, « High Efficiency Photovoltaic Source Simulator with Fast Response Time for Solar Power Conditioning Systems Evaluation », *IEEE Transactions on Power Electronics*, vol. 29, nº 3, p. 1285‑1297, mars 2014, doi: 10.1109/TPEL.2013.2262297.

[12] Z. Shi, Y. Xie, Y. Wang, H. Ma, et J. Zhang, « Improved model predictive control for three-phase Vienna rectifiers », *IEICE Electronics Express*, vol. 15, nº 12, p. 20180398‑20180398, 2018, doi: 10.1587/elex.15.20180398.

[13] Z. Chen, J. Qiu, et M. Jin, « Adaptive finite-control-set model predictive current control for IPMSM drives with inductance variation », *IET Electric Power Applications*, vol. 11, nº 5, p. 874‑884, mai 2017, doi: 10.1049/iet-epa.2016.0861.

[14] Z. Kara, K. Barra, et A. Y. Cherif, « Predictive algorithm for matrix converter control in wind energy conversion system based DFIG », in *2018 9th International Renewable Energy Congress (IREC)*, Hammamet, mars 2018, p. 1‑6, doi: 10.1109/IREC.2018.8362530.

[15] V. Yaramasu et B. Wu, *Model Predictive Control of Wind Energy Conversion Systems*. Hoboken, NJ, USA: John Wiley & Sons, Inc., 2017.

[16] M. J. Rana et M. A. Abido, « Energy management in DC microgrid with energy storage and model predictive controlled AC–DC converter », *IET Generation, Transmission & Distribution*, vol. 11, nº 15, p. 3694‑3702, oct. 2017, doi: 10.1049/iet-gtd.2016.1934.

[17] A. Olama, P. R. C. Mendes, et E. F. Camacho, « Lyapunov-based hybrid model predictive control for energy management of microgrids », *IET Generation, Transmission & Distribution*, vol. 12, nº 21, p. 5770‑5780, nov. 2018, doi: 10.1049/iet-gtd.2018.5852.

[18] R. B. A. Cunha, S. G. Di Santo, A. J. S. Filho, et F. F. Costa, « Finite control set applied to the current control of interleved boost converter of PV systems », in *2017 IEEE 6th International*

Conference on Renewable Energy Research and Applications (ICRERA), San Diego, CA, nov. 2017, p. 580‑584, doi: 10.1109/ICRERA.2017.8191127.

[19] D. Lopez, F. Flores-Bahamonde, S. Kouro, M. A. Perez, A. Llor, et L. Martinez-Salamero, « Predictive control of a single-stage boost DC-AC photovoltaic microinverter », in *IECON 2016 - 42nd Annual Conference of the IEEE Industrial Electronics Society*, Florence, Italy, oct. 2016, p. 6746‑6751, doi: 10.1109/IECON.2016.7793637.

[20] A. K. Bonala, S. R. Sandepudi, et V. P. Muddineni, « Selective finite-states model predictive control of grid interfaced three-level neutral point clamped photovoltaic inverter for inherent capacitor voltage balancing », *IET Power Electronics*, vol. 11, nº 13, p. 2072‑2080, nov. 2018, doi: 10.1049/iet-pel.2018.5021.

[21] W. Zhang, « DC-DC converter based photovoltaic simulator with a double current mode controller », p. 67.

[22] A. Cordeiro, D. Foito, et V. Fernao Pires, « A PV panel simulator based on a two quadrant DC/DC power converter with a sliding mode controller », in *2015 International Conference on Renewable Energy Research and Applications (ICRERA)*, Palermo, nov. 2015, p. 928‑932, doi: 10.1109/ICRERA.2015.7418545.

[23] H. Wang, F. Blaabjerg, M. G. Simões, et Y. Yang, « Power control flexibilities for grid-connected multi-functional photovoltaic inverters », *IET Renewable Power Generation*, vol. 10, nº 4, p. 504‑513, avr. 2016, doi: 10.1049/iet-rpg.2015.0133.

[24] H. Dehghani Tafti *et al.*, « Low-voltage ride-thorough capability of photovoltaic grid-connected neutral-point-clamped inverters with active/reactive power injection », *IET Renewable Power Generation*, vol. 11, nº 8, p. 1182‑1190, juin 2017, doi: 10.1049/iet-rpg.2016.0544.

[25] O. Abdel-Rahim, H. Funato, et J. Haruna, « Gird-connected boost inverter for low-power PV applications with model predictive control », *The Journal of Engineering*, vol. 2017, nº 7, p. 318‑326, juill. 2017, doi: 10.1049/joe.2017.0070.

[26] M. B. Shadmand, M. Mosa, R. S. Balog, et H. A. Rub, « Maximum power point tracking of grid connected photovoltaic system employing model predictive control », in *2015 IEEE Applied Power Electronics Conference and Exposition (APEC)*, Charlotte, NC, USA, mars 2015, p. 3067‑3074, doi: 10.1109/APEC.2015.7104789.

[27] M. K. Das, K. C. Jana, et A. Sinha, « Performance evaluation of an asymmetrical reduced switched multi-level inverter for a grid-connected PV system », *IET Renewable Power Generation*, vol. 12, nº 2, p. 252‑263, févr. 2018, doi: 10.1049/iet-rpg.2016.0895.

[28] M. B. Shadmand, X. Li, R. S. Balog, et H. A. Rub, « Model predictive control of grid-tied photovoltaic systems: Maximum power point tracking and decoupled power control », in *2015 First Workshop on Smart Grid and Renewable Energy (SGRE)*, Doha, Qatar, mars 2015, p. 1‑6, doi: 10.1109/SGRE.2015.7208726.

[29] S. Taghizadeh, M. J. Hossain, et J. Lu, « An Enhanced Orthogonal Signal Generator for a Single-phase Grid-Connected Converter », p. 11.

[30] R. Chan, J. Baek, et S. Kwak, « Simple algorithm with fast dynamics for cascaded H-bridge multilevel inverter based on model predictive control method », in *2017 IEEE Applied Power Electronics Conference and Exposition (APEC)*, Tampa, FL, USA, mars 2017, p. 696‑702, doi: 10.1109/APEC.2017.7930770.

Chapter IV

Cascaded Predictive Direct Power Control for Photovoltaic Systems: stand-alone system with integrated energy storage and grid-connected system

IV. Cascaded predictive direct power control for photovoltaic systems : for stand-alone system with integrated energy storage and grid-connected system

IV.1. Introduction

Actually, some countries are deficient in hydrocarbons, but most of them have the critical potential of green energies, namely: biomass energy, hydraulic energy, wind energy, solar energy, and other kinds. The use of these renewable energies increases the economy of these countries and gives our planet more safety and more vitality. Recent studies on power generation provide the most significant potential and the highest margin of progression for solar energy. This last, can fulfil the world's energy demands due to their inexhaustible natural renewable, easy installation and low-maintenance with pollution-free operation [1-3]. However, many constraints hinder the progress of this green energy, such as manufacturing cost, large area requirement, and discontinuous solar irradiance. Therefore, these constraints stimulate more innovative and advanced researches [2].

Decentralized energy production is based on renewable energies, and it is occupying an increasing share in the global power market under the so-called micro grids, which can be helpful for the global utility grid. The energy challenges between micro grids and utility grid such as power quality, reliability and availability make the technology of smart grids more vulnerable. The photovoltaic energy is one of the clean energies that represent the principal source of energy in each micro grid installation due to its increasing rate of growth and a decreasing trend in the PV panel costs (from 4,9 $/W in 1998 to 0,52 $/W in 2019). Based on these statistics, the predictions indicate that the most significant potential and the highest margin of progression are for photovoltaic energy compared to wind energy [4], [5].

Power electronic converters have been becoming an essential part of today's photovoltaic energy conversion systems. Even they can imitate the non-linear PV characteristics (PV emulators), such as in [6], they can be used to ensure the Maximum Power Point Tracking (MPPT) algorithms functioning by extracting the available power from PV panels (off-grid), and they are used in grid-tied configurations to transmit the PV power to the utility grid [1].

The fundamental theory of power converters as repetitive switching states and their structures of single-input-single-output or the multilevel topologies are the main criteria to define the output power quality such as waveform and lower current and voltage Total Harmonic Distortion (THD) [5]. Moreover, the way in which the power converter devices are controlled has also a critical factor in power quality and switching losses [7]. Many new types of research focused on multilevel converters and their advanced control algorithms such as in [5, 8-9].

Model predictive control (MPC) is one of the promising available control techniques that proved its high performance compared to linear controllers. MPC control methods are grouped in the same functioning principle, where they are all able to predict the future behavior in a predefined horizon and maintain the best control action based on a minimized objective cost function [1], [9]. Further, during the last decade, researchers have proposed the Finite Set Model Predictive Control (FS-MPC); this control technique is much more intended for power converters because of the finite number of the switching states of the converter [5]. After several theoretical analysis on this method. MPC has been tested experimentally on different system applications such as electrical drives [10], wind energy conversion systems (WECS) [11] and photovoltaic applications [1], [5] using several topologies of power converters (DC-DC converters [5], two-level inverters [1], multi-level converters [5], [8] and matrix converters [11]) in a wide range of low, medium and high-power conversion [4]. The performance of the FS-MPC has been investigated in several research papers, which show that FS-MPC technique outperforms the linear control on dynamic response, low current and voltage ripples and reference tracking even during system parameters mismatch. Moreover, the FS-MPC gives more flexibility to control cascaded power converter topologies in one stage [12]. An optimized cost function is formulated, which contains errors between the predicted values of the variables and their references, these errors may be current errors, voltage errors or power errors, where, the proposed Cascade Predictive Direct Power Control (CPPC) uses the power errors to give more flexibility to the system control. The CPPC able to minimizes the optimized cost function that contains several errors and generates the optimal switching states for all cascade converters in the system [13], [14].

IV.2. Photovoltaic emulator based on the predictive power control

The presented predictive PV emulator (P-PVE) shown in Fig. IV.1 is based on a stabilized power supply, Buck converter, resistive load, and a control card. The power supply feds the

resistive load through the controlled buck converter. The control block contains two main control loops: the first one is the PV panel model (TE-505) that generates the reference power, where, the second is a predictive power control that uses the generated reference to formulate the optimized cost function and attack the MOSFET trigger. The resistive load is set to a value that maintains the P-PVE to operate at the Maximum Power Point (MPP). Otherwise, if it is changed from zero to a high value, the system can imitate exactly the I-V and P-V characteristics of the PV panel.

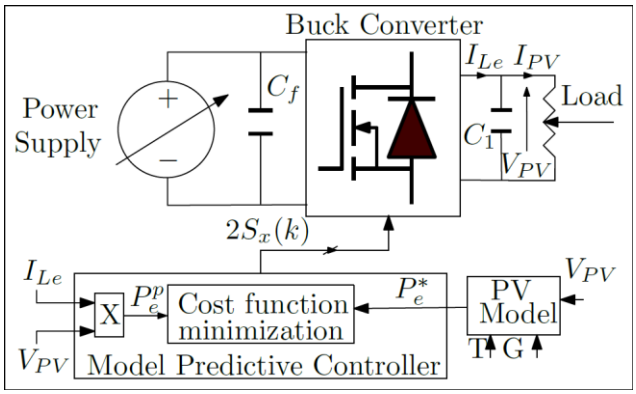

Figure IV.1: The PV emulator based on a buck converter.

IV.2.1. Predictive modelling of the buck converter

The predictive model of the buck converter is obtained using its operation principle when the switch is "ON", then when it is "OFF" and with the help of Euler approximation, we can find these equations:

When the switch is ON:

$$\begin{cases} I_{Le}(k+1) = \left(1 - \left(\frac{T_s}{L_e} * r_{Le}\right)\right) * I_{Le}(k) - \frac{T_s}{L_e} * \left(V_{PV}(k) - V_{C_f}(k)\right) \\ V_{PV}(k+1) = \left(1 - \frac{T_s}{R.C_1}\right) * V_{PV}(k) + \frac{T_s}{C_1} * I_{Le}(k) \end{cases} \quad \text{(IV.1)}$$

Then, when the switch is turned OFF:

$$\begin{cases} I_{Le}(k+1) = \left(1 - \left(\frac{T_s}{L_e} * r_{Le}\right)\right) * I_{Le}(k) - \frac{T_s}{L_e} * V_{PV}(k) \\ V_{PV}(k+1) = \left(1 - \frac{T_s}{R.C_1}\right) * V_{PV}(k) + \frac{T_s}{C_1} * I_{Le}(k) \end{cases} \quad \text{(IV.2)}$$

Where, r_{Le} is the internal resistance of the buck inductanceL_e, T_s is the sampling time.

These equations are rearranged in a common predictive model, and they are represented by a matrix form corresponding to the switch state S as given by:

$$\begin{bmatrix} I_{Le}(k+1) \\ V_{PV}(k+1) \end{bmatrix} = \begin{bmatrix} (1-\frac{r_{Le}}{L_e}T_s) & -\frac{T_s}{L_e} \\ \frac{T_s}{C_1} & (1-\frac{T_s}{R.C_1}) \end{bmatrix} . \begin{bmatrix} I_{Le}(k) \\ V_{PV}(k) \end{bmatrix} + \begin{bmatrix} \frac{T_s}{L_e}S \\ 0 \end{bmatrix} . V_{C_f}(k) \qquad (IV.3)$$

Then, the predicted power of the PV emulator is given by:

$$P^{p}_{emul} = I_{Le}(k+1) \times V_{PV}(k+1) \qquad (IV.4)$$

Fig. IV.2 gives the proposed predictive power control algorithm for PV emulators, and it can be explained as follows:

a- In each sampling period, the P-PVE of Fig. IV.2 receives the measures as: the input voltage V_{Cf}, the inductance current I_{Le} and the output voltage V_{PV}. When V_{Cf} feds the resistive load through the buck converter, the current I_{Le} begins to move and the predicted power model is calculated based on inputs and switch states according to (IV.3) and given by (IV.4), where, the PV panel model generates the reference power P^{ref}_{emul}.

b- The cost function g is formulated that contains the predicted power error, and it is given by (IV.5), where it is subject to minimization, and the optimal switching state is selected to be applied in the next sampling interval.

$$g = \left| P^{p}_{emul} - P^{ref}_{emul} \right| \qquad (IV.5)$$

IV.3. Stand-alone photovoltaic system with integrated energy storage using cascaded predictive direct power control

Recently, Distributed Energy Resources (DERs) use several renewable energies as principal sources to fulfill energy demands such as factories, public lighting, electronic-based office, and home appliances...etc. To make power balancing between these clean energies and demanded powers of loads, adaptation stages and energy storage systems, are integrated using divers of power electronic converters, to form configurations so-called AC or DC Micro-grids (MGs) [15], [16]. One of the essential parts in MGs system is the design and control method of Energy Management System (EMS), and as depicted in [16] that an EMS plays a role of divers of functions to optimize MGs operations as analyzing, forecasting of DERs power generation and

monitoring, load consumption....etc. In fact, DC MGs have several advantages over AC MGs, among them, the power electronic converters, where DC MGs uses less switches and simple configuration of converters than AC MGs. Another one, that the DC MGs generate DC power with the lack of reactive power, so it minimizes the regulation loop of the reactive power compensation [17], [18].

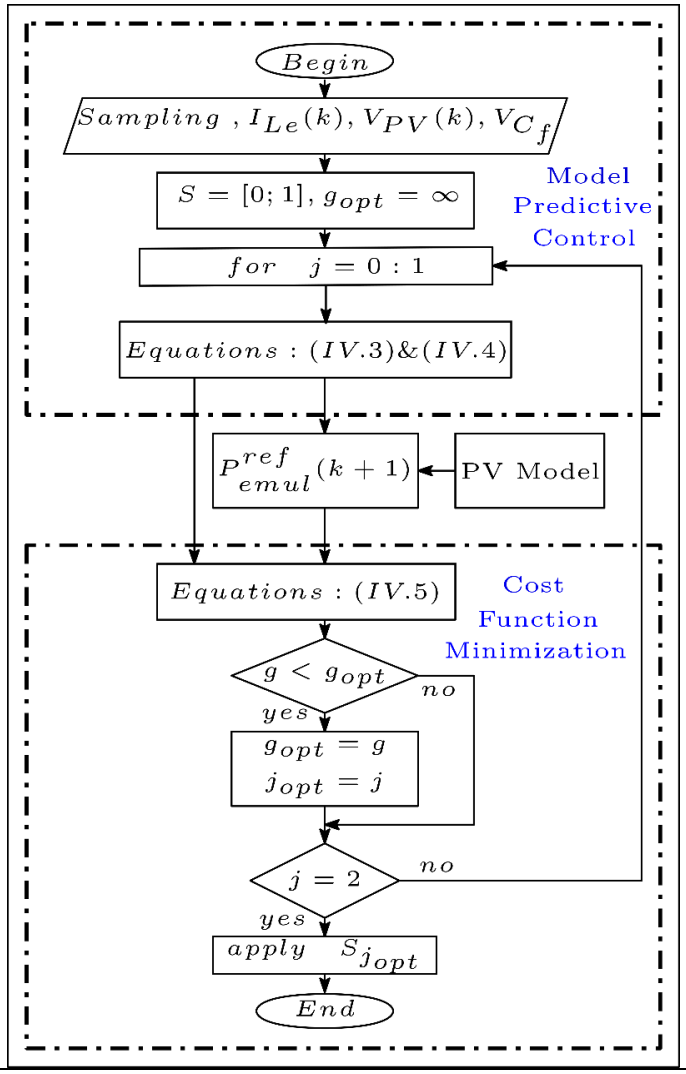

Figure IV.2: Flowchart of the proposed predictive power control algorithm for P-PVE.

The use of power electronic converters in DC MGs conversion system is the essential element to make the system able to transfer the produced energy demanded by the DC loads, and the way to assemble these power converters and their control, affect directly on the quality of the produced energy and the efficiency of the system [19]. Despite the development of a single-stage PV system with integrated energy storage using a Quasi Z-Source Inverter (qZSI) such as in [20], the double stage PV systems with energy storage are the most used architectures

in MGs. Their efficacy on the system lies in the advanced control methods, such as the Model Predictive Control (MPC) [21].

Finite Set Model Predictive Control (FS-MPC) is the easiest predictive control that much more intended for the control of power electronic converters because of its simple principle that based on the switching states of the converter and its predictive model. This method outperforms the linear controllers on low current and voltage ripples, dynamic response, and reference tracking even in the transient state [12], [19]. After making equations from the functioning sequences of the converter, its predictive model obtained using the Euler forward approximation technique. An optimized cost function is formulated, which contains errors between the predicted values of the variables and their references. These errors may be current errors, voltage errors, or power errors, where the proposed Cascade Predictive Direct Power Control (CPPC) uses the power errors to give more flexibility to the system control. The CPPC able to minimizes the optimized cost function that contains several errors and generates the optimal switching states for all cascade converters in the system [12], [22].

The studied configuration is shown in Fig. IV.3 contains three parts with three DC/DC converters, namely: buck converter, boost converter, and bi-directional converter. The buck converter is used for the P-PVE. It can imitate the behavior of real PV panels and recuperates exactly its I-V and P-V characteristics. Based on a stabilized power supply, a buck converter and the PV mathematical model of the used PV panel (two panels in series of TE-5O5) that generates the reference power for the predictive controller. The boost converter is used to ensure the MPPT functioning, by extracting the maximum available power from the P-PVE, using a hybrid algorithm between the conventional Incremental Conductance algorithm (Inc-Cond) and the Model Predictive Control (MPC). So, the Inc-Cond allows generating the correct reference power for the MPC that minimizes the square error of the reference power and the predicted one and produces the optimal switching state. The bi-directional converter is used to ensure the charge and discharge cycles of the batteries (three AGM batteries of 12V connected in series). It allows the balancing power between the P-PVE, batteries, and load demand.

IV.3.1. Predictive model of the DC/DC converters

The buck converter predictive model is obtained based on its operation principle when the switch is "ON," then when it is "OFF," and with the use of Euler approximation. It is given in the previous section.

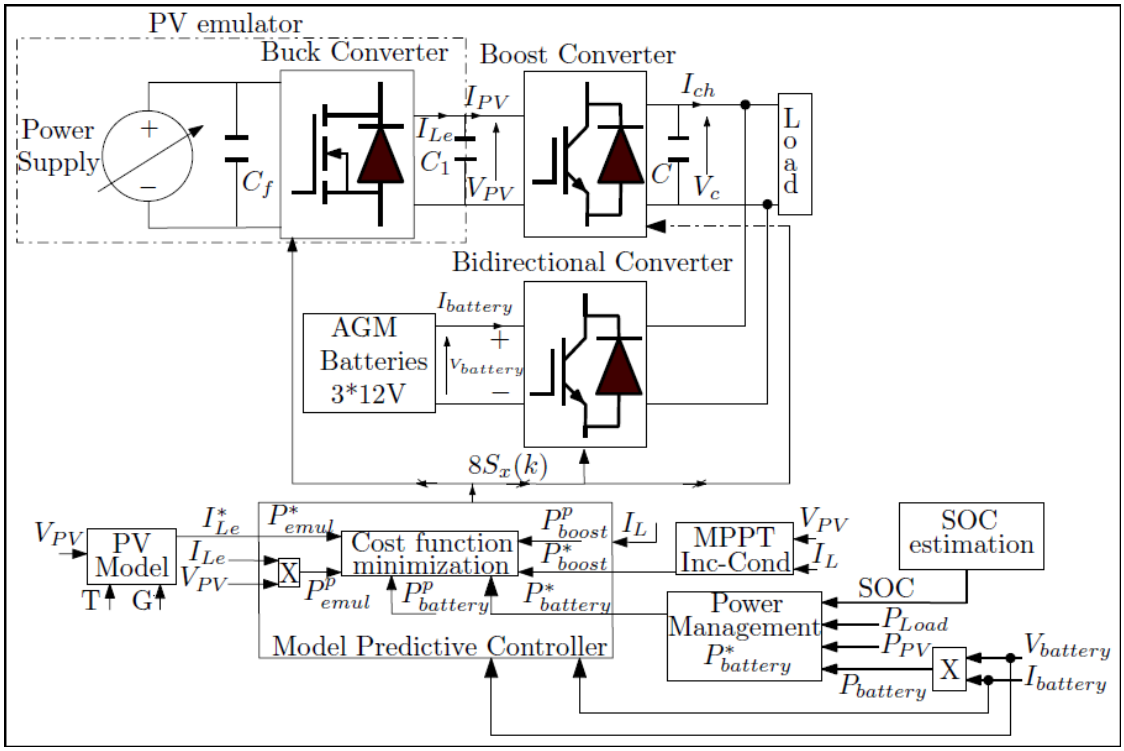

Figure IV.3: The global control scheme of the stand-alone PV system with integrated energy storage using the CPPC.

IV.3.1.1. Boost converter predictive modelling

The boost converter ensures the functioning of the MPPT algorithm, where, its predictive model is obtained according to its operation sequences using Euler approximation formula as follows:

When the switch is ON:

$$\begin{cases} I_L(k+1) = \left(1 - \left(\frac{T_s}{L} * r_L\right)\right) * I_L(k) - \frac{T_s}{L} * V_{PV}(k) \\ V_{PV}(k+1) = V_{PV}(k) + \frac{T_s}{C_1} * (I_{Le}(k) - I_L(k)) \end{cases} \quad \text{(IV.6)}$$

Then, when it is OFF, we get:

$$\begin{cases} I_L(k+1) = \left(1 - \left(\frac{T_s}{L} * r_L\right)\right) * I_L(k) - \frac{T_s}{L} * (V_{PV}(k) - V_C(k)) \\ V_{PV}(k+1) = V_{PV}(k) + \frac{T_s}{C_1} * (I_{Le}(k) - I_L(k)) \end{cases} \quad \text{(IV.7)}$$

Where, r_L is the internal resistance of the boost inductance L.

The equations (IV.6) and (IV.7) are rearranged in view to minimize current sensors, and they represented by:

$$\begin{bmatrix} I_L(k+1) \\ V_{PV}(k+1) \end{bmatrix} = \begin{bmatrix} \left(1 - \left(\frac{T_s}{L} * r_L\right)\right) & \frac{T_s}{L} & -(1-S) * \frac{T_s}{L} \\ 0 & 2 & 0 \end{bmatrix} . \begin{bmatrix} I_L(k) \\ V_{PV}(k) \\ V_C(k) \end{bmatrix} + \begin{bmatrix} 0 \\ -1 \end{bmatrix} . V_{PV}(k-1) \quad \text{(IV.8)}$$

Then, the predicted power of the boost converter is given by:

$$P^p_{boost} = I_L(k+1) \times V_{PV}(k+1) \quad \text{(IV.9)}$$

IV.3.1.2. Bi-directional converter predictive modelling

The Bi-directional converter used for batteries charge and discharge is modelled based on only two functioning sequences. When the main switch is "ON" and when it is turned "OFF" (the same as for a buck converter), and the predictive equations are obtained using Euler approximation technique as follows:

When the main switch is ON:

$$I_{L_{ba}}(k+1) = \left(1 - \left(\frac{T_s}{L_{ba}} * r_{L_{ba}}\right)\right) * I_{L_{ba}}(k) - \frac{T_s}{L_{ba}} * \left(V_{battery}(k) - V_C(k)\right) \quad \text{(IV.10)}$$

Then, the main switch is turned OFF, we get:

$$I_{L_{ba}}(k+1) = \left(1 - \left(\frac{T_s}{L_{ba}} * r_{L_{ba}}\right)\right) * I_{L_{ba}}(k) - \frac{T_s}{L_{ba}} * V_{battery}(k) \quad \text{(IV.11)}$$

Where, $r_{L_{ba}}$ is the internal resistance of the bi-directional inductance (L_{ba}) and $I_{L_{ba}}$ is the inductor current of the bi-directional converter and it is equal to:

$$I_{L_{ba}} = -I_{battery} \quad \text{(IV.12)}$$

The equations (IV.10) and (IV.11) are rearranged, and represented by (IV.13).

$$\left[I_{L_{ba}}(k+1)\right] = \left[\left(1 - \left(\frac{T_s}{L_{ba}} * r_{L_{ba}}\right)\right) \quad -\frac{T_s}{L_{ba}}\right] . \begin{bmatrix} I_{L_{ba}}(k) \\ V_{battery}(k) \end{bmatrix} + \left[\frac{T_s}{L_{ba}} S\right] . V_C(k) \quad \text{(IV.13)}$$

Then, the predicted power of the Bi-directional converter is given by (IV.14):

$$P^{p}_{battery} = I_{L_{ba}}(k+1) \times V_{battery}(k) \quad \text{(IV.14)}$$

IV.3.2. Proposed cascaded predictive power control for the stand-alone system with energy storage integration

The proposed CPPC control algorithm is shown in Fig. IV.4, it contains three parts to be treated before generating the control signals for the converters, and that can be explained as:

a- After making voltage and current measures as inputs, the predictive models of the three converters are obtained, as mentioned in the previous section.

b- The reference powers are generated as follows:

- The reference power for the P-PVE is generated from the mathematical PV model [22] as given by (IV.15).

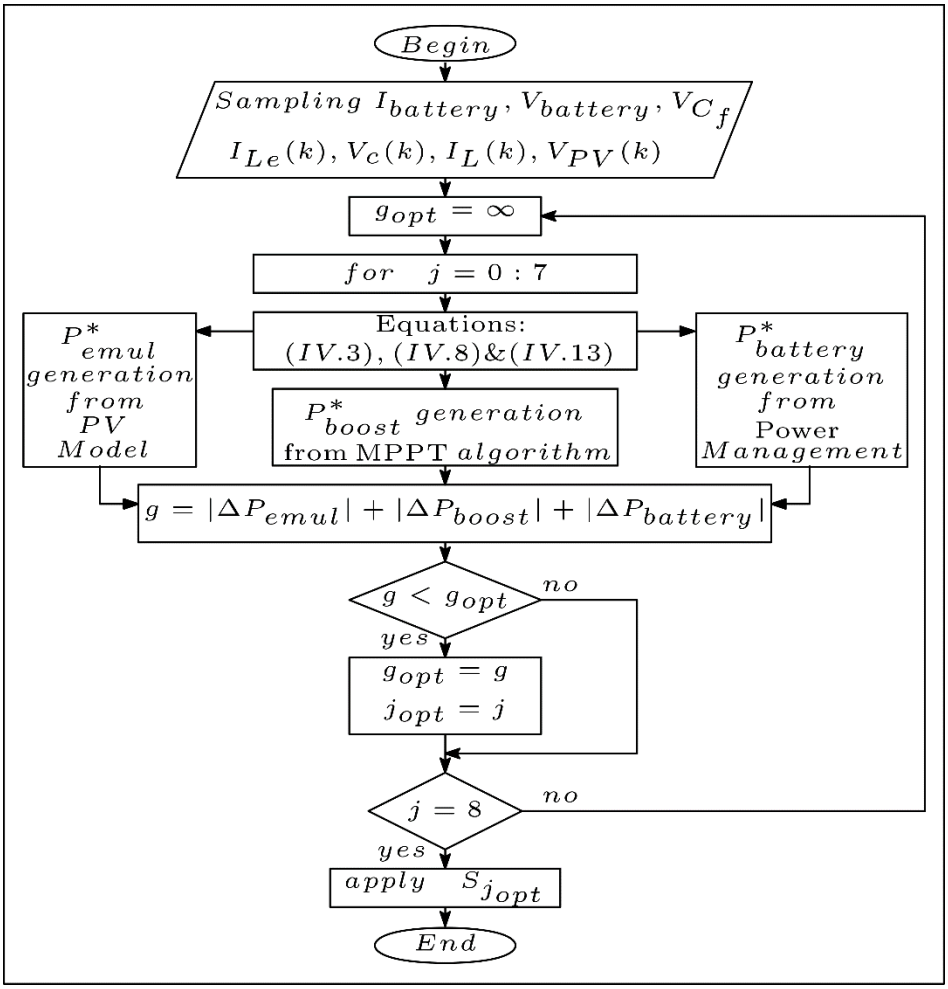

Figure IV.4: Flowchart of the CPPC for the stand-alone system with energy storage integration.

$$\begin{cases} I_{PV} = I_{ph} - I_s\left(e^{\frac{V_{PV}+I_{PV}R_s}{nN_{se}V_t}} - 1\right) - \frac{V_{PV}+I_{PV}R_s}{R_{sh}} \\ V_{PV}(k+1) = 2 \times V_{PV}(k) - V_{PV}(k-1) \\ P_{emul}^{ref} = I_{PV} \times V_{PV}(k+1) \end{cases} \quad \text{(IV.15)}$$

Where, q is the elementary charge (1.6×10^{-19}C), k is Boltzmann constant (1.38×10^{-23}J/K) and T is P − N junction temperature in kelvin. Where, R_s and R_{sh} are the serie and shunt resistances of the solar panel respectively, I_s is the dark saturation current, V_t is the solar cell thermal voltage defined as $V_t = kT/q$, n is the diode quality factor, N_{se} is the number of series-connected PV cells in the PV panel.

- The reference power for the boost converter is generated from the Inc-Cond MPPT algorithm, as given by Fig. III.8 in the previous chapter.
- The reference power for the bi-directional converter is generated from the power management algorithm given by Fig. IV.5, where, the algorithm is based on the P-PVE power, batteries power, the load power and especially the instantaneous state of charge (SoC) of the batteries, which can be obtained with the Coulomb Counting Method (CCM) using the equation (IV.16) [23] as given by Fig. IV.6.

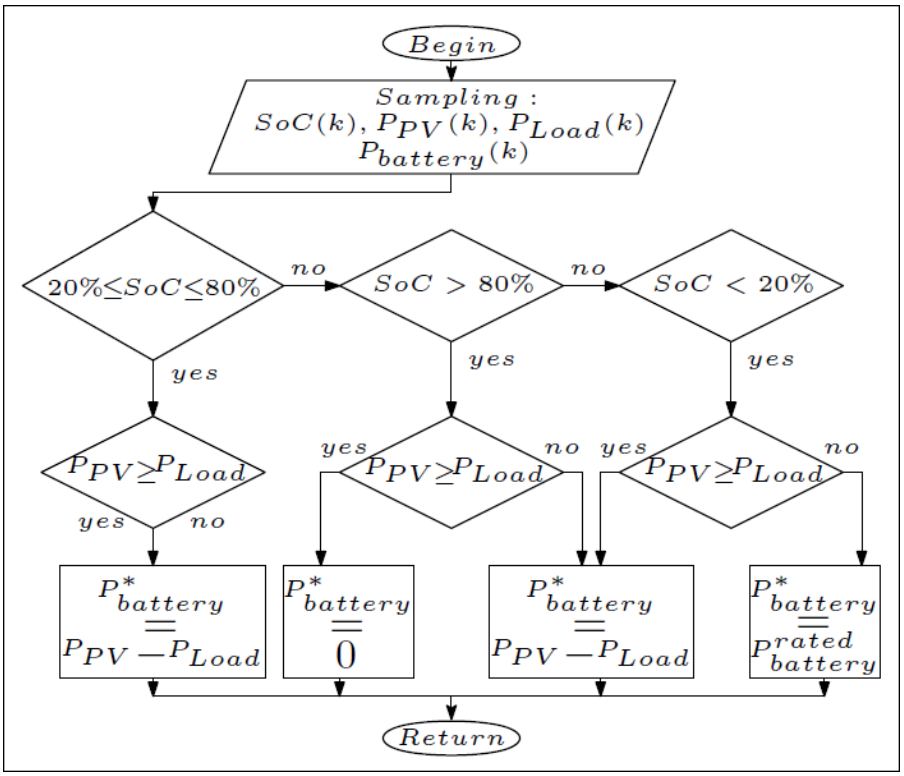

Figure IV.5: The Flowchart of power management algorithm.

$$SoC(t) = SoC(t_0) - \frac{1}{C_n}\int_{t_1}^{t_2} I_{battery}(t)dt \quad \text{(IV.16)}$$

Where, $SoC(t_0)$ is the initial state of charge of batteries, C_n is the nominal capacity of batteries expressed in Ah (1Ah=3600C) [23].

c- The cost function g is generated and contains three power square errors. This cost function should be minimized before selecting the optimal switching states for each converter, as shown by Fig. IV.4 and it given by (IV.17).

$$g = \left|P^{p}_{emul} - P^{ref}_{emul}\right| + \left|P^{p}_{boost} - P^{ref}_{boost}\right| + \left|P^{p}_{battery} - P^{ref}_{battery}\right| \quad \text{(IV.17)}$$

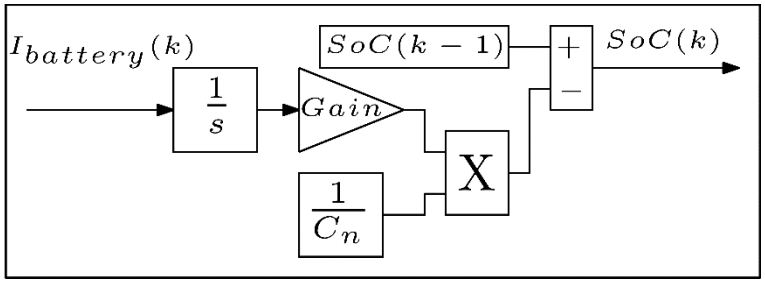

Figure IV.6: The Coulomb counting method used for SoC estimation.

IV.4. Proposed cascaded predictive power control for grid-connected PV systems

As depicted in [12], [13] it is considered to reduce the computation burden while keeping a high grid current waveform, good THD performance and reduced global control loop of the system using the FS-MPC with Predictive Current Control (PCC). This paper proposes a cascaded predictive direct power control for three power converters namely: Buck converter used as a predictive PV emulator (P-PVE), Boost converter and a three-phase voltage source inverter, this configuration deals with a grid-connected photovoltaic application. The proposed cascaded predictive power control (CPPC) takes the performance of the FS-MPC (switching states of each converter) and combines only the possible switching states (28 switching states), this combination can eliminate the redundant switching states in each sampling time and maintain excellent controllability and optimal control of the power system.

Fig. IV.7 shows a Grid-Connected Photovoltaic System (PVGCS) that is based on the P-PVE, boost converter and a three-level voltage source inverter (3P-VSI). The P-PVE emulator replaces the real PV panel modules, and it is used to properly test the system under different

sudden variations of climatic conditions. In contrast, the boost converter is used to ensure the functionality of the system at its maximum power point tracking and extracts the maximum available power from the P-PVE, and the three-phase voltage source inverter is used to transfer and injects the PV power to the utility three-phased grid.

The DC link stage is adopted to an appropriate power value by controlling the AC side, so the DC link voltage V_C is kept to 100V for a 25V/50Hz AC three-phase grid system. The injected current is shaped to be purely sinusoidal and synchronized with the grid voltage using an orthogonal function based block, and its amplitude was calculated by the method given in [14].

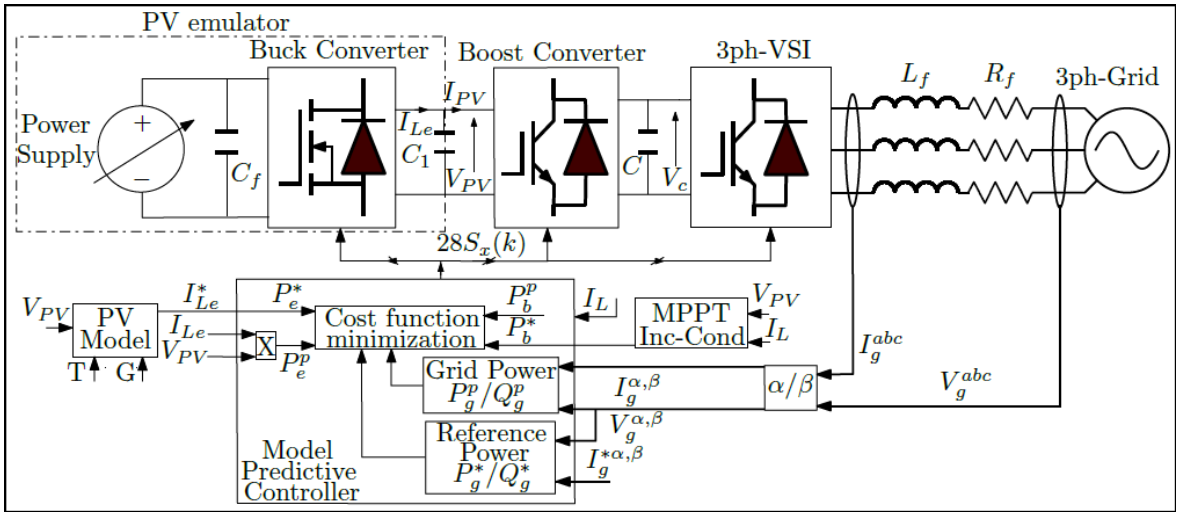

Figure IV.7: Scheme of the proposed cascaded predictive power control (CPPC) for grid connected PV system (GCS).

IV.4.1. The voltage source inverter predictive modelling

The predictive models of the buck converter and the boost one are depicted in the previous sub-sections. The three-phase inverter is used to ensure the PV power injection with an optimal decoupled power control, and its predictive model can be obtained according to the following equations:

The output inverter voltage vector v(k) is related to the DC link voltage V_C by the following equation [14]:

$$v(k) = \Psi(t) \times V_C(k) \qquad \text{(IV.18)}$$

Where:

$$\Psi(t) = \sqrt{\frac{2}{3}}\left(S_a + S_b e^{j\frac{2\pi}{3}} + S_C e^{j\frac{4\pi}{3}}\right) \quad \text{(IV.19)}$$

The control of the three-phase inverter requires a discrete-time model of the grid, which can be defined from the following continuous-time equation:

$$v(k) = R_f . I_{g_{\alpha,\beta}}(k) + L_f \frac{dI_{g_{\alpha,\beta}}(k)}{dt} + V_{g_{\alpha,\beta}}(k) \quad \text{(IV.20)}$$

Where $I_{g_{\alpha,\beta}}$ is the grid currents, R_f is the grid filter resistance, L_f is the grid filter inductance and $V_{g_{\alpha,\beta}}$ is the grid voltage vectors, and they are assumed to be sinusoidal with constant frequency and constant amplitude.

Then the predicted grid currents for one-step-ahead can be given as:

$$I_{g_{\alpha,\beta}}(k+1) = (1 - R_f \frac{T_S}{L_f})\, I_{g_{\alpha,\beta}}(k) + \frac{T_S}{L_f}(v(k) - V_{g_{\alpha,\beta}}(k)) \quad \text{(IV.21)}$$

This predicted current model is used to calculate the future active and reactive power of the grid side, P_g^p and Q_g^p as follows:

$$P_g^p = V_{g_\alpha}(K+1) I_{g_\alpha}(K+1) + V_{g_\beta}(K+1) I_{g_\beta}(K+1) \quad \text{(IV.22)}$$

$$Q_g^p = V_{g_\beta}(K+1) I_{g_\alpha}(K+1) + V_{g_\alpha}(K+1) I_{g_\beta}(K+1) \quad \text{(IV.23)}$$

The reference active and reactive power is obtained as follows:

$$P_g^{ref} = V_{g_\alpha}(K+1) I_{g_\alpha}^{ref}(K+1) + V_{g_\beta}(K+1) I_{g_\beta}^{ref}(K+1) \quad \text{(IV.24)}$$

$$Q_g^{ref} = V_{g_\beta}(K+1) I_{g_\alpha}^{ref}(K+1) + V_{g_\alpha}(K+1) I_{g_\beta}^{ref}(K+1) \quad \text{(IV.25)}$$

Where, the value of the reference grid current is obtained by using (IV.26), and it is shaped to be purely sinusoidal in phase with the grid voltage.

$$I_g^{ref_{max}} = \frac{P_b^p}{V_g} \quad \text{(IV.26)}$$

The formulated cost function is given by (IV.27) as follows:

$$g = \left|P_e^p - P_e^{ref}\right| + \left|P_b^p - P_b^{ref}\right| + \left|P_g^p - P_g^{ref}\right| + \left|Q_g^p - Q_g^{ref}\right| + \lambda . N_s \qquad \text{(IV.27)}$$

IV.4.2. The cascaded predictive power algorithm

The proposed algorithm is based on hybrid predictive and Incremental conductance (Inc-Cond) algorithms [1], as shown in Fig. IV.8 considers the three cascaded power converter as a single converter and controls them at the same time with the same optimized cost function as in the case of an indirect matrix converter. This algorithm aims to:

a- Simplify the global control system and gives it more controllability.

b- Offer optimal control by using the theory of decoupled power control and by including the MPPT in the algorithm.

c- Allow the system able to compensate for the undesired reactive power on the grid side.

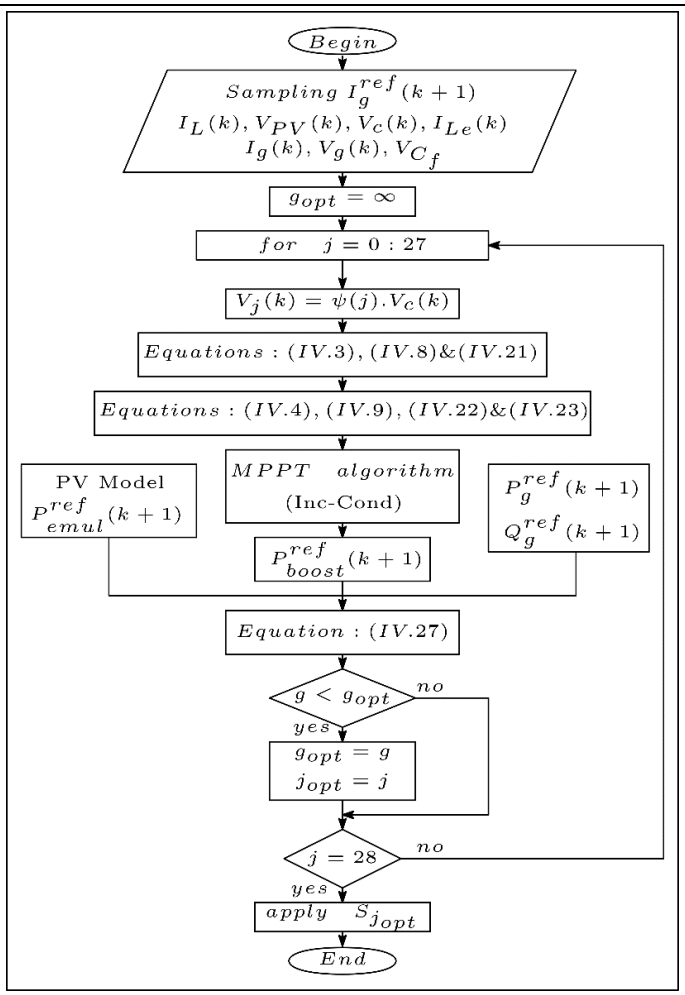

Figure IV.8: Flowchart of the CPPC algorithm applied to GCS.

IV.5. Simulations and discussions

In order to confirm the efficacy of the proposed configurations, simulations are done under MATLAB/SIMULINK software. Specifications of the used parameters are indicated in Table IV.1. The sampling time T_s for P-PVE and GCS is set to 50µs and for the PV system with batteries is set to 10µs. Three panels in series are used in the PV panel model (3*TE-505) for P-PVE and GCS tests, whereas two panels in series (2*TE-505) are used for the PV system with batteries.

Table IV.1: Active switching states of the CPC-GCS application.

Parameter	Symbol	Values for P-PVE	Values for P-PVE with batteries	Values for GCS	Unit
PV maximum power	P_{MPP}	3*49.26	2*49.26	3*49.26	W
PV maximum current	I_{MPP}	2.8	2.8	2.8	A
Short circuit current	I_{SC}	3.1	3.1	3.1	A
PV maximum voltage	V_{MPP}	3*17.6	2*17.6	3*17.6	V
Open circuit voltage	V_{OC}	3*21.7	2*21.7	3*21.7	V
Input voltage	V_{Cf}	82	62	82	V
DC Link voltage	V_C	100	67	100	V
Grid voltage	V_g	-	-	50	V
Filter resistor	R_f	-	-	0.2	Ω
Filter inductor	L_f	-	-	30	mH
Buck converter capacitor	C_1	0.68	0.68	0.68	mF
Boost converter capacitor	C	-	1.1	1.1	mF
Bi-directional converter capacitor	C	-	1.1	-	mF
Input capacitor	C_f	0.68	0.68	0.68	mF
Buck converter inductor	L_e	10	10	10	mH
Boost converter inductor	L	-	10	3	mH
Bi-directional converter inductor	$L_{battery}$	-	10	-	mH

To affirm the functioning of the P-PVE using the predictive power control. A sudden irradiance variation test is done in the range [1 - 0.7 - 0.55 - 0.85] kW/m². Fig. IV.9 shows the less oscillation of the P-PVE power P_{PV} the current I_{Le} and voltage V_{PV}, also high dynamic response is achieved and confirmed by the reference current I_{Le}^{ref} tracking even under hard irradiance variations.

To illustrate the good functioning of the studied system using the CPPC. A hard irradiance variation test is done in the range [1 - 0.5 - 0.7] kW/m². Fig. IV.10 shows the less oscillation of

the P-PVE current I_{Le} and a stable state of the voltage V_{PV} also the DC link voltage V_C have a quasi constant value even under hard irradiance variations, and that confirms the good power balancing between the P-PVE power and batteries power against the load demanded power.

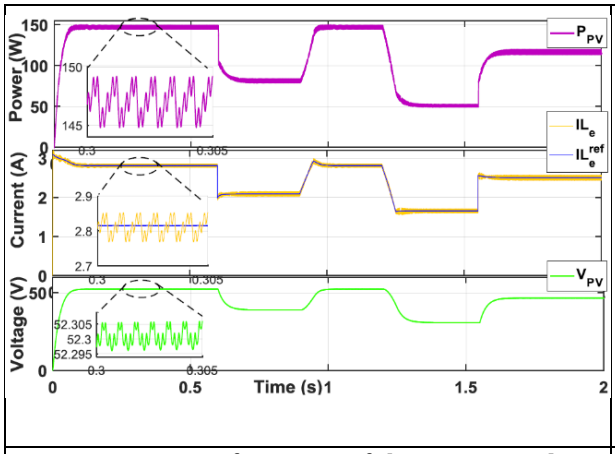

Figure IV.9: Performance of the P-PVE under irradiance variation test.

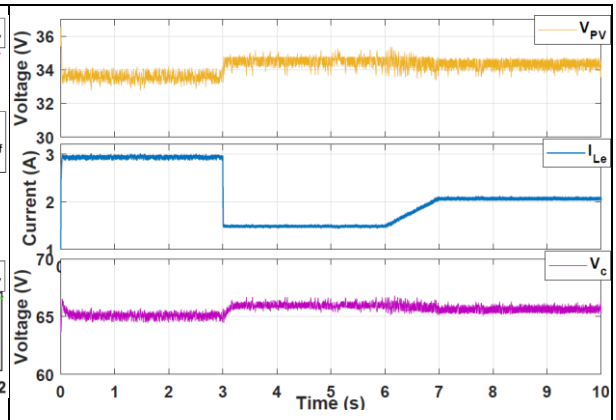

Figure IV.10: P-PVE voltage and current with the DC link voltage.

The good functioning of the power management included in the CPPC control algorithm is confirmed also for both irradiance variation levels. For a sudden change of illumination from [1 - 0.5] kW/m² at 3s and smooth irradiance rising in the time range [6 - 7] s from [0.5 - 0.7] kW/m², where, the demanded power still constant and the P-PVE power is perfectly balanced with the batteries power as illustrated by Fig. IV.11. Then, the batteries charge and discharge performance is illustrated by Fig. IV.12. where, the batteries voltage and current indicate the phase of charge from [0 - 3] s when the irradiance is equal to 1 kW/m² (the P-PVE power can fulfil the load demand, and the SoC increases from 50 % to 50.0042%), then, the phase of discharge from [3 - 6] s when the irradiance is equal to 0.5 kW/m² (the P-PVE power cannot fulfil the load demand, and the SoC decreases from 50.0042% to 50.0015%), then, when the irradiance is fixed to 0.7 kW/m², one can see that the demanded power and the P-PVE power are equal to each other and the batteries power has a stable state (the SoC is constant and it is equal to 50.0015%).

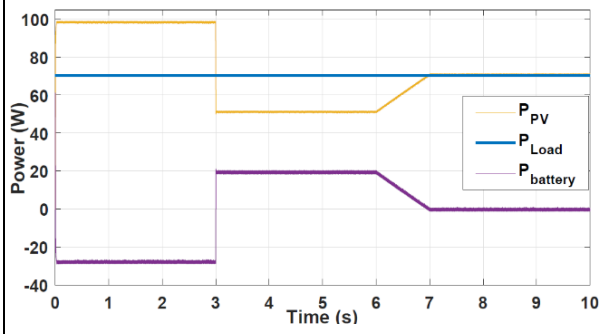

Figure IV.11: Balancing power between PV power, demanded power and batteries power.

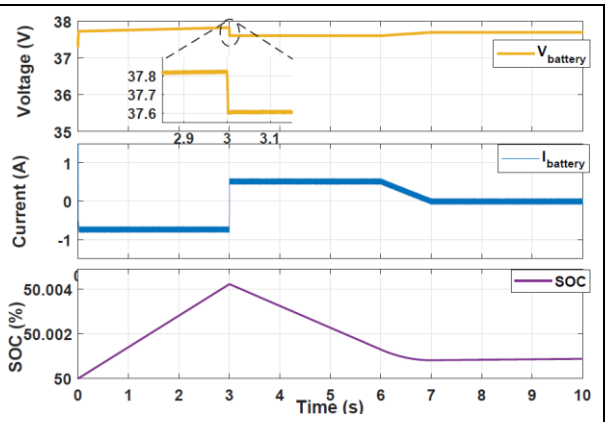

Figure IV.12: Performance of the batteries under charge and discharge cycles.

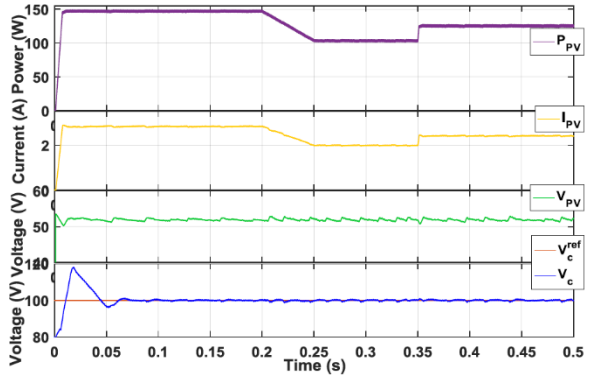

Figure IV.13: Performance in the DC side of the GCS.

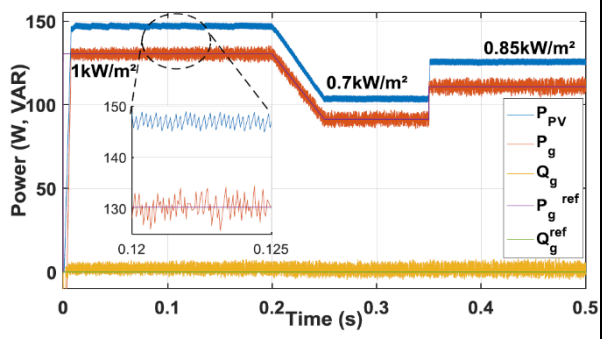

Figure IV.14: PV power with the grid side active and reactive powers.

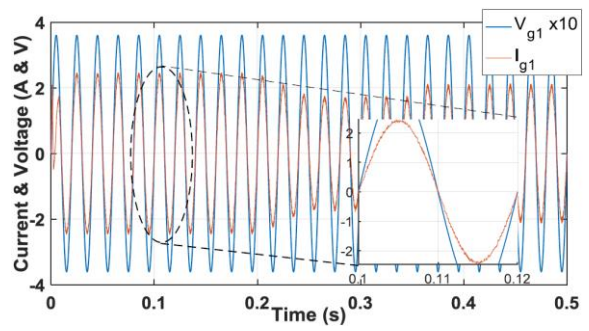

Figure IV.15: Grid side voltage and current.

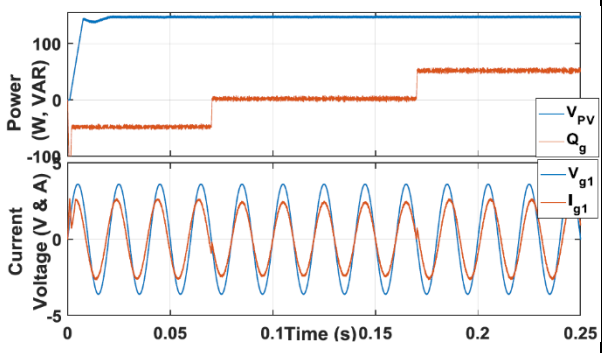

Figures IV.16: Grid side reactive power test.

The good performances of the GCS with the proposed control algorithm are also confirmed for both tests: smooth irradiance degradation in the time range [0.2 - 0.25] s from [1 - 0.7] kW/m², then for a sudden change of illumination from [0.7 - 0.85] kW/m² at 0.35 s. Simulation results show the performance of the system in their both sides (DC side and AC side). Fig. IV.13 shows the proper functioning of the GCS for the previous profile of the irradiance

changes where the PV power achieves its Maximum Power Point (MPP) and gives its maximum available power P_{PV} even under low irradiance levels. Fig. IV.14 shows the P_{PV} around the MPP in the DC side, whereas in the grid side, active grid power P_g and reactive grid power Q_g track closely their references with low ripples (Q_g^{ref}=0). It is clear to see from Fig. IV.15 that the grid current I_g is perfectly in phase with the grid voltage V_g and it seems sinusoidal with low THD of about [1.89 - 3.08 - 2.58] % under irradiance levels [1 - 0.7 - 0.85] kW/m² respectively. The GCS with the proposed CPPC is able to eliminate the undesired surplus of the Q_g or to provide the reactive power lack as it is shown in Fig. IV.16, where the reactive power reference is settled respectively to [-50 - 0 - +50] VAR.

IV.6. Experimental validations

The global experimental bench for testing the studied systems is shown in Fig. IV.17 and Fig. IV.18 using a dSPACE 1104 board. The buck converter used for P-PVE is realized using a MOSFET (500V/20A), the boost converter, the bi-directional converter, and voltage source inverter are those of SEMIKRON IGBT (750V/30A). The current and voltage sensors are those of LA-25 and LV-25, respectively. The sampling time for P-PVE test is set to 50µs and 90µs for PV system with energy storage and GCS tests.

The P-PVE is now validated experimentally, Fig. IV.19 shows high dynamic response, low power ripples and good current reference I_{Le}^{ref} tracking under the same irradiance variation levels of simulations given by Fig. IV.9.

The PV system with batteries integration is now tested experimentally, under hard irradiance variation test, Fig. IV.20 shows the performance of the P-PVE, where the P-PVE voltage V_{PV} and current I_{Le} are obtained with their MPP values, and the DC link voltage V_C is kept to a quasi-constant value, where, the load demand is fulfilled, by means that the MPPT algorithm and the power management are well operated under the CPPC control. Fig. IV.21 shows the balancing power between the P-PVE power and the batteries power against the demanded power, where, they compensate each other to fulfil the load demands under any irradiance variation levels.

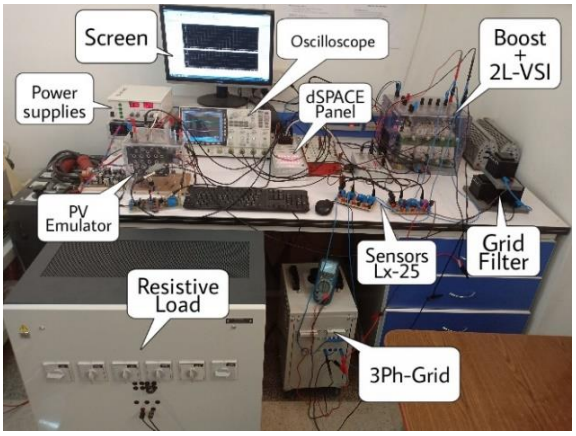

Figure IV.17: The experimental bench used for GCS tests.

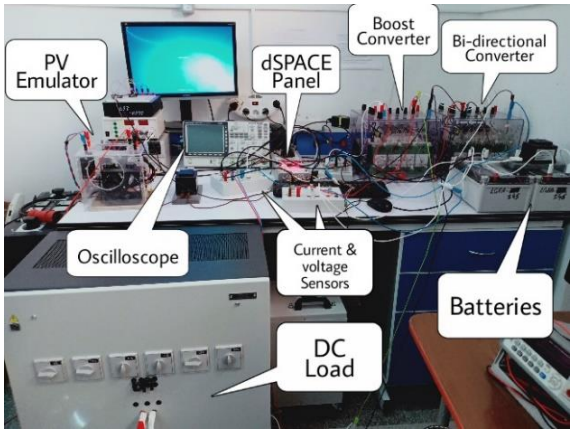

Figure IV.18: The experimental bench used for P-PVE and energy storage system.

One can see from Fig. IV.22 that the batteries are charged and discharged according to the extracted P-PVE power and the demanded power, where, the batteries voltage $V_{battery}$ and current $I_{battery}$ indicate the cycle of charge from [0 - 3] s when the irradiance is equal to 1 kW/m² (the P-PVE power can fulfil the load demand, and the SoC increases from 50.015 % to 50.0192 %), then, the cycle of discharge from [3 - 6] s when the irradiance is equal to 0.5 kW/m² (the P-PVE power cannot fulfil the load demand, and the SoC decreases from 50.0192 % to 50.016 %), then, when the irradiance is set to 0.7 kW/m² one can see that the demanded power and the P-PVE power are equal to each other and the batteries power has a stable state (the SoC is constant and is equal to 50.016 %).

The proposed GCS based on CPPC is validated experimentally with high dynamic performances as those obtained in simulations (Fig. IV.13), From Fig. IV.23 one can see that the DC side of the GCS proves high dynamic response with fewer ripples of the (P_{PV}, I_L, V_{PV}). In addition, the DC link voltage V_C is kept constant to 100 V. Also, the grid active power P_g follows the same profile of the PV power P_{PV} and the grid reactive power Q_g oscillates around zero as it is shown in Fig. IV.24. Fig. IV.25 shows the three-phase currents $I_{a,b,c}$ under irradiance variation from 1 kW/m² to 0.7 kW/m². The AC side of the GCS is illustrated in Fig. IV.26, which shows that the grid current is in phase with the grid voltage V_g having a sinusoidal form with less THD of about [2.92 - 4.18 - 3.29] % under irradiance levels [1 - 0.7 - 0.85] kW/m² respectively. The high efficacy of the proposed CPPC for GCS is confirmed by Fig. IV.27, where, the system is able to estrange the undesired surplus of the Q_g or to provide the reactive power lack without any perturbation in the transmitted PV power P_{PV}.

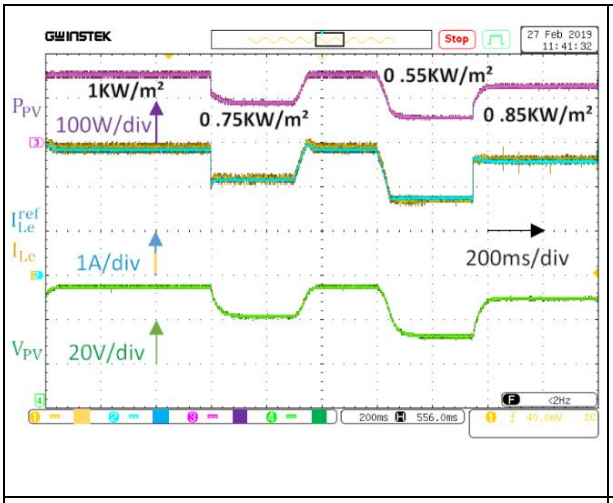

Figure IV.19: Experimental performance of the P-PVE under irradiance variation test.

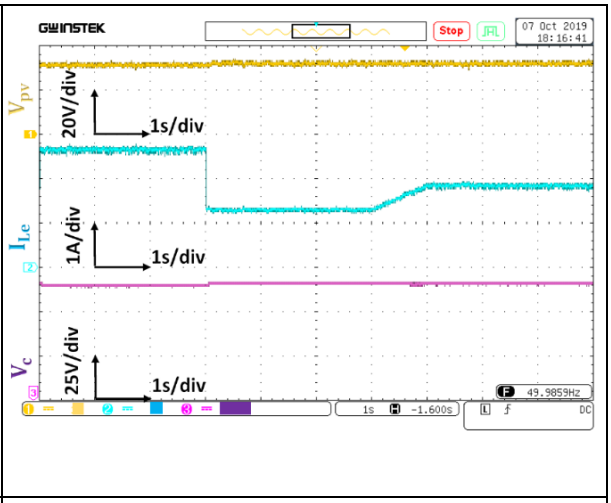

Figure IV.20: Experimental results of the P-PVE with energy storage system.

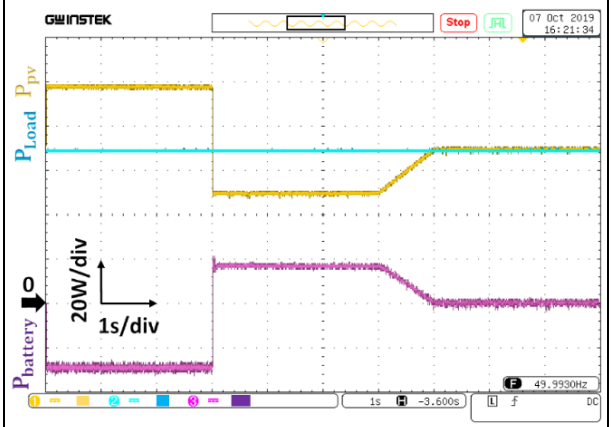

Figure IV.21: Experimental balancing power between PV power, demanded power and batteries power.

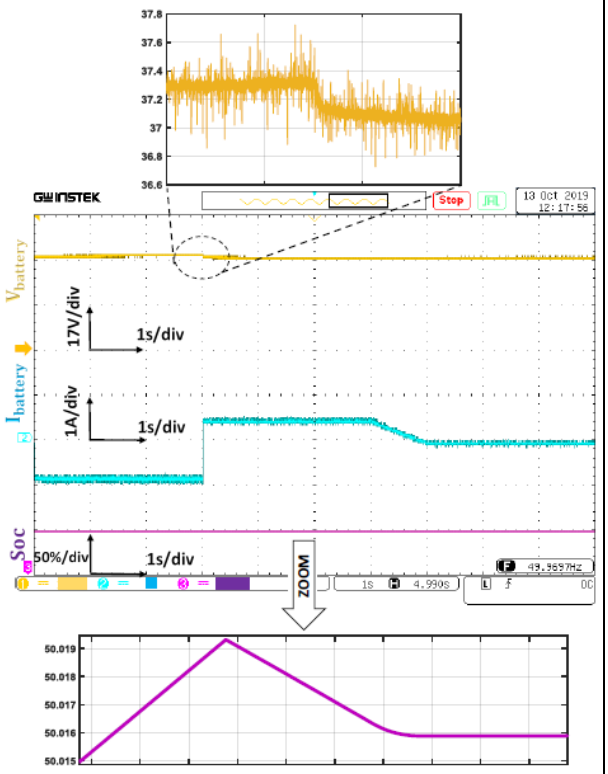

Figure IV.22: Experimental performance of the batteries under charge and discharge cycles.

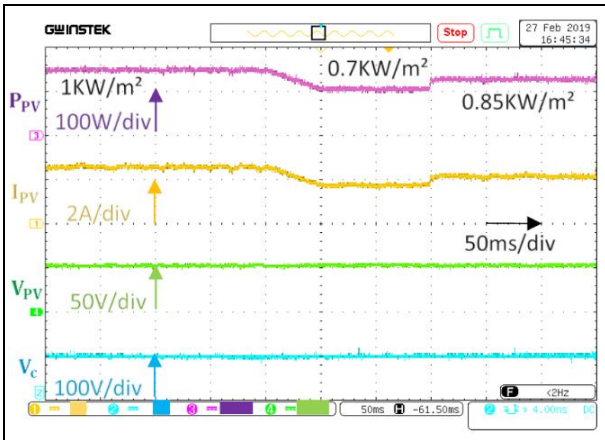

Figure IV.23: Experimental performance in the DC side of the GCS.

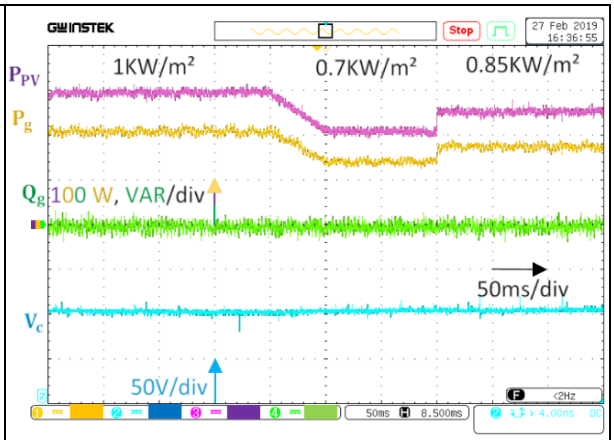

Figure IV.24: Experimental PV power with the DC link voltage and the grid powers of the GCS.

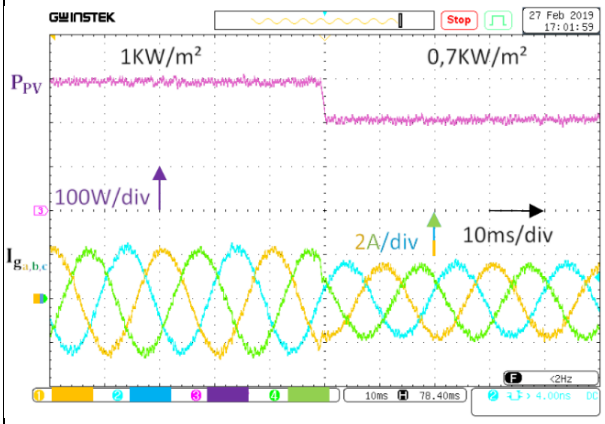

Figure IV.25: The three phase currents under irradiance variations.

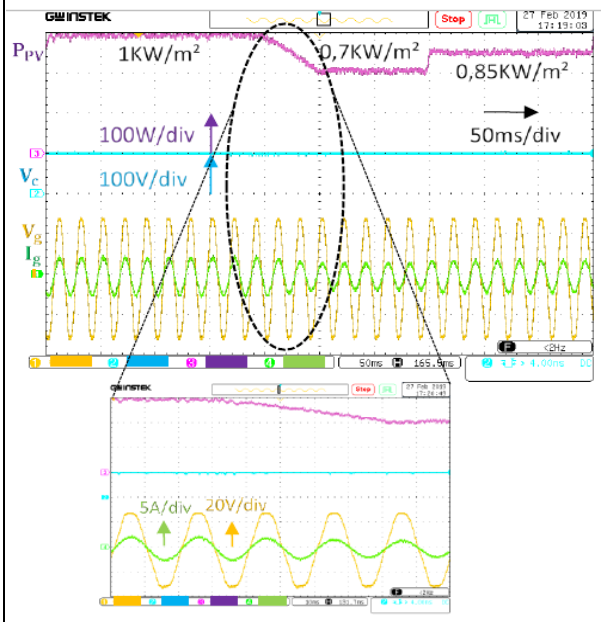

Figure IV.26: Experimental performance in the AC side of the GCS.

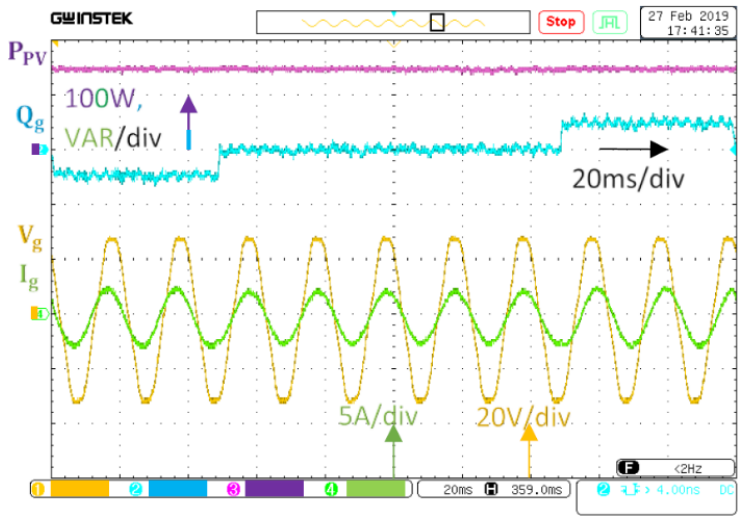

Figure IV.27: Grid side reactive power experimental test.

IV.7. Conclusion

The present chapter deals with three kinds of photovoltaic configurations. The first one is dedicated to a predictive power control algorithm well suited for PV emulators. The second one deals with the cascaded control of three DC/DC converters used in a stand-alone photovoltaic system with integrated energy storage. The power management of the studied system between the P-PVE power, batteries power and demanded power, is directly included in the proposed control, so this last ensures the MPPT functioning by extracting the available power from the P-PVE and also the batteries charge and discharge cycles with fewer ripples all depending on the demanded power of the load. The third one presents a new Cascaded Predictive Power Control destined for Grid-Connected PV System. The CPPC is used to control the cascaded power converters simultaneously at the same time with the same optimized cost function, as shown in Fig. IV.17. Consequently, more flexibility and simple controllability are obtained and allowed the system able to compensate for the undesired grid reactive power (see Fig. IV.16 and Fig. IV.27). A set of simulations and experimental tests are done to illustrate well the high efficacy of the P-PVE and the proposed CPPC strategy under several hard tests of irradiance levels variations.

IV.8. References

[1] S. El Islam Remache et K. Barra, « Performance comparison among boost and multi level boost converters for photovoltaic grid connected system using finite set model predictive control », in *2018*

9th International Renewable Energy Congress (IREC), Hammamet, mars 2018, p. 1‑6, doi: 10.1109/IREC.2018.8362483.

[2] J. P. Ram, H. Manghani, D. S. Pillai, T. S. Babu, M. Miyatake, et N. Rajasekar, « Analysis on solar PV emulators: A review », *Renewable and Sustainable Energy Reviews*, vol. 81, p. 149‑160, janv. 2018, doi: 10.1016/j.rser.2017.07.039.

[3] M. Azharuddin, T. S. Babu, N. Bilakanti, et N. Rajasekar, « A Nearly Accurate Solar Photovoltaic Emulator Using a dSPACE Controller for Real-time Control », *Electric Power Components and Systems*, vol. 44, nº 7, p. 774‑782, avr. 2016, doi: 10.1080/15325008.2015.1131763.

[4] V. Yaramasu et B. Wu, *Model Predictive Control of Wind Energy Conversion Systems*. Hoboken, NJ, USA: John Wiley & Sons, Inc., 2017.

[5] H. Dehghani Tafti *et al.*, « Low-voltage ride-thorough capability of photovoltaic grid-connected neutral-point-clamped inverters with active/reactive power injection », *IET Renewable Power Generation*, vol. 11, nº 8, p. 1182‑1190, juin 2017, doi: 10.1049/iet-rpg.2016.0544.

[6] R. Ayop et C. W. Tan, « A comprehensive review on photovoltaic emulator », *Renewable and Sustainable Energy Reviews*, vol. 80, p. 430‑452, déc. 2017, doi: 10.1016/j.rser.2017.05.217.

[7] R. P. Aguilera *et al.*, « Selective Harmonic Elimination Model Predictive Control for Multilevel Power Converters », *IEEE Transactions on Power Electronics*, vol. 32, nº 3, p. 2416‑2426, mars 2017, doi: 10.1109/TPEL.2016.2568211.

[8] J. Ebrahimi, E. Babaei, et G. B. Gharehpetian, « A New Multilevel Converter Topology With Reduced Number of Power Electronic Components », *IEEE Transactions on Industrial Electronics*, vol. 59, nº 2, p. 655‑667, févr. 2012, doi: 10.1109/TIE.2011.2151813.

[9] C. Xue, W. Song, X. Wu, et X. Feng, « A Constant Switching Frequency Finite-Control-Set Predictive Current Control Scheme of a Five-Phase Inverter With Duty-Ratio Optimization », *IEEE Transactions on Power Electronics*, vol. 33, nº 4, p. 3583‑3594, avr. 2018, doi: 10.1109/TPEL.2017.2707440.

[10] J. Rodriguez et P. Cortes, *Predictive Control of Power Converters and Electrical Drives: Rodriguez/Predictive Control of Power Converters and Electrical Drives*. Chichester, UK: John Wiley & Sons, Ltd, 2012.

[11] Z. Kara, K. Barra, et A. Y. Cherif, « Predictive algorithm for matrix converter control in wind energy conversion system based DFIG », in *2018 9th International Renewable Energy Congress (IREC)*, Hammamet, mars 2018, p. 1‑6, doi: 10.1109/IREC.2018.8362530.

[12] X. Chen, J. Liu, S. Song, S. Ouyang, H. Wu, et Y. Yang, « Modified Increased-Levels Model Predictive Control Methods With Reduced Computation Load for Modular Multilevel Converter », *IEEE Transactions on Power Electronics*, p. 1‑1, 2018, doi: 10.1109/TPEL.2018.2882690.

[13] Y. Li, Z. Zhang, et M. P. KaTmierkowski, « Cascaded Predictive Control for Three-Level NPC Power Converter Fed Induction Machine Drives Without Weighting Factors », in *2018 IEEE International Power Electronics and Application Conference and Exposition (PEAC)*, Shenzhen, nov. 2018, p. 1‑5, doi: 10.1109/PEAC.2018.8590301.

[14] O. Abdel-Rahim, H. Funato, et J. Haruna, « Gird-connected boost inverter for low-power PV applications with model predictive control », *The Journal of Engineering*, vol. 2017, nº 7, p. 318‑326, juill. 2017, doi: 10.1049/joe.2017.0070.

[15] A. T. Elsayed, A. A. Mohamed, et O. A. Mohammed, « DC microgrids and distribution systems: An overview », *Electric Power Systems Research*, vol. 119, p. 407‑417, févr. 2015, doi: 10.1016/j.epsr.2014.10.017.

[16] M. S. B. Arif et M. A. Hasan, « Microgrid architecture, control, and operation », in *Hybrid-Renewable Energy Systems in Microgrids*, Elsevier, 2018, p. 23‑37.

[17] L. Zhang, N. Tai, W. Huang, J. Liu, et Y. Wang, « A review on protection of DC microgrids », *Journal of Modern Power Systems and Clean Energy*, vol. 6, nº 6, p. 1113‑1127, nov. 2018, doi: 10.1007/s40565-018-0381-9.

[18] M. F. Zia, E. Elbouchikhi, et M. Benbouzid, « Microgrids energy management systems: A critical review on methods, solutions, and prospects », *Applied Energy*, vol. 222, p. 1033‑1055, juill. 2018, doi: 10.1016/j.apenergy.2018.04.103.

[19] S. El Islam Remache, A. Y. Cherif, K. Barra, et A. Reama, « Cascaded Predictive Direct Power Control for Grid Connected Photovoltaic System », in *2019 1st Global Power, Energy and Communication Conference (GPECOM)*, Nevsehir, Turkey, juin 2019, p. 302‑307, doi: 10.1109/GPECOM.2019.8778582.

[20] A. Lashab, D. Sera, J. Martins, et J. M. Guerrero, « Model Predictive-Based Direct Battery Control in PV Fed Quasi Z-Source Inverters », in *2018 5th International Symposium on Environment-Friendly Energies and Applications (EFEA)*, Rome, sept. 2018, p. 1‑6, doi: 10.1109/EFEA.2018.8617084.

[21] M. B. Shadmand, R. S. Balog, et H. Abu-Rub, « Model Predictive Control of PV Sources in a Smart DC Distribution System: Maximum Power Point Tracking and Droop Control », *IEEE Transactions on Energy Conversion*, vol. 29, nº 4, p. 913‑921, déc. 2014, doi: 10.1109/TEC.2014.2362934.

[22] S. el islam Remache, A. Yahia Cherif, et K. Barra, « Optimal Cascaded Predictive Control for Photovoltaic Systems: application based on predictive emulator », *IET Renewable Power Generation*, août 2019, doi: 10.1049/iet-rpg.2019.0068.

[23] W.-Y. Chang, « The State of Charge Estimating Methods for Battery: A Review », *ISRN Applied Mathematics*, vol. 2013, p. 1‑7, 2013, doi: 10.1155/2013/953792.

GENERAL CONCLUSION AND FUTURE WORK

General conclusion and future work

This PhD thesis focused much more on improving experimental performance of PV solar systems using developed and proposed control algorithms based on FS-MPC.

The research in the first section has begun by reviewing various interesting researches and contributions on PV systems integrated in DC micro-grids and related to DERs. In addition, the benefits and drawbacks of each important control method are summarized and compared, in order to well investigate the given improvement for the studied systems.

The second section is devoted to the theoretical study of the FS-MPC applied to PV systems and power electronics, its basic principle, the flexibility of the cost function and weighting factors determination. In the second part of this section, a performance comparative study between two different topologies of DC/DC converters is presented in stand-alone and grid-connected systems. In this study, a proposed predictive current control including a hybrid MPPT algorithm is presented, and analyzed in view to demonstrate its flexibility given for these systems. Moreover, a set of simulation results is given and discussed to well present the comparison study in terms of the reference current tracking, dynamic response, DC link voltage stabilization, and switching number (average frequencies).

For the experimental validation of the obtained results, a P-PVE is developed and realized in the LGEA laboratory, it is based on synchronous buck converter. Its predictive control algorithm is compared to the conventional PI controller, in terms of less oscillation, reference current tracking, and robustness under load variations, where it proved its superiority over the compared one. In addition, a CPC is proposed and presented for a single-phase grid PV connected system, the flexibility of this control algorithm allow us to add in the same cost function a secondary control objective such as the switching number minimization. The studied system is subject to several experimental tests to prove its robustness, and many results are presented and discussed.

Always in search for system optimization, a CPPC algorithm is proposed and presented for a three-phase grid PV system. The control algorithm is based on the decoupling power control strategy and it aims to control all cascaded converters of the conversion chain simultaneously with the same cost function which contains the P-PVE power error, the MPPT power error, the active and reactive powers errors and the fifth term for switching number minimization. The five terms are minimized together in one loop without any complication. This flexibility allows

the system to be able to compensate the reactive power, ensures the grid injection and extracts the maximum of PV power without any perturbation. The system is tested experimentally under the same tests of simulations and it proved high performance. Additionally, the CPPC is applied for an islanded system with integrated energy storage, where it works in parallel with the power management algorithm to ensure batteries' charge and discharge. Experimental results are carried out to prove the effectiveness of the proposed control algorithm.

The researches in this dissertation have open the door for new challenges and shed a light on more contributions and investigations that could be our future work and that could be listed as follows:

- As a first future work, we will increase PV penetration and the injected power into the grid side (rise up to KW level), and that leads to more investigations on system control and stabilization.
- Developing a DC micro-grid based on PV panels, batteries, fuel cell and wind turbine by making interactions with the demanded loads and the AC grid. This challenge will be followed by new control techniques, new power management algorithms and more advanced interfaces for practical analysis.
- Developing power converters topologies for DC micro-grids and enhancing their behavior by developing new control techniques.
- We will try to overcoming the drawbacks of the FS-MPC and proposing new techniques to enhance its benefits, like fixing the switching frequency, proposing new cost functions based on new control variables, and proposing new methods for the weighting factor selection.

Abstract

Photovoltaic power generation systems gain popularity day by day, where photovoltaic energy became the first one used in distributed energy resources. This dissertation focuses on experimental platforms and advanced control algorithms: Finite Set Model Predictive Control. The first research treats in simulations the use of the FS-MPC to photovoltaic systems, and it is applied to stand alone PV systems with two different topologies of DC/DC converters, and to grid-connected systems using AC converters.

A PV emulator based on DC/DC buck converter represents the second aspect of this work, where the PV platform experimentations are tested under real climatic conditions. For that, a hybrid MPPT based on MPC and the incremental inductance algorithm was developed in order to extract the maximum of power from the PV emulator. The studied PV grid-tied system is also subject to a proposed predictive control that uses predicted models of the three-cascaded converters, and that allows flexibility to control them simultaneously after minimization of a single cost function. This suppleness gives the possibility to add a minimization of the switching numbers as a fourth term in the cost function.

In the third aspect, the research investigates a cascaded predictive algorithm with decoupled active and reactive powers control. The proposed control aims to give more controllability to the system and improve its efficiency. This section's first studied system contains three converters, These lasts are controlled simultaneously with one cost function; the used control strategy provides more robustness to the system by means that the global system can now compensate the undesired reactive power on the grid side without any other regulator and any perturbation in the DC side. The second studied system deals with a standalone PV system with integrated energy storage. The predictive power control algorithm used for it; includes power management. Besides, it assures the battery's charge and discharge cycles with fewer ripples, all depending on the load's demanded power. The both systems are tested experimentally under several conditions.

Résumé

Les systèmes de production de l'énergie photovoltaïque gagnent en popularité de jour en jour, où l'énergie photovoltaïque est devenue la première énergie utilisée dans les ressources énergétiques distribuées. Cette thèse se concentre sur les plates-formes expérimentales et les algorithmes de contrôle avancés tel que la commande prédictive à ensemble fini. La première recherche de ce travail traite en simulation l'utilisation de la FS-MPC appliquée aux systèmes photovoltaïques, autonomes avec deux topologies différentes de convertisseurs DC / DC, et à des systèmes connectés au réseau utilisant des convertisseurs AC.

Un émulateur PV basé sur un convertisseur dévolteur DC / DC représente la deuxième contribution de ce travail, où les plateformes PV sont testées expérimentalement et dans des conditions climatiques réelles. Pour cela, un MPPT hybride basé sur l'MPC et l'algorithme incrémentation de l'inductance a été développé afin d'extraire le maximum de puissance de l'émulateur PV. Le système PV lié au réseau étudié est également soumis à une commande prédictive proposée qui utilise des modèles prédits des trois convertisseurs cascadés, et qui permet une flexibilité pour les contrôler simultanément après la minimisation d'une fonction de coût unique. Cette souplesse permet d'ajouter une minimisation des nombres de commutation comme quatrième terme dans la fonction de coût.

Dans cette contribution, le travail étudie un algorithme prédictif en cascade avec une commande découplée des puissances actives et réactives. La commande proposée vise à donner plus de contrôlabilité au système et à améliorer son efficacité. Le premier système étudié de cette section contient trois convertisseurs. Ces derniers sont contrôlés simultanément avec une fonction de coût ; la stratégie de commande utilisée fournit plus de robustesse au système où le système global peut maintenant compenser la puissance réactive indésirable côté réseau sans aucun régulateur et aucune perturbation côté DC. Le deuxième système étudié concerne un système PV autonome avec stockage d'énergie intégré. L'algorithme de commande utilisé pour ce système inclut la gestion des puissances. En outre, il assure les cycles de charge et de décharge de la batterie avec moins d'ondulations, tout en fonction de la puissance demandée par la charge. Le système est testé expérimentalement sous plusieurs conditions.

ملخص

تكتسب أنظمة توليد الطاقة الكهروضوئية شعبية يومًا بعد يوم، حيث أصبحت الطاقة الكهروضوئية هي الأولى من حيث الاستخدام في مصادر الطاقة الموزعة. تركز هذه الرسالة على المنصات التجريبية وخوارزميات التحكم المتقدمة: التحكم التنبئي بنموذج المجموعة المحدودة. يعالج البحث الأول محاكاة للأنظمة الكهروضوئية باستخدام FS-MPC، ويتم تطبيقه على الأنظمة الكهروضوئية القائمة بذاتها مع نوعين مختلفتين من محولات التيار المستمر DC / DC، والأنظمة المتصلة بالشبكة باستخدام محولات التيار المتردد AC.

يمثل المحاكي الكهروضوئي المستند إلى محول مخفض الجهد DC / DC الجانب الثاني من هذا العمل، حيث يتم اختبار تجارب منصة PV في ظل ظروف مناخية حقيقية. من أجل ذلك، تم تطوير خوارزمية MPPT الهجين على أساس MPC وخوارزمية الحث التزايدي من أجل استخراج أقصى طاقة من محاكي PV. يخضع النظام المرتبط بالشبكة الكهروضوئية المدروسة أيضًا لعنصر تحكم تنبؤي مقترح يستخدم النماذج المتوقعة للمحولات الثلاثة المتتالية، والتي تتيح المرونة للتحكم في هذه المحولات في وقت واحد بعد تقليل دالة التكلفة الفردية. حيث تمنح هاته الليونة إمكانية إضافة تصغير لأرقام التبديل أو لمتوسط التردد كمصطلح رابع في دالة التكلفة.

في هذا الجانب، يطرح البحث خوارزمية تنبؤيه متتالية مع التحكم المنفصل في القوى النشطة والتفاعلية. يهدف التحكم المقترح إلى إعطاء مزيد من التحكم في النظام وتحسين كفاءته. يحتوي أول نظام تمت دراسته في هذا القسم على ثلاثة محولات، يتم التحكم في هذه المحولات في وقت واحد مع وظيفة تكلفة واحدة؛ توفر استراتيجية التحكم المستخدمة مزيدًا من المتانة للنظام من خلال أن النظام الكلي يمكنه الآن تعويض الطاقة التفاعلية غير المرغوب فيها على جانب الشبكة دون أي منظم آخر وأي اضطراب في جانب التيار المستمر. النظام الثاني المدروس يتعامل مع نظام PV المستقل والذي يحتوي بذاته على نظام متكامل لتخزين الطاقة. تتضمن خوارزمية التحكم التنبئي للقدرة المستخدمة لهذا النظام إدارة الطاقة المنتجة. بالإضافة إلى ذلك، فإنه يضمن دورات شحن وتفريغ البطارية مع تموج أقل، وكل ذلك يعتمد على الطاقة المطلوبة بواسطة الحمل. تم اختبار النظام تجريبيا تحت عدة ظروف.